Timing test of the NeuRad neutron detector prototype*

D. Kostyleva[1,2,3], *A. Bezbakh*[2,4], *V. Chudoba*[2,5], *A. Fomichev*[2], *A. Gorshkov*[2,4], *O. Kiselev*[3], *S. Krupko*[2,4], *I. Mukha*[3], *and I. Muzalevsky*[2,6]

[1]JLU Giessen, Germany; [2]FLNR JINR Dubna, Russia; [3]GSI Helmholtzzentrum, Darmstadt; [4]FSBI NRC "Kurchatov Institute" - ITEP, Moscow, Russia; [5]Silesian University in Opava, Czech Republic; [6]Dubna State University, Russia

The NeuRad neutron detector is constructed out of scintillation fibers and is aimed on measuring the neutron - heavy fragment angular correlations from exotic neutron decays. The results of the first test of NeuRad prototype timing properties are presented in this report.

The EXPERT (EXotic Particle Emission and Radioactivity by Tracking) is a part of the physics program of the Super-FRS Experiment Collaboration [1]. The EXPERT experiments are aimed at studies of the unknown exotic nuclear systems beyond the proton and neutron drip-lines. These experiments will use the first half of the Super-FRS as a radioactive beam separator and its second half as a high-resolution spectrometer. NeuRad detector will provide precise information on angular correlations between nuclear-decay neutrons and the charged decay products measured by the rest of EXPERT setup. An information on angular correlations will be used to determine the decay energy of the precursor, its life time and mode of the decay.

The detector is designed in order to provide sufficient detection efficiency and fine position resolution for neutrons at expected energies about 200-800 MeV interacting with the material of fibers, in particular, via elastic scattering. The detector will be constructed of scintillating fibers ($\approx 10^3$ units) with 3x3 mm^2 cross section and the length of 1 m each, which will be grouped into bundles. Two multi-anode PMT's will be mounted on each side of bundle, each side of fiber will be read out by one pixel. Bundles will be oriented along beam axis meaning that the frontal PMT will be penetrated by neutrons. The detector will be placed at distance of $\approx$ 30 m from the focal plane FRF1. Such setup will ensure total angular acceptance of the detector up to $\pm$6 mrad which reflects low transfer momentum, corresponding to the decay energy expected at the range of 0.1-100 keV.

One of the significant NeuRad characteristics is the time resolution. The first neutron hit has to be determined in order to distinguish between one multi-scattered neutron and the event with multiple neutrons. The longitudinal (z) position, which enhances angular resolution, will be extracted from the time difference between the signals collected on both sides of the detector. In order to obtain required angular resolution, a position resolution about 6 cm is needed. This corresponds to the time-uncertainty of $\sim$ 0.5 ns. Test measurements of timing characteristics has been performed with NeuRad detector demonstrator at FLNR JINR recently.

The demonstrator consists of one bundle of BCF12 fibers 25 cm long coupled with two PMT's H9500. It has been irradiated with a γ-source ^{60}Co in a shielded black box. Unamplified signals from the PMTs were collected by DRS4 digitizer board [2] and Tektronix MSO7354 oscilloscope for further offline analysis. Qualitative difference between signals acquired by both devices, despite differences in sampling rate (5 GS/s of DRS4 board and 10 GS/s of the oscilloscope), bandwidth (750 MHz of DRS4 and 2 GHz of the oscilloscope) and amplitude resolution (12 bit and 10 bit correspondingly), has not been observed.

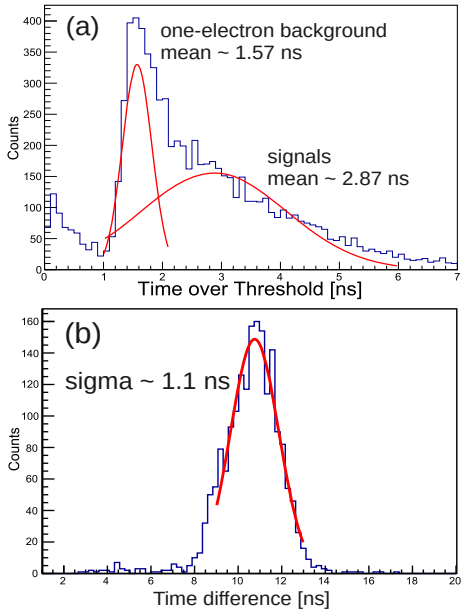

Figure 1: (a) Time-over-threshold spectra of PMT signals, (b) difference between times of γ-ray registration from opposite sides of NeuRad obtained using time-over-threshold selection.

Data have been processed using time difference measurement techniques (Constant Fraction Discrimination, Leading Edge Analysis, fitting the shape of rising edge etc.) which were implemented in ExpertRoot software [3]. Time-over-threshold spectra allowed to implement signal selection avoiding noise and one-electron PMT background, see Fig.1(a). Time uncertainty between two opposite ends of one fiber was determined to be of about 1 ns (σ), see Fig.1(b).

A reference measurement conducted with the same con-

* The work was partly supported by grants provided by MEYS Czech Republic (projects LTT17003 and LM2015049) and RSF (project No. 17-12-01367), A.B., A.G. and S.K have been supported by FAIR-Russia Research Center as well.

figuration of the setup but a thin (4 mm thick) BC-420 square scintillator has shown that the time resolution can be improved down to $\sigma \approx$ 0.5 - 0.7 ns.

The next test of NeuRad prototype is planned with the multi-channel electronics from the company PET SYS Electronics [4].

References

[1] J. Aysto et al. Nucl. Inst. Meth. in Phys. Res. B376 (2016) 111

[2] https://www.psi.ch/drs/evaluation-board

[3] http://er.jinr.ru

[4] http://www.petsyselectronics.com/web/

DOI:10.15120/GR-2017-1

Time-of-Flight measurements with a liquid Cherenkov detector as a possible TOF detector for the Super-FRS

N. Kuzminchuk-Feuerstein[*1], *B. Voss*[1], *E. Fiks*[2], *and the SFRS collaboration*[1]
[1]GSI, Darmstadt, Germany; [2]National Research Tomsk Polytechnic University, Tomsk, Russia

Aiming to develop a system with a precision down to about 50 ps in time and resistant to a high radiation rate of relativistic heavy ions of up to 10^7 per spill (at the second focal plane), we have shown a conceptual design for a Cherenkov detector envisioned for the future TOF measurements employing a fluid radiator. After search of suitable radiator an Iodine-Naphthalene liquid ($C_{10}H_7I$) is proposed [1]. The choice of the radiator was motivated by its high refractive index (n=1.7003) and relatively low density allowing to detect low-energetic particles with minimized deterioration of the beam quality.

The first proof of principle experiment with a Cherenkov TOF prototype detector using a $C_{10}H_7I$ radiator was performed at the experimental place CaveC of the SIS facility at GSI in April 2014 with ^{58}Ni beam at 300 - 1500 MeV/u [2] [3]. In the summer 2016 a time-of-flight was measured with ^{124}Xe ions with 600 MeV/u at CaveC.

Fig. 1 shows a layout of our experimental setup used in the measurements with xenon ions. A quadratic plastic scintillator (S) is used as a start detector for time-of-flight measurements. Scintillator has a size of 5.5 x 5.5 x 2 cm^2 and placed in the vacuum chamber perpendicular to the beam direction, directly at the beginning of HTD-beam line. The scintillation light is directly read out by 4 PMTs (S_u, S_d, S_l, S_r), placed on the top, bottom, left and right sides of the scintillator. For high accuracy timing measure-

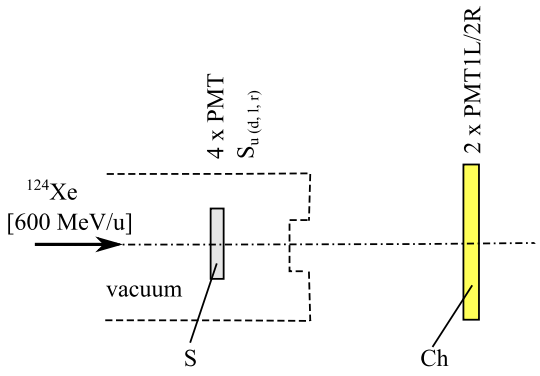

Figure 1: Detector arrangement used in timing measurements with xenon ions at CaveC.

ments the VME - Module VFTX (VME-FPGA-TDC) [4] was used. First, the signals from two ends of the Cherenkov detector (PMT1L, PMT2R) and four ends of the scintillator counter were delivered to CFD. Then the TOF between (Ch) and (S) was recorded by TDC.

The timing of the detectors is calculated by taking the average time detected by four PMTs of a plastic scintillator $< T_S >$ and by two PMTs of a Cherenkov detector $< T_S >$. Time-of-flight distribution between (Ch) and (S) detectors was measured as:

$$TOF(Ch-S) =< T_{Ch} > - < T_S > \quad (1)$$

The width of the time distribution is given by

$$\sigma_{TOF} = \sqrt{\sigma^2_{T_{Ch}} - \sigma^2_{T_S}} \quad (2)$$

where σ is the accuracy of the TOF measurement. Fig. 2 shows resulting time-of-flight distribution $TOF(Ch-S)$.

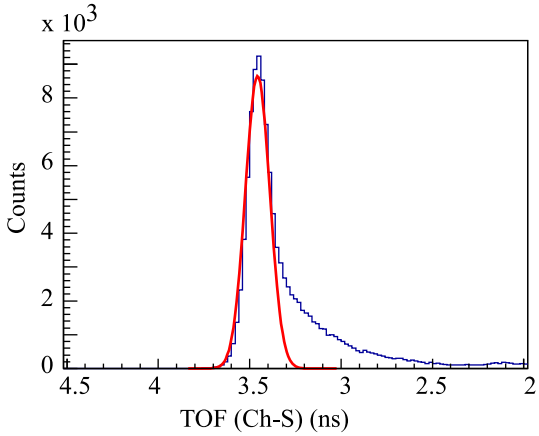

Figure 2: Time-of-flight spectra TOF(C-S) measured with xenon ions between Cherenkov detector and plastic scintillator. The Gaussian fit is indicated with a red solid line. The width of the distribution equals 63 ps.

References

[1] N. Kuzminchuk-Feuerstein et. al., GSI Scientific Report 2013, 103.

[2] N. Kuzminchuk-Feuerstein et. al., GSI Scientific Report 2014, 141.

[3] N. Kuzminchuk-Feuerstein et. al., First beam test of a liquid Cherenkov detector prototype for a future TOF measurements at the Super-FRS, submitted to Nucl. Instrum. and Meth. A (2017).

[4] J. Frühauf et. al., GSI Scientific Report 2012, 300.

* n.kuzminchuk@gsi.de

Systematic investigations of charge states and purity of projectile and fission fragments extracted from the stopping cell of the (Super-)FRS *

I. Miskun[1], *A.-K. Rink*[1], *F. Greiner*[1], *S. Ayet*[1,2], *S. Bagchi*[2], *J. Bergmann*[1], *P. Constantin*[3], *T. Dickel*[2], *J. Ebert*[1], *A. Finley*[4], *H. Geissel*[1,2], *E. Haettner*[2], *C. Hornung*[1], *S. Kaur*[5], *W. Lippert*[1], *I. Mardor*[6,7], *B. Mei*[3], *I. Moore*[8], *J.-H. Otto*[1], *S. Pietri*[2], *A. Pikhtelev*[9], *W. R. Plaß*[1,2], *I. Pohjalainen*[8], *A. Prochazka*[2], *S. Purushothaman*[2], *C. Rappold*[2], *M. P. Reiter*[4], *C. Scheidenberger*[1,2], *Y. Tanaka*[2], *H. Toernqvist*[2], *H. Weick*[2], *J. S. Winfield*[2], *X.Xu*[2], *and M. Yavor*[10]

[1]JLU, Gießen, Germany; [2]GSI, Darmstadt, Germany; [3]ELI-NP, Bucharest, Romania; [4]TRIUMF, Vancouver, Canada; [5]Saint Mary's Univ., Halifax, Canada; [6]Tel Aviv University, Israel; [7]Soreq NRC, Yavne, Israel; [8]Univ. of Jyväskylä, Finland; [9]Inst. for Energy Problems of Chem. Phys., RAS, Chernogolovka, Russia; [10]IAI, RAS, St. Petersburg, Russia

The prototype of the cryogenic stopping cell (CSC) [1] for the Low-Energy Branch of the Super-FRS has been developed and successfully commissioned as a part of the FRS Ion Catcher experiment [2] at GSI. In several experiments various ^{238}U and ^{124}Xe projectile and fission fragments were produced, separated and range-bunched in the FRS, thermalized, extracted from the CSC and identified. The measured charge states of the extracted ions are shown in the bottom section of each element in Fig.1. In the top section of each element the predicted charge states are presented, based on the assumption that charge exchange processes in the CSC are defined by the ionization potential of its contaminants and dominated by N_2 molecules, which are present in trace amounts in the He buffer gas. The results indicate that this assumption is correct and there are no contaminants such as O_2, oil, water, etc. in the CSC. Further purification of the buffer gas can result in the survival of higher charge states of the thermalized ions and, therefore, limitations of the mass range of the ions transmitted by the RF carpet. In the future [3] trace gases will be used to control the charge state of thermalized ions.

Operation with high intensity beams causes high ionization and reveals contaminants introduced together with the He buffer gas. These are light molecules containing noble gases, which do not harm ion survival, but can still spoil the measurement. An example can be seen in Fig.2a, where a time-of-flight spectrum of ^{124}Xe primary beam taken with the multiple-reflection time-of-flight mass spectrometer (MR-TOF-MS) [4] is dominated by Kr molecules. These contaminants can be removed by using a collision induced dissociation (CID) process [5] together with two-stage mass separation [6] in the RFQ beamline downstream of the CSC. It proved to be a universal and effective tool for beam purification. In Fig.2b a spectrum is shown, where this method was applied. It can be seen that all of the contaminants are removed from the spectrum, including the isobar of ^{124}Xe with a mass difference of only $\approx$ 300 keV. This enables a precision measurement of ^{124}Xe, the ion of interest in this case.

*This work was supported by the BMBF under contracts No. 05P12RGFN8 and 05P16RGFN1, by the HMWK through the LOEWE Center HICforFAIR, by HGS-HIRe, by JLU Gießen and GSI under the JLU-GSI strategic Helmholtz partnership agreement.

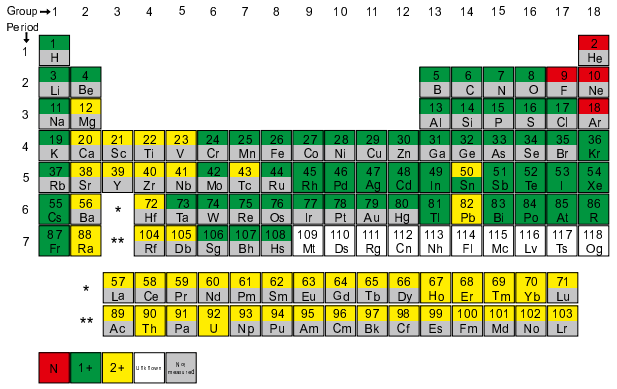

Figure 1: Periodic table showing the charge states in which the ions are extracted from the CSC. Upper section of each element: predicted; lower section: measured.

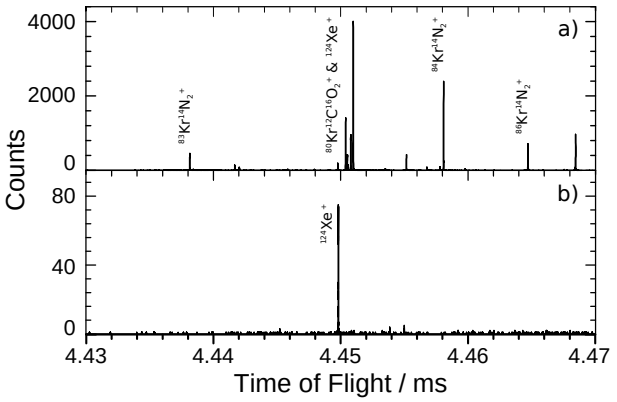

Figure 2: Multi-turn TOF spectra of ^{124}Xe primary beam: (a) no CID applied, the spectrum is dominated by contaminants; (b) CID applied, the contaminants are removed.

References

[1] M. Ranjan et al., Europhys. Lett. 96 (2011) 52001.

[2] W.R. Plaß et.al., NIM B 317 (2013) 457-462.

[3] T. Dickel et al., NIM B 376 (2016) 216.

[4] T. Dickel et al., NIM A 777 (2015) 172-188.

[5] F. Greiner, Master thesis, JLU, Gießen, Germany, 2017.

[6] I. Miskun, Diploma thesis, TPU, Tomsk, Russia, 2015.

DOI:10.15120/GR-2017-1

Complete ion identification by proton and mass number via high-resolution mass spectrometry at the (Super-)FRS *

C. Hornung[1], S. Ayet[1,2], S. Bagchi[2], J. Bergmann[1], P. Constantin[3], T. Dickel[2], J. Ebert[1], A. Finlay[4], H. Geissel[1,2], F. Greiner[1], E. Haettner[2], S. Kaur[5], W. Lippert[1], I. Mardor[6], B. Mei[3], I. Miskun[2], I. D. Moore[7], J.-H. Otto[1], S. Pietri[2], A. Pikhtelev[8], W. R. Plaß[1,2], I. Pohjalainen[7], A. Prochazka[2], S. Purushothaman[2], C. Rappold[2], M. P. Reiter[4], A.-K. Rink[1], C. Scheidenberger[1,2], Y. Tanaka[2], H. Toernqvist[2], H. Weick[2], J. S. Winfield[2], X. Xu[1,2], and M. I. Yavor[9]

[1]JLU, Gießen, Germany; [2]GSI, Darmstadt, Germany; [3]ELI-NP, Bucharest, Romania; [4]TRIUMF, Vancouver, Canada; [5]Astronomy and Phys. Dep., Saint Mary's Univ., Halifax, Canada; [6]Soreq NRC, Yavna, Israel; [7]Univ. of Jyväskylä, Finland; [8]Inst. for Energy Problems of Chem. Phys., RAS, Chernogolovka, Russia; [9]IAI, RAS, St. Petersburg, Russia

Ion identification and separation are important at all present and future rare-isotope facilities. The in-flight separators FRS / Super-FRS [1, 2] use the $B\rho - \Delta E - B\rho$ method to achieve isotopic-spatial separation. At relativistic velocities the verification of the particle identification (PID) by proton number (Z) and mass number (A) of the selected bare ions can be easily performed with particle detectors via velocity, energy-deposition and magnetic rigidity measurements in coincidence. Still the separation and identification require both an elaborated absolute calibration. At lower velocities (300 MeV/u), the fragments emerge from the target in different ionic charge states which makes an unambiguous PID very difficult. Here, we demonstrate that high-resolution mass spectrometry represents a universal method to provide an unambiguous PID at the final focal plane of the FRS.

In our previous FRS experiments we reached a mass resolving power (MRP) of 450000 with the multiple-reflection time-of-flight mass spectrometer (MR-TOF-MS) [3]. It is part of the FRS Ion Catcher [4], which is a test bench for the Low-Energy-Branch (LEB) of the Super-FRS [2] at FAIR. Together with a cryogenic gas-filled stopping cell (CSC) the MR-TOF-MS has the capability to perform a complete PID of exotic nuclei based on their mass-to-charge ratio only.

In Fig. 1 we illustrate the ensemble of isotopes which enters the CSC for two experiments centered either on ^{94}Ag or ^{202}Os fragments. Although the number of possibly implanted isotopes is relatively large due to the applied monoenergetic degrader and the selected kinetic energy domain of 300 MeV/u, all ions involved can be uniquely identified with the achieved MRP.

In our latest experiment uranium projectile fragments were produced at 300 MeV/u, spatially separated in-flight, energy bunched and efficiently stopped in the CSC, fast extracted and finally analyzed with the MR-TOF-MS. The 300 MeV/u corresponds to the energy at the LEB. The nuclides could be identified unambiguously already with a modest MRP of 75000 (Fig. 2).

*This work was supported by the BMBF under contracts No. 05P12RGFN8 and 05P16RGFN1, by the HMWK through the LOEWE Center HICforFAIR, by HGS-HIRe, by JLU Gießen and GSI under the JLU-GSI strategic Helmholtz partnership agreement.

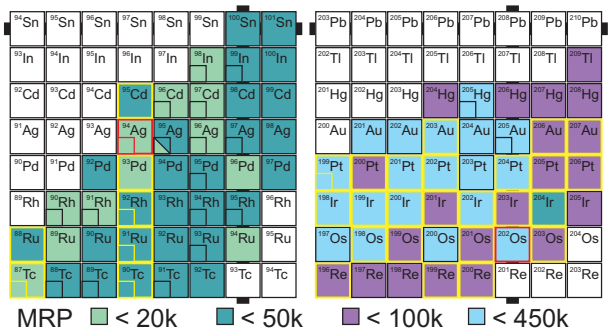

Figure 1: Required MRP to achieve unique PID in two typical isotope domains (^{94}Ag and ^{202}Os). An MRP corresponding to twice the mass difference between adjacent isobars has been assumed. The fragments were produced and separated at 300 MeV/u. All fragments which are stopped together with the goal fragment (red frame) in the CSC got a yellow frame.

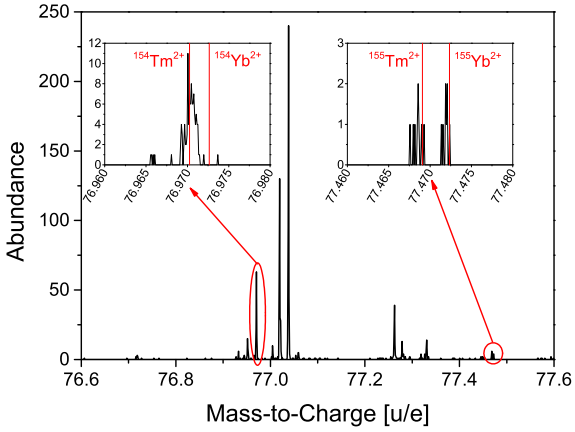

Figure 2: Measured mass-to-charge-spectrum of the uranium fragments under LEB conditions.

References

[1] H. Geissel et al., Nucl. Instrum. Methods B 70 (1992) 286.
[2] H. Geissel et al., Nucl. Instrum. Methods B 204 (2003) 71.
[3] T. Dickel et al., Nucl. Instrum. Methods A 777 (2015) 172.
[4] W.R. Plaß et al., Nucl. Instrum. Methods B 317 (2013) 457.

Excitation of baryonic resonances in projectiles of ^{124}Xe at 600A MeV

J.L. Rodríguez-Sánchez[1], J. Benlliure[1], S. Bagchi[2], J. Díaz-Cortes[1], H. Geissel[2], E. Haettner[2], H. Lenske[3], A. Prochazka[2], C. Scheidenberger[2], Y. Tanaka[2], I. Vidaña[4], H. Weick[2], and J.S. Winfield[2]

[1]University of Santiago de Compostela, Spain; [2]GSI, Germany; [3]Justus-Liebig-Universität Giessen, Germany; [4]University of Coimbra, Portugal

The structure of baryons, such as the Δ and Roper (N*) resonances, and their excitation spectrum is one of the unsolved issues of strong interaction physics. Recently, the early appearance of Δ-isobars in dense nuclear matter has inspired many studies relevant to neutron stars [1] and heavy-ion collisions [2]. In particular, very compact stellar configurations are reached due to the introduction of Δ-isobars [1]. However, the in-medium properties of baryon resonances are not well understood. Up to now, the in-medium effects of Δ-isobars have been studied in heavy-ion collisions at kinetic energies above the production threshold using pion-nucleus and nucleon-nucleus reactions [3, 4], where there is not a good control over the production of residual fragments and thus over the number of collisions. Further investigations were performed with isobar charge-exchange reactions at SATURNE using nucleus-nucleus collisions [5]. This kind of reaction allows us to constrain the nucleus-nucleus collision to one nucleon-nucleon reaction at the surface of both nuclei. However, the experiments carried out at SATURNE did not permit to measure the pion emitted in the decay of the resonances in coincidence with the isobar charge-exchange reaction.

To go a step further, we propose to perfome complete kinematics measurements of isobar charge-exchange reactions, detecting the residual nucleus in coincidence with pions in order to separate the quasi-elastic and inelastic componets observed in the missing-energy spectrum [6]. The GSI experimental facilities provide us unique conditions to perform these measurements with high quality allowing us to identify the isobaric charge-exchange reactions from the determination of the atomic and mass number of the residual fragments event-by-event. For the measurement of the pions, a specific setup (based on a solenoid magnet and tracking detectors) will be installed in the middle focal plane of the fragment separator FRS in order to deflect and trace the pions. We plan to perform this measurement with the WASA detector [7].

In this work we report on the results from a experimental test carried out at the FRS in July of 2016 for the phase 0 of this new generation of experiments. We measured the excitation of isobar charge-exchange reactions in stable projectiles of ^{124}Xe impinging in a carbon target of 89 mg/cm^2 placed in the intermediate focal plane of the FRS, using vacuum in the experimental areas S0, S1, S2, and S3 in order to reduce the energy and angular straggling of the projectiles and residual fragments. In Fig. 1 we display the missing-energy spectrum for the isobar charge-exchange reaction ^{12}C(^{124}Xe, ^{124}Cs)X at 600A MeV. The peak close to zero corresponds to the quasi-elastic channel (n, p) and the peak around -300 MeV represents the inelastic contribution due to the excitation of the Δ and Roper (N*) resonances. Thanks to the thin carbon target and the use of vacuum we obtained this spectrum with an energy resolution of 7 MeV, improving the resolution in a factor two with respect to previous experiment performed at FRS [8] or at SATURNE [5].

The new generation of experiments at the FRS will help us to separate the quasi-elastic and inelastic componets observed in the missing-energy spectrum, leading to a full identification of the baryonic resonances excited in the nuclear medium.

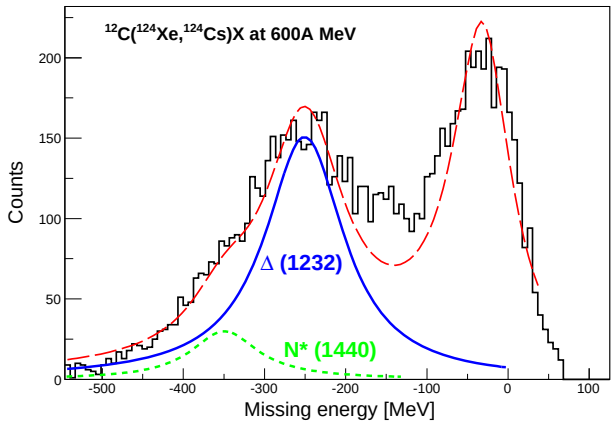

Figure 1: Missing-energy spectrum for the isobar charge-exchange reaction ^{124}Xe + ^{12}C at 600A MeV going to ^{124}Cs. Solid and short-dashed lines show the Δ and Roper (N*) contributions obtained by fitting the spectrum to Breit-Wigner distributions, respectively.

References

[1] A. Drago et al., Phys. Rev. C **90**, 065809 (2014).

[2] Z.-Q. Feng, Phys. Rev. C **94**, 054617 (2016).

[3] S. B. Kaufman et al., Phys. Rev. C **20**, 2293 (1979).

[4] J. Chiba et al., Phys. Rev. Lett. **67**, 1982 (1991).

[5] D. Bachelier et al., Phys. Lett. B **172**, 23 (1986).

[6] I. Vidaña et al., EPJ Web of Conferences **107**, 10003 (2016).

[7] C. Bargholtz et al., Nucl. Instrum. Meth. A **594**, 339 (2008).

[8] J. Vargas et al., Nucl. Instrum. Meth. A **707**, 16 (2013).

DOI:10.15120/GR-2017-1

Measurements of hypernuclear decay fragments at FRS for Phase0-FAIR hypernuclear experiment

C.Rappold[*1,2], *T.R. Saito*[1,3,4], *and C. Scheidenberger*[1,2]

[1]GSI, Darmstadt, Germany; [2]Justus-Liebig-Universität Giessen, Germany; [3]Johannes Gutenberg-Universität, Mainz, Germany; [4]The Helmholtz Institute Mainz, Mainz, Germany

The first experiment of the HypHI collaboration demonstrated the feasibility of the hypernuclear spectroscopy by means of heavy ion beam induced reactions. The phase 0 experiment was performed with a ^{6}Li beam at 2AGeV impinged on a stable ^{12}C target material. The main results of the experiment showed the reconstruction and identification of decay vertexes of Λ particle and $^{3}_{\Lambda}$H, $^{4}_{\Lambda}$H [1, 2, 3].

A novel experiment at the FRS fragment separator for the FAIR-Phase 0 beam-time period is proposed in order to assess the existence of the nnΛ possible bound state. A new experimental concept have been under development and their designs have been already reported [4, 5]. In order to assess if this experimental method is viable, a experiment with similar conditions of the previously successful experiment will be performed. Light hypernuclei $^{3}_{\Lambda}$H, $^{4}_{\Lambda}$H and nnΛ will be the species of interest that will be aimed to be reconstructed and identified by invariant mass method.

After the two-body decay, a narrow magnetic rigidity acceptance window will be set for the FRS in order to measure precisely the momentum of outgoing decay fragment. The detection apparatus at the S2 experimental area will be responsible for the measurement of a large portion of the emitted π^{-}. The acceptance and measurement efficiency of the S2-S4 section of the FRS is assessed by means of MOCADI simulations.

The full phase-space distribution in position and momentum is simulated by Geant4 simulations. The Geant4 simulation code is responsible for the detail treatment of the hypernuclear decay, the tracking within the experimental apparatus placed in the S2 area, and the hit digitalization within the different detection systems in the S2 area. decay π^{-} and other light particles produced in the reaction and in the hypernuclear decay are measured in the dedicated apparatus in S2, while fragments continue up to the S2 exit.

Detectors placed at the S2 exit register the full phase-space of the outgoing fragments. Specific code for loading Geant4 events as input event into MOCADI simulations was implemented and allowed a event by event simulations in the continuity of Geant4 simulations. A Bρ scanning is then possible in order to assess the decay fragment measurement efficiency of the S2-S4 section of the FRS. Fig. 1a shows the phase-space distribution as a function of Bρ of decay ^{3}He of $^{3}_{\Lambda}$H at the entrance and exit of the S2-S4 section of the FRS.

Fig. 1b shows the differential efficiency of S2-S4 section for FRS setting center at Bρ of 12.6 Tm for ^{3}He decay fragment of $^{3}_{\Lambda}$H. After performing the Bρ scanning over the full phase-space, the maximum efficiency of measurement between S2-S4 was determined. The average measurement efficiency for ^{3}He, ^{4}He and d are around 40% respectively.

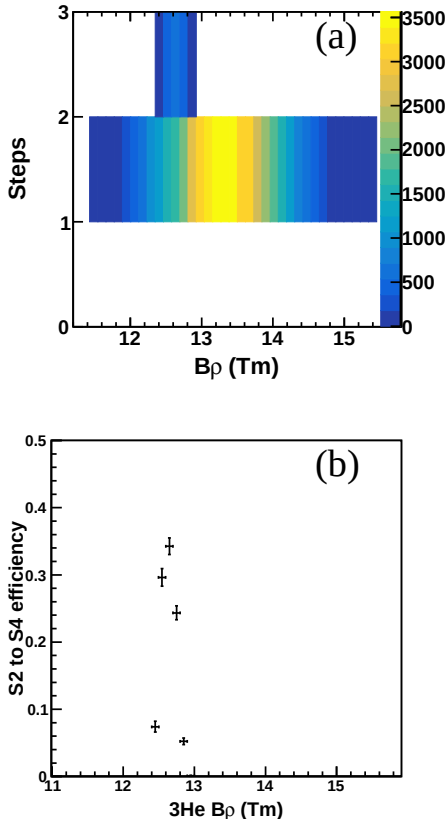

Figure 1: Differential efficiency of the S2-S4 section of the FRS for the momentum measurement of decay ^{3}He of $^{3}_{\Lambda}$H. The central Bρ of 12.6 Tm was set in the MOCADI simulations.

References

[1] C. Rappold *et al.*, Nucl. Phys. A **913**, 170 (2013).

[2] C. Rappold *et al.*, Phys. Rev. C **88**, 041001 (2013).

[3] C. Rappold *et al.*, Phys. Lett. B **747**, 129 (2015).

[4] C. Rappold *et al.*, GSI Scientific Report 2014 [GSI Report 2015-1] (2015) p. 135.

[5] C. Rappold *et al.*, GSI Scientific Report 2014 [GSI Report 2015-1] (2015) p. 136.

* c.rappold@gsi.de

Particle identification using cylindrical detector system for Phase0-FAIR hypernuclear experiment

C.Rappold[*1,2], *T.R. Saito*[1,3,4], *and C. Scheidenberger*[1,2]

[1]GSI, Darmstadt, Germany; [2]Justus-Liebig-Universität Giessen, Germany; [3]Johannes Gutenberg-Universität, Mainz, Germany; [4]The Helmholtz Institute Mainz, Mainz, Germany

The feasibility of the hypernuclear spectroscopy by means of heavy ion beam induced reactions was demonstrated by the results obtained in the first experiment of the HypHI collaboration. A ^{6}Li beam at 2AGeV impinged on a stable ^{12}C target. The main results of the experiment showed the measurements of Λ hyperon and $^{3}_{\Lambda}$H, $^{4}_{\Lambda}$H. Results on the invariant masses, lifetime and production cross sections were published [1, 2, 3].

For the FAIR-Phase 0 beam-time a new hypernuclear spectroscopy experiment is proposed in order to assess the existence of the nnΛ possible bound state. This novel experiment will take place at the FRS fragment separator. The section TA-S1-S2 of FRS will use to deliver the stable beam with a energy of 2AGeV to the S2 experimental area. In the S2 area, the possibility to install a cylindrical detector system that involved a solenoid magnet is considered as described in [4]. A target will placed around 40 cm to 60 cm upstream to this detection system. The light hadrons, π^-, π^+, K$^+$, K$^-$, and protons will be able to be measured by the cylindrical system. A central drift chamber and hodoscope barrel will be responsible for the main tracking system for the momentum measurement. Additional planar tracker stations will be placed in the upstream area of the detection system. The most important aspect of this cylindrical detector system will be to precisely measure the decay π^- from the nnΛ and other produced hypernuclei. As well the produced kaons from the strangeness s-$\bar{\text{s}}$ production will be possible to be measured and identified. After the hypernuclear two-body decay, a narrow magnetic rigidity acceptance window will be set for the S2-S4 section of FRS in order to measure precisely the momentum of outgoing decay fragment.

The full phase-space distribution in position and momentum is simulated by Geant4 simulations. The Geant4 simulation code is responsible for the detail treatment of the hypernuclear decay, the tracking within the experimental apparatus placed in the S2 area, and the hit digitalization within the different detection systems in the S2 area. The MOCADI simulations are then used for the study of the S2-S4 section of FRS efficiency. Decay π^- and other light particles produced in the reaction and in the hypernuclear decay are measured in the dedicated apparatus in S2, while fragments continue up to the S2 exit. Fig. 1 shows the results of the particle identification of track reconstruction of the Geant4-simulated events. The tracking is based on Kalman Filter and the framework developed for full data analysis of the Phase 0 experiment. A time-of-flight resolution of 150 ps was assumed in the simulations. Fig. 1a shows the β-momentum correlation while the mass distribution, $m = p\sqrt{\beta^{-2}-1}$, of the reconstructed light hadrons is shown in Fig. 1b. A clear identification and separation between π, kaon and proton is visible in each plot.

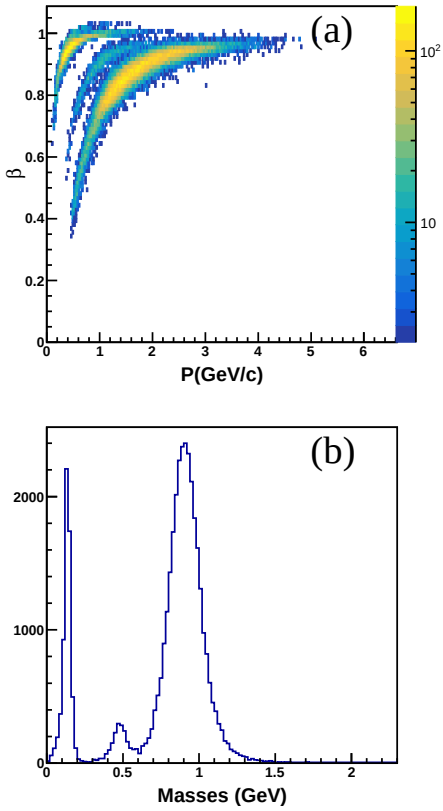

Figure 1: Particle identification plots for light hadrons within the cylindrical detector system. (a) The β-momentum correlation shows clear distinction between π, kaons and protons. (b) The mass distribution spectrum of light hadrons calculated from β and momentum.

References

[1] C. Rappold *et al.*, Nucl. Phys. A **913**, 170 (2013).

[2] C. Rappold *et al.*, Phys. Rev. C **88**, 041001 (2013).

[3] C. Rappold *et al.*, Phys. Lett. B **747**, 129 (2015).

[4] C. Rappold *et al.*, GSI Scientific Report 2014 [GSI Report 2015-1] (2015) p. 135.

* c.rappold@gsi.de

DOI:10.15120/GR-2017-1

Simulations of RCE, ChR & HWC channeling

H. Geissel[1], *O.V. Bogdanov*[*2], *C. Scheidenberger*[1], *Yu.L. Pivovarov*[2], *N. Kuzminchuk-Feuerstein*[1], *E.I. Rozhkova*[2], *T.A. Tukhfatullin*[2], *and the Super-FRS Experiment Collaboration*[1]

[1]GSI, Darmstadt, Germany; [2]National Research Tomsk Polytechnic University, Russia

The perspective atomic physics experiments are the part of Super-FRS collaboration program [1], in particular for the first time to observe the nuclear Okorokov effect of resonant coherent excitation (RCE) of relativistic nuclei passing through a crystal [2]. The RHI beam energy at Super-FRS is up to 1500 MeV/u, and perturbation harmonic energy at axial channelling in a crystal is equal to $\hbar\omega_n = (2\pi\hbar c/d) \cdot \gamma \cdot \beta \cdot n$, n=1,2,.., where d is the spacing between atoms in the crystal axis, γ is the relativistic factor and $\beta = v/c$, with v being RHI velocity. For RCE, the transition energy between ground and excited state of projectile nucleus should match perturbation harmonic energy. For a case of ¡100¿ channelling in W crystal, the harmonic energy equals $\hbar\omega_n = 3.92 \cdot \gamma \cdot \beta \cdot n$ keV [2]. Therefore, at $\gamma\beta \cong 2$ the energies of the first three strong perturbation harmonics are $\hbar\omega_1$=7.84 keV, $\hbar\omega_2$=15.68 keV and $\hbar\omega_3$=23.52 keV. At Super-FRS, RCE experiments will be performed with exotic nuclei. Detailed simulations of nuclear RCE using the BCM-2.0 code [3] are in progress.

The first measurements of the Cherenkov radiation (ChR) from RHI with the present FRS have revealed that the well known Tamm-Frank theory cannot describe the observed results [4]. The new models [5] [6] predict that at the Super-FRS energies the slowing-down of the ions in the radiator leads to broadening and complex diffraction structures of the spectral and angular distributions (Fig. 1). These distributions are very sensitive to the charge and

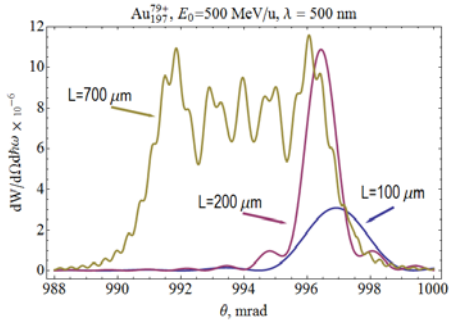

Figure 1: ChR angular distribution from 500 MeV/u Au ions in a 100, 200, and 700 μm diamond radiator.

velocity of RHI, and radiator thickness [7], thus the experiments with the Super-FRS will contribute to the detailed understanding of ChR from RHI ions and will lay the ground for improved and novel detector developments, like velocity selector [8]. These studies will be performed

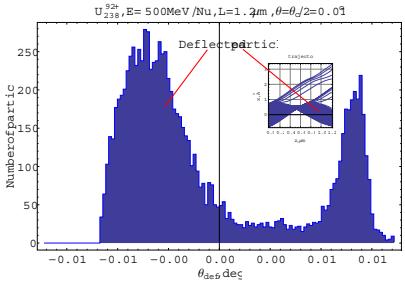

Figure 2: Deflection of 500 MeV/u uranium ions by (200) tungsten HWC. Critical channelling angle θ_C = 0.02 °.

in close collaboration with the detector laboratory at GSI, which investigate ChR in liquid radiator as a diagnostic tool for RHI [9].

The FRS research division is already active in channelling experiments [10], all the necessary equipment exists and can be used to continue these experiments at the Super-FRS. We suggest to include into experimental program the studies of channelling in a Half-Wave Crystal (HWC), which is the very recent trend in high-energy physics [11]. According to the simulations, achievable deflection angle through the mirror effect is of the order of critical channelling angle θ_C (Fig. 2). The possible applications are: effective beam deflector and even charge/velocity selector.

References

[1] I. Tanihata, H. Geissel et. al., 'Conceptual Design Report for the Scientific Program of the Super FRS Experiment Collaboration', GSI Report 2016, 3.

[2] Yu.L. Pivovarov, H. Geissel, C. Scheidenberger. Nucl. Instrum. and Meth. B 256 (2007) 109.

[3] S.V. Abdrashitov, O.V. Bogdanov, B. Korotchenko et. al., Nucl. Instrum. and Meth. B 402 (2017) 106.

[4] J. Ruzicka, et. al., Vacuum 63, Issue 4 (2001) 591.

[5] E.I. Fiks, et. al., Nucl. Instrum. and Meth. B 309 (2013) 146.

[6] E.I. Fiks, et. al., Nucl. Instrum. and Meth. B 314 (2013) 51.

[7] E.I. Fiks, Yu.L. Pivovarov, Phys. Lett. A 380 (2016) 2386.

[8] T. Yamaguchi et. al., Nucl. Instrum. and Meth. B 766 (2014) 123

[9] N. Kuzminchuk-Feuerstein et. al., Nucl. Instrum. and Meth. A 866 (2017), 207.

[10] D. Dauvergne et al., Phys. Rev. A 59 (1999) 2813.

[11] W. Scandale et. al., Phys. Lett. B 734 (2014) 1.

* bov@tpu.ru

A gas degrader for the low-energy branch of the Super-FRS at FAIR *

S. Purushothaman[1], *T. Dickel*[1,2], *S. Ayet*[1,2], *S. Bagchi*[1], *K.-H.Behr*[1,2], *J. Bergmann*[2], *T. Blatz*[1,2], *P. Constantin*[5], *J. Ebert*[2], *A. Finley*[6], *H. Geissel*[1,2], *F. Greiner*[2], *E. Haettner*[1], *C. Hornung*[2], *S. Kaur*[10], *W. Lippert*[2], *B. Lommel*[1], *I. Mardor*[8,9], *B. Mei*[5], *I. Miskun*[1,2], *I. Moore*[3], *J.-H. Otto*[1], *S. Pietri*[1], *A. Pikhtelev*[7], *W. R. Plass*[1,2], *I. Pohjalainen*[3], *A. Prochazka*[1], *C. Rappold*[1,2], *M. P. Reiter*[6], *A.-K. Rink*[2], *C. Scheidenberger*[1,2], *B. Szczepanczyk*[1], *Y. Tanaka*[1,2], *H. Weick*[1], *and J. S. Winfield*[1]

[1]JLU, Gießen, Germany; [2]GSI, Darmstadt, Germany; [3]Univ. of Jyväskylä, Finland; [4]IAI, RAS, St. Petersburg, Russia; [5]ELI-NP, Bucharest, Romania; [6]TRIUMF, Vancouver, Canada; [7]Inst. for Energy Problems of Chem. Phys., RAS, Chernogolovka, Russia; [8]Tel Aviv Univ., Tel Aviv, Israel; [9]Soreq NRC, Yavna, Israel; [10]Astronomy and Phys. Dep., Saint Mary's Univ., Halifax, Canada

At the Low Energy Branch (LEB) of the Super-FRS at FAIR the exotic nuclei produced and separated at relativistic energies are thermalised (∼eV) and delivered to dedicated experimental setups to perform spectroscopy and decay studies (MATS/LaSpec). The only universal technique available for this procedure is to slow the nuclei down to few MeV·u^{-1} in degraders, thermalise them in a noble gas filled stopping cell and then extract using a combination of electric fields and gas flow. The magnetic rigidity of the main-separators of the Super-FRS is 20 Tm whereas it is 7 Tm at the LEB. Therefore, the ion beam must first be slowed down (e.g. $\leq$300 MeV·u^{-1} for ^{238}U) using a homogeneous degrader. The stochastic processes during the production and slowing down of exotic nuclei introduce a momentum spread which is orders of magnitude larger than that of the primary beam. To overcome this problem the ion beam is spatially dispersed according to the momentum using a magnetic stage and the difference is then compensated by passing through a wedge-shaped degrader [1].

A final fine tuning of ion energy is required for an efficient implantation in a gas stopping cell. A thickness-tunable homogeneous degrader which can achieve areal densities lesser than that is possible using a technically feasible aluminum degrader is required for this purpose. Due to the large beam size at the LEB and the requirement of a large dynamic range of tuning, a gas-based degrader is proposed. A prototype of such a density controllable gas degrader was tested at the FRS Ion Catcher (FRSIC) setup [2] during the 2016 beam time at GSI. A Multiple-Reflection Time-of-Flight Mass-Spectrometer (MR-TOF-MS) was used to identify and quantify the thermalized ions extracted from the stopping cell.

The prototype gas degrader consists of a cylindrical stainless steel chamber of 1500 mm length and 125 mm radius. The beam entrance and exit windows were made of 100 μm Kapton foils. The dimensions of the windows were 200 mm$\times$100 mm. The Kapton beam windows were coated with a thin layer of carbon to avoid beam induced charging up and destruction of the beam windows by electrical discharge. These two windows contribute 2$\times$20 mg·cm^{-2} to the total areal density of the gas degrader. Dry nitrogen was used as the degrader material. The areal density of the nitrogen gas inside the chamber can be tuned between 0–160 mg·cm^{-2} with an accuracy of $\pm$0.2 % using a pressure controller.

For the test measurements the FRSIC setup was equipped with a tunable homogeneous aluminum degrader besides the gas degrader. Tests were performed for two gas degrader pressure settings (525 mbar and 800 mbar). The optimal ion energy for the efficient stopping in the gas cell was found by scanning the thickness-tunable homogeneous aluminum degrader. To study the effect of the curvature of the gas degrader beam window on the areal density a scan was also repeated for off-axis beams. No noticeable effect of the window curvature was found. The results of these tests (see Figure 1) show the technical feasibility of a gas degrader system for the LEB of the Super-FRS.

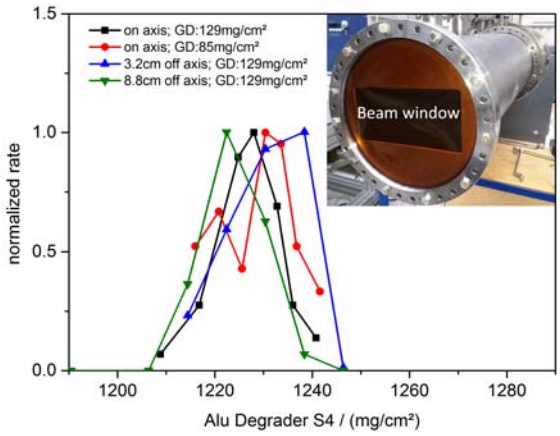

Figure 1: Stopping efficiency of ions in the gas stopping cell as a function of the sum of the areal densities of the thickness-tunable homogenous degrader and the gas degrader (GD) in aluminum equivalent. Photograph of the gas degrader chamber is shown in the inset.

*This work was supported by the BMBF under contracts No. 05P12RGFN8 and 05P16RGFN1, by the HMWK through the LOEWE Center HICforFAIR, by HGS-HIRe, by JLU Gießen and GSI under the JLU-GSI strategic Helmholtz partnership agreement.

References

[1] H. Weick et al., NIMB 164 (2000) 168-179

[2] W.R. Plaß et al., NIMB 317 (2013) 457-462

DOI:10.15120/GR-2017-1

Systematic measurement of total interaction cross sections in medium mass nuclei

J. Díaz-Cortés[1], *J.L. Rodríguez-Sánchez*[1], *J. Benlliure*[1], *D. Dragosavac*[1], *D. Pérez*[1], *H. Álvarez-Pol*[1], *B. Blanck*[2], *E. Casarejos*[1], *V. Fohr*[3], *M. Gascón*[1], *W. Gawlikowicz*[4], *A. Heinz*[5], *K. Helariutta*[6], *L. Pienkowski*[4], *M. Staniou*[3], *K. Subotic*[7], *K. Summerer*[3], *B. Pietras*[1], *J. Taieb*[8], *A. Trzcinska*[4], *D. Rossi*[6], *H. Simon*[6], *J. Vargas*[1], *and B. Voss*[6]

[1]University of Santiago de Compostela, Spain; [2] Centre d'Etudes Nucleaires,Bordeaux-Gradignan Cedex, France; [3]GSI, Darmstadt, Germany; [4]University of Warsaw, Poland; [5]University of Chalmers, Sweeden; [6]University of Helsinki, Finland; [7]Institute of Nuclear Science Vinca, Belgrade, Serbia; [8]CEA DAM, Bruyeres-le-Chatel, France

Radial distributions of protons and neutrons are fundamental properties of nuclei that are fairly well understood for stable nuclei, but in neutron-rich nuclei signatures of unconventional behavior have been reported [1].

Several methods can be used to determine the matter distribution in nuclei, but in general they are all model dependent. X-ray spectroscopy of anti-protonic atoms [2] or the probability for collective excitation as the giant-dipole resonances (GDR) or the spin-dipole resonance (SDR) [3] are some of them.

Interaction cross sections (σ_I) of relativistic projectiles can give access to matter radii and nuclear density distributions [4]. One of the most interesting features of unstable nuclei is the existence of skins [5]. These data provide a unique opportunity to systematically investigate the evolution of neutron-skin structures in medium-mass nuclei.

The experiment took place at the GSI facility where we used secondary beams produced in the fragmentation of ^{132}Xe and fision of ^{238}U at energies around 1000 MeV/A to produce nuclei between Cadmium and Xenon over a broad range in isospin. The FRagment Separator was used as a two-independent magnetic spectrometers, each with a different magnetic setting. In the first part of the FRS, fission and fragmentation fragments produced by the primary beams were unambiguously identified in mass and charge. At the intermediate focal plane of the FRS, a beryllium target of 2591 $\pm$ 7 mg/cm^2 was placed in order to induce the fragmentation reactions. Then, the second part of the FRS was used to identify the fragmentation products.

Total interaction cross sections were determined using the transmission method, counting the number of projectiles impinging in the fragmentation target and the number of projectiles arriving at the final focal plane of the FRagment Separator. The number of counts were corrected by the optical transmission of the ions along the spectrometer, detection efficiency and reactions in other layers of matter by using measurements without the fragmentation target.

These cross sections will be compared to Glauber model calculations in order to investigate the evolution of the neutron and proton density distributions along the isotopic chain [6]. By comparing the spread of the neutron density to that of the proton density for the most neutron-rich nuclei, the difference between the neutron (r_n) and proton (r_p) radii can be obtained. The thickness of the neutron skin is defined as the differrence between the matter radii of the two different nucleon species ($S_n = r_n - r_p$), so this measurements will allow us to evaluate the existence of a neutron skin in medium-mass neutron rich nuclei .

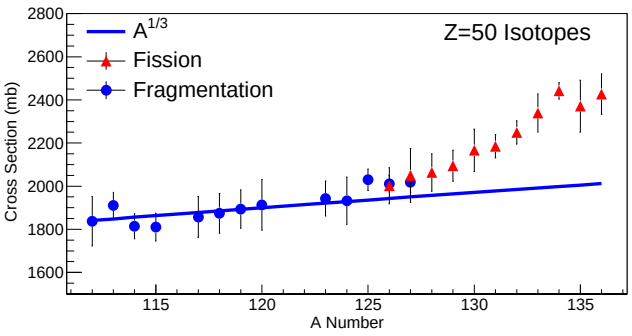

Figure 1: Total interaction cross sections for different tin isotopes (Z=50) from N = 63 to N = 85. The blue line shows the A$^{1/3}$ dependence.

In Fig. 1 we depict the preliminary total interaction cross sections for different tin isotopes measured in this work (points) as a function of the projectile mass number. The blue line shows the A$^{1/3}$ dependence normalized to the ^{112}Sn.The total interaction cross sections for the most neutron deficient tin isotopes increase slowly with the mass but for the most neutron-rich isotopes this increase is much faster. This increment would indicate that the size of the most neutron-rich tin isotopes is bigger than predicted and this could be a signature of the existence of a neutron skin.

References

[1] R.Kanungo et al., Phys. Rev. C **83**, (2011).

[2] A. Trzcinska et al., Phys. Rev. Lett. **87**, 082501 (2001)

[3] T. Kasznahorkay et al., Nucl. Phys. A **731**, (2004)

[4] A.Ozawa et al., Nucl. Phys. A **709**, (2002).

[5] A.Ozawa et al., Nucl. Phys. A **693**, (2001).

[6] T.Suzuki et al., Phys. Rev. Lett. **75**, 3241 (1995).

DOI:10.15120/GR-2017-1

DOI:10.15120/GR-2017-1

Offline analysis of Beam Spill structure measurement at GSI

S. Saha [*1,2], *M. Reese*[1], *H. Schaffner*[1], *J. Vesic*[1,3], *J. Gerl*[1], *and M. Górska*[1]

[1]GSI, Darmstadt, Germany; [2]Technical University Darmstadt, Darmstadt, Germany; [3]Jozef Stefan Institute, Ljubljana, Slovenia

Uniform spill structure of high energy ion beams is required for various spectroscopy experiments carried out in GSI fragment separator. We have carried out an offline analysis of the Beam spill structure from beam obtained at Cave C during an experiment in June 2016.

Resonance extraction of particles from SIS can have some fluctuations from various non-coherent as well as coherent sources [1]. These fluctuation leads to non uniformity of the beam current. The random fluctuations in the beam current can significantly lower the detection efficiency of events in slow response detectors like HPGe.

The incoming particles of a steady beam current can be considered as homogeneous Poisson events occurring at a uniform rate. The time of occurrence of each event is independent of the time of a previous event. The waiting time distribution of such events should fall exponentially with increasing time interval. The rate of beam current is given by the decay time of this distribution.

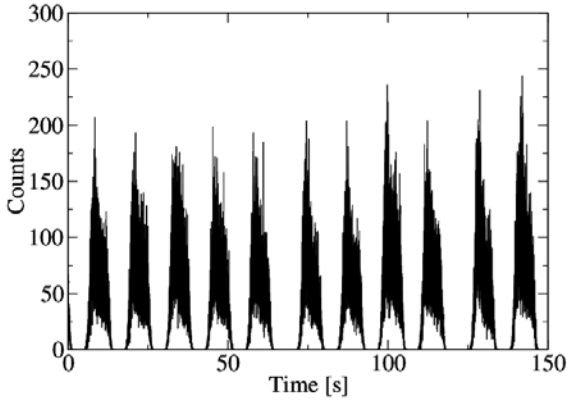

Figure 1: Beam Spill structure over a time period during experiment.

The data was taken during the GSI beam time in June 2016. The ^{124}Xe primary beam at 600 MeV/u energy was extracted from the SIS. The count rate at the detector was maintained at 10 kHz. The signal from the incident events were collected when the beam particles pass through a plastic scintillator detector placed across the beam direction. The event by event time information was collected using a discriminator and a VME time stamper module [2].

The events recorded in the experiment is first sorted with respect to an increasing time stamp. Then the average number of events recorded per 5 milliseconds is plotted against

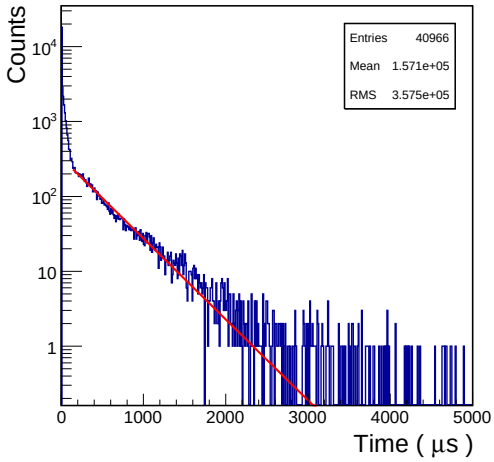

Figure 2: Waiting time statistics over a duration of beam time. The exponential fit to the distribution is shown in red.

time to obtain the spill structure as shown in Figure 1. The figure clearly shows the fluctuation in beam current over a given spill structure. The data was further analysed by extracting the waiting time distribution of all events with respect to the previous event over a given run time. In Figure 2 the statistics of the waiting time distribution for a typical run time is plotted. The data is fitted with an exponential function to obtain the avarage event rate. The Figure 2 clearly shows that the beam current cannot be regarded as uniform over time as the exponential distribution exhibits a steeper ascent within a time window of 100 μs. The rate of the wait time distribution is constant over time beyond 200 μs. More than two orders of magnitude higher statistics is observed within a wait time of 100 μs.

The experiment and subsequent analysis concludes the presence of random fluctuation in the beam current. The fluctuation can be more than two order of magnitude higher than the avarage current. As 100 μs is also the typical event processing time, an excessive number of events in this time domain reduces the trigger throughput.

References

[1] U. Blell, "A feedback system to improve the spill structure of a synchrotron." GSI, Darmstadt, Germany.

[2] VULOM (VME Universal Logic Module with 48 ECL I/Os), GSI.

* ssaha@gsi.de

DOI:10.15120/GR-2017-1

Neutron flux mapping in an ion-beam environment employing an improved neutron activation technique using thick foils

P. Koseoglou[1,2,*], M.L. Cortés[1,2], J. Gerl[2], T. Habermann[1,2], I. Kojouharov[2], C. Lizarazo[1,2], N. Pietralla[1], H. Schaffner[2], S. Stoulos[3], E. Vagena[3], J. Vesic[2]

[1] *Institut für Kernphysik, Technische Universität Darmstadt, 64289 Darmstadt, Germany*
[2] *GSI Helmholtzzentrum für Schwerionenforschung GmbH, 64291 Darmstadt, Germany*
[3] *Nuclear Physics Lab., School of Physics, Aristotle University of Thessaloniki, 54124 Thessaloniki, Greece*
(Dated: 13/02/2017)

* *Corresponding author. E-mail address: pkoseoglou@ikp.tu-darmstadt.de*

Purpose and method:

Measurements have been performed during summer 2016 at GSI in order to determine the neutron background in the ion beam environment. An advanced neutron activation method has been used to allow determination of low neutron fluxes [1][2]. Thick foils, instead of thin, have been used in the past for the determination of the neutron flux spectrum on the sub nuclear assembly-reactor of Aristotle University of Thessaloniki [1] and on a medical LINAC environment [2]. Due to the thickness of the samples low neutron fluxes can be "detected", at the same time, corrections for the self-shielding of the neutrons and the gammas by the materials have been applied [2]. In previous studies, the sensitivity of the technique has been proven to be lower than 3000 thermal neutrons/s/cm^2 [1]. The main purpose of the experiment performed was to test the applicability of the specific method in an ion-beam environment in order to investigate the neutron background of it.

Experiment:

The measurements have been performed using three different ion beams, uranium, xenon and carbon. The samples have been irradiated in several position near the ion beam and not in it. These positions were along FRS (S1, S2, S3 and S4, for S4 in both the exit of the last dipole and in the AGATA frame) and in Cave C (HTC and HTD) (see Figure 1). Limitations on the number of foils did not allow simultaneous irradiation in more than three to four areas. In Table 1 the activated samples are shown for each combination of beam and area tested, the combinations of beam and irradiation areas that were not tested are mark with a "-".

Being a parasitic measurement, the beam parameters changed according to the needs of other experiments. An estimation we can make at this point for the average energy of the beam (e.g. for uranium beam) during the activations is ~300MeV/u and for the average intensity ~10^8pps. The exact values of each beam during the irradiations will be considered on the analysis.

Early results:

Some "in-beam" observations are the following:

- Only (n,γ) reactions and no threshold reactions were detected.
- The activated samples were: Au, As, In, Ir, Mn, Sn and W (see Table 1). The expected reactions was occurred; the ones with the higher cross-section.
- The fluxes of the thermal neutrons were lower than 100 n/cm^{2}s, so a "weak" activation of the samples was achieved. This estimation was derived from the comparison of the count rates from these measurements with the ones obtained during the experiment in the sub-critical nuclear assembly [1].
- The technique can be used in an ion-beam environment.

Further analysis:

In the on-going analysis the activation of each reaction will be studied and the neutron flux spectrum will be calculated using the SAND-II unfolding code [3]. The conclusions will be connected to the different beams and beam intensities during the irradiations.

DOI:10.15120/GR-2017-1

Table 1. Samples activated per beam and irradiation area. The combinations of beams and irradiation areas that were not tested are mark with a "-".

Beam\Area	FRS				Cave-C	
	S1	S2	S3	S4	HTC	HTD
U	-	Au, In, Ir, Mn, W	-	In, Ir, Sn	-	-
Xe	-	In	-	W	Au, In, W	No activation
C	Au	Ir	Au, As, Ir	-	-	-

This work is supported by Helmholtz Graduate School for Heavy Ion Research for FAIR.

References

[1] Koseoglou, P.; Vagena, E.; Stoulos, S.; Manolopoulou M. Neutron spectrum determination in a sub-critical assembly using multi-disc neutron activation technique. Radiation Effects and Defects in Solid, **2016**, 171, 9-10, 766-774. (http://dx.doi.org/10.1080/10420150.2016.1262370)

[2] Vagena, E.; Stoulos, S.; Manolopoulou M. Analysis of improved neutron activation technique using thick foils for application on medical LINAC environment. Nuclear Instr. Methods A, **2016**, 806, 271-278. (http://www.sciencedirect.com/science/article/pii/S0168900215012346)

[3] SAND II, (https://rsicc.ornl.gov/codes/ccc/ccc1/ccc-112.html)

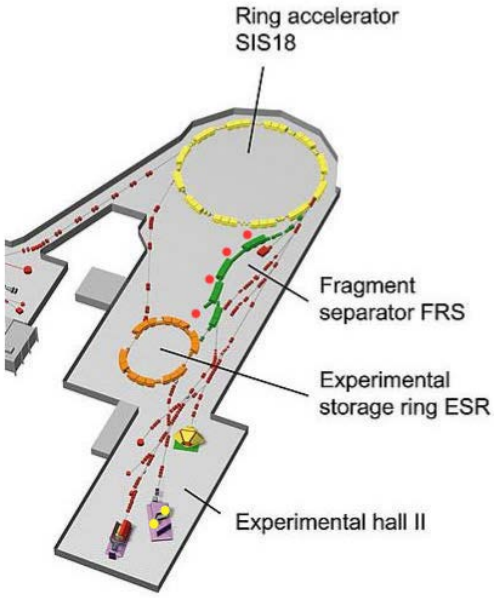

Figure 1. Areas of irradiation. The red bullets represents the areas along FRS where the samples were placed. And the yellow in Cave-C.

Tests of Sunpower CryoTel CT Stirling cooling engine for DEGAS*

W. Witt[1,2], *P. Koseoglou*[1,2], *I. Kojouharov*[2], *and J. Gerl*[2]
[1]IKP TU Darmstadt, Darmstadt, Germany; [2]GSI, Darmstadt, Germany

Introduction

As one of the four pillars of the FAIR project the NUSTAR collaboration aims at investigating exotic beams provided by the Super-FRS to study NUclear STructure, Astrophysics and Reactions. High-resolution DEcay SPECtroscopy of short-lived nuclei and isotopes is performed within the DESPEC experiment, which is located at the low-energy branch of the facility. γ-decays following the ion implantation in the active silicon detector (AIDA) are to be detected using the DEGAS germanium-array making DEGAS a key instrument of DESPEC. It is currently under development and planned to be used starting at the SIS/FRS beam-time 2019 as part of the NUSTAR phase-0 program.

Cooling of DEGAS Ge-crystals

Based on γ-ray interactions in semi-conducting matter, high-purity Germanium (HPGe) detectors such as DEGAS operate at temperatures around 90K, which makes cooling an essential aspect of the operation and for design considerations. Previous studies have shown a need for cooling power of $<$ 8W per DEGAS triple-Ge-cluster [1]. As opposed to the usual liquid nitrogen cooling, free-piston Stirling cooling (i.e. a heat engine operated within the Stirling circle to transfer heat) was chosen for DEGAS cooling. The main reason for that is the box geometry of the array adapted to the focal plane of the Super-FRS that would require a specifically tailored dewar too small for reliable operation and difficult to find. Next to smaller size and mass and lack of failures due to refilling (lifetimes of 10 years have been achieved), electrical coolers offer a cooling power of up to 10W at 77K, which satisfies the needs for DEGAS cooling. However, the piston's motion causes vibrations of the cooler, which affect the detector performance. The CryoTel CT cooler from Sunpower [2] is one of such electric coolers and was taken into operation at GSI for the planned investigation of the vibration effects and for testing counter-measures.

Ongoing tests of CryoTel CT cooling engine

The cooling engine was delivered by Sunpower around mid of 2016 including an active vibration cancellation system (AVC by Ametek) to reduce the vibrations typical for such coolers. A holding structure as well as a flange adapter for connection with a DEGAS cluster-cryostat were designed and constructed. The cooling engine, the AVC, the thermal Pt-100 sensors, the power supply and the corresponding controller were connected and the system was taken into operation by the end of 2016 (see fig. 1). Cooler vibrations too strong for reliable operation of the Ge detector excluded further tests and the system was moved to Helmholtz-Institute Mainz early 2017, where it is currently being set up.

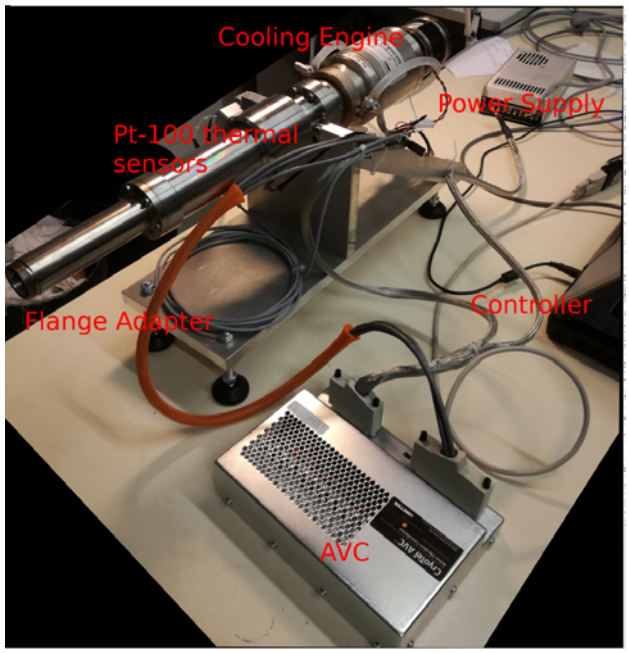

Figure 1: Cooler system setup at GSI end of 2016 including AVC, controller and temperature sensors and power supply

Perspective

The cooler will be taken into operation at the Mainz lab in the near future to verify and quantify the observed vibrations. If a defect or wrong setting of the AVC can be excluded it is foreseen to study the vibrations employing acceleration sensors at different positions of the cooling system. For the readout a BeagleBone plug-in board will be used.
After quantification of the oscillations a reduction of them is a considered option.
Operation of such coolers for astronomical detectors [3] encountered vibration problems as well and solved this issue by mechanically decoupling (see fig. 2) the cooler from

* Work supported by Helmholtz Graduate School for Hadron and Ion Research at FAIR.

DOI:10.15120/GR-2017-1

the rest of the system (i.e. here the holding structure and the cryostat connection). Using leaf-springs and vacuum bellows a mechanical low-pass filter can be created to reduce oscillations for certain frequencies. In the mentioned case a reduction of the oscillations caused by the piston's movement by a factor of 500 was achieved.

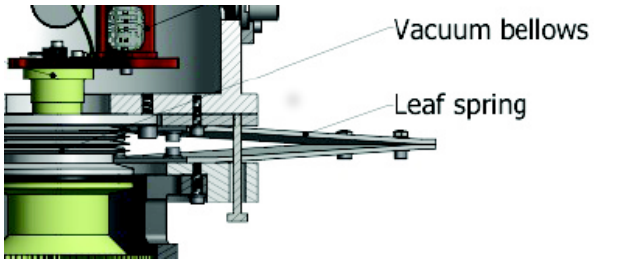

Figure 2: Mechanical decoupling of cooler vibrations from holding structure via vacuum bellows and leaf springs as done in ref. [3]. Shown in green is the cooling engine.

Conclusion

As it currently stands the Sunpower CryoTel CT cooling engine is unfit to be used as planned for DEGAS due to too strong vibrations. In case of a previous AVC malfunction, minor (e.g. frequency) setting changes could solve this problem.
However, should the oscillation reduction of the AVC remain insufficient, oscillation measurements and simulations followed by design and construction of changes to the mechanical structure would be necessary.
The consideration of another electrical cooling engine could be a valid option.

References

[1] Technical Design Report for DEGAS (2014)

[2] Sun Power CryoTel User Manual V.7, http://sunpowerinc.com/cryocoolers/ cryotel-family/ct/ (2012)

[3] G. Raskin et al., Compact Stirling cooling of astronomical detectors, https://arxiv.org/pdf/1311.0685.pdf (2013)

Bayes-Tracking – A novel approach to γ-ray tracking

P. Napiralla[1,2], H. Egger[3], P. R. John[2], N. Pietralla[2], M. Reese[1], and C. Stahl[2]

[1]Institut für Kernphysik, TU Darmstadt, Darmstadt, Germany; [2]GSI, Darmstadt, Germany; [3]AG Numerik und wissenschaftliches Rechnen, TU Darmstadt, Darmstadt, Germany

The Advanced GAmma Tracking Array AGATA [1] will be the key instrument for nuclear structure investigations in the upcoming HISPEC and DESPEC experimental campaigns at the Facility for Antiproton and Ion Research FAIR.
In the photon energy range of $0.2 - 8$ MeV, the Compton-scattering is the dominating interaction process in HPGe detectors. This leads to numerous Compton-escaped photons, which are typically suppressed or appear as background in the γ-ray spectra. Although it is possible to reconstruct photon paths between different HPGe detectors of AGATA using *Pulse Shape Analysis* [5] and γ-ray tracking algorithms [3], photons that have Compton-scattered and subsequently left the array still only contribute to the background of the γ-ray spectra. Using Bayesian inference, some of these events can be reconstructed via a new type of γ-ray tracking algorithm, called *Bayes-Tracking*, when it is most likely that they originate from Compton-escape.

In contrast to existing γ-ray tracking algorithms based on the Forward/Back-Tracking method [3], the *Bayes-Tracking* algorithm quantifies the probability of an initially incident photon, given the measured hit pattern in the detector. It is based on Bayes' Theorem [2, 4]

$$P(B|A) = \frac{P(A|B) \cdot P(B)}{P(A)} . \tag{1}$$

The conditional probability for two arbitrary events A and B is defined as

$$P(A|B) := \frac{P(A \cap B)}{P(B)} . \tag{2}$$

The incident photon energy E_γ can be identified in the case of full energy absorption (photoelectric effect at last interaction point) **and** in the case of a Compton-escaped photon. In contrast to existing tracking algorithms, the latter events can be partially recovered.

Using Bayes' theorem and the measured deposited energies $\{E_{\text{dep}_1}, \ldots, E_{\text{dep}_N}\}$ at the corresponding interaction points $\{\vec{x}_1, \ldots, \vec{x}_N\}$ identified via *Pulse Shape Analysis* [5], a conditional probability distribution P for hypothetical incident photon energies e_0 can be derived

$$\begin{aligned} &P\left(e_0 | \left\{\{\vec{x}_1, E_{\text{dep}_1}\}, \ldots, \{\vec{x}_N, E_{\text{dep}_N}\}\right\}\right) \\ &\propto \sum_\pi \mathcal{L}\left(\pi\left(\{\vec{x}_1, E_{\text{dep}_1}\}, \ldots, \{\vec{x}_N, E_{\text{dep}_N}\}\right) | e_0\right) . \end{aligned} \tag{3}$$

π denotes the permutation function over all possible permutations of the measured energies E_{dep_i} (at interaction points $\vec{x}_i$) and $\mathcal{L}$ the corresponding *likelihood function* (corresponds to $P(A|B)$ in Equation (1)). By using the principle of so-called *marginalization* [4], a calculable form of the likelihood function can be derived.

A *Geant4* simulation of a simplified cubic Germanium detector (edge length 8 cm) with incident photon energy $E_\gamma = 1.5$ MeV has been used to firstly realize Bayes-Tracking and test its performance. The amount of interactions inside the detector has been limited to $N = 3$. Altogether, 5055 photons (4000 Compton-escaped, 1055 photo-absorbed) have been used. The Bayes-tracked photon spectrum compared to the Add-Back energy spectrum (traditional detector response) is shown in Figure 1.

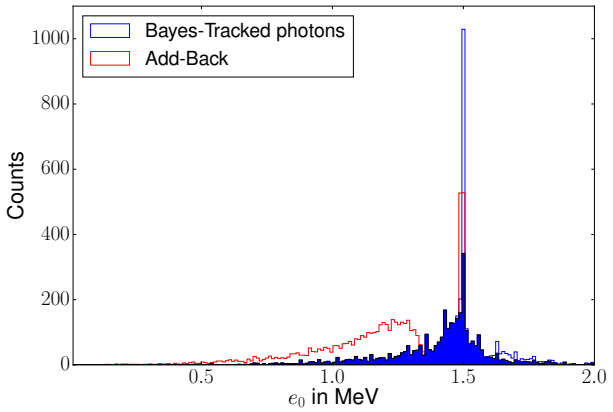

Figure 1: Comparison of Add-Back energy spectrum (red) to Bayes-tracked photon energy spectrum (blue). The tracked photon energies of the Compton-escaped photons are shown in solid blue.

The Peak-to-Total ratios in this simulated detector are:

- Add-Back: 20.77 %
- Bayes-tracked: 24.35 %

Hence, a gain in the Peak-to-Total ratio by around 3.6 percentage points absolute has been achieved by simply using the Bayes-Tracking on this dataset.

Future work on the Bayes-Tracking algorithm will include testing on real data sets taken with AGATA detectors, the incorporation of pair-production and embedding

DOI:10.15120/GR-2017-1

the algorithm into the AGATA framework *Femul* to enable the usage of the Bayes-Tracking on upcoming AGATA experiments.

Especially for radioactive ion beam experiments with limited intensities, this algorithm can be applied with the aim to increase the statistics in the γ-ray peaks. It will potentially decrease the statistical uncertainties of future HISPEC experiments with very exotic relativistic radioactive ion beams using AGATA at FAIR.

References

[1] A. Akkoyun et al., AGATA – Advanced GAmma Tracking Array, *Nuclear Instruments and Methods in Physics Research A*, 668:26–58, March 2012.

[2] H.-O. Georgii. *Stochastik – Einführung in die Wahrscheinlichkeitstheorie und Statistik*, volume 4. Walter de Gruyter, Berlin, 2009.

[3] A. Lopez-Martens et al. γ-ray tracking algorithms: a comparison. *Nuclear Instruments and Methods in Physics Research A*, 533:454–466, 2004.

[4] D. Sivia and J. Skilling. *Data Analysis – A Bayesian Tutorial*, volume 2. Oxford University Press, Oxford, 2006.

[5] R. Venturelli and D. Bazzacco. Adaptive Grid Search as Pulse Shape Analysis Algorithm for γ-Tracking and Results. *LNL Annual Report*, 2004.

DOI:10.15120/GR-2017-1

Upgrade and commissioning of the Lund-York-Cologne CAlorimeter*

B. Fu[1], *K. Wolf*[1], *P. Reiter*[1], *M. A. Bentley*[2], *P. Coleman-Smith*[4], *S. Fox*[2], *C. Goergen*[1], *P. Golubev*[3], *I. Lazarus*[4], *C. Lorenz*[3], *D. Rudolph*[3], *L. Scruton*[2], *and S. Thiel*[1]

[1]IKP, Universität zu Köln, Germany; [2]University of York, UK; [3]Lund University, Sweden; [4]STFC Daresbury Laboratory, UK

Introduction

The Lund-York-Cologne CAlorimeter (LYCCA) is a charged-particle detector for the FAIR/NUSTAR collaboration, to discriminate heavy ions produced in nuclear reactions of relativistic radioactive-ion beams (RIB). The charge number Z and mass number A of the reaction products can be determined measuring their Time-of-Flight (ToF), energy loss and total energy. Employing the position sensitivity of LYCCA the flight paths of the reaction products can be tracked event-by-event, enabling the HIgh-resolution in-beam γ-ray SPECtropscopy (HISPEC) far from the line of stability (concept and design of LYCCA see Ref. [1]).

Upgrade of Electronics

The precursor LYCCA-0 using 12 ΔE-E telescopes and analog electronics was employed in the PreSPEC campaign from 2009 to 2014. A high resolution of Z and A was proven for proton number around 33 and mass region around 100 [2,3,4]. Afterwords the major upgrade from analog to digital electronics for LYCCA was carried out by the STFC Daresbury Laboratory. Using high-integrated Front-End Electronics (FEE) with Application-specific Integrated Circuits (ASICs), the electronic arrangement and data-acquisition process were significantly simplified. As

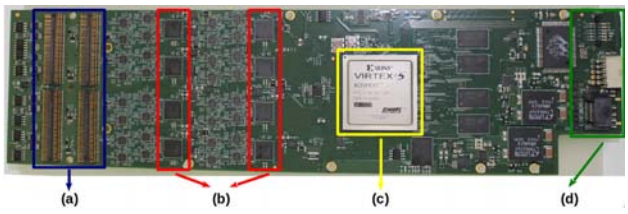

Figure 1: The view of a FEE-card. (a) four 16-channel ASICs; (b) eight 14-bit ADCs; (c) Virtex-5 PowerPC; (d) Connections: HDMI (Clock), Power and Gbit-Ethernet.

shown in Fig. 1, each FEE card contains four 16-channel ASICs, which amplify the signals from all 64 channels of one Double-Sided Silicon Strip Detector (DSSSD). The ASIC is optimized for high dynamic range with excellent linearity and noise performance. Each ASIC covers three energy ranges: (i) high gain up to 20 MeV, (ii) medium gain up to 1 GeV, and (iii) low gain up to 20 GeV. The pre-amplified signals are digitalised in ADCs, processed in the Virtex-5 PowerPC and then stored in a LYCCA-Server. A master-slave control delivers a synchronous time stamp via HDMI-cables on all FEE cards in use. The Multi-Instance Data-Acquisition System (MIDAS) ensures the hardware configuration, experiment control, data merging and data storage.

Commissioning at IKP Cologne

Since 2016 the LYCCA setup is located at the Cologne tandem accelerator. A new three-stage beam tube was built for LYCCA, which allows for three different distances between target position and the DSSSD-wall (cf. Fig. 2). Thus, the corresponding opening-angles range from 1.5 to 16 degree. Currently 25 FEE modules and 14 ΔE-E telescopes are installed on LYCCA. In order to check the specifications and energy resolutions of the DSSSDs with the new digital FEE modules, measurements were performed with a triple-alpha source. Employing the Multi-Instance-Data-Acquisition System (MIDAS) experiment data were stored, sorted event by event and analyzed using the data-analysis framework ROOT. The results show that more than 99% DSSSD-channels were working successfully. A consistent energy resolution of around 1.1% at 5.8 MeV was obtained for all 14 DSSSDs in use. At the IKP several in-beam experiments were also curried out to test the performance of the LYCCA system. In collaboration with the University of York, a 2 mm thick plastic scintillator for later ToF-measurement was tested on the LYCCA setup in March 2016. A ^{12}C beam with an en-

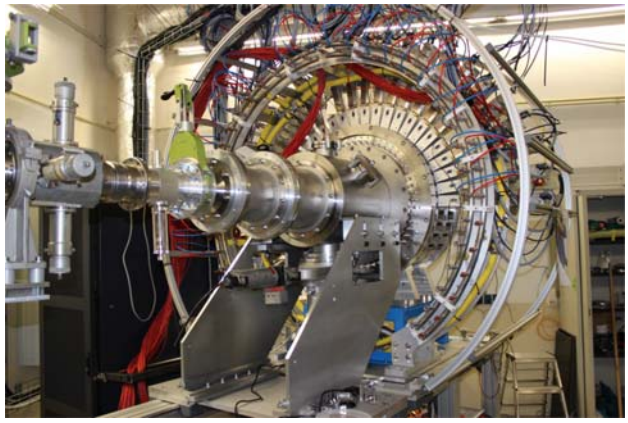

Figure 2: The current LYCCA-construction in the IKP Cologne. With the 25 installed FEE-modules all DSSSDs can be operated.

* This work supported by the German BMBF (05P12PKFNE TP5) and GSI F&E KREITE 1416.

DOI:10.15120/GR-2017-1

ergy of 60 MeV was scattered on the ^{197}Au target with a thickness of 0.2 mg/cm^2, and stopped in the ToF-detector. The generated light signals were detected with 32 photomultipliers (PMTs) mounted around the plastic scintillator. Together with the Lund University in May 2016, another beam time was scheduled to test the performance of the ΔE-E telescopes. A proton beam with an energy of 18 MeV was scattered on a thin gold foil and then detected in the DSSSDs and CsI-detectors. In November 2016 a further in-beam experiment of elastic scattering of heavy ions was conducted. In this measurement the medium-gain range (up to 1 GeV) of the FEE modules was tested successfully for the first time. A ^{12}C beam with a kinetic energy of 60 MeV was scattered on the ^{197}Au target with a thickness of 0.17 mg/cm^2. At a distance of 120 cm between the target and the DSSSDs, a continuous scattering-angle coverage of 1.5 to 9.5 degrees was obtained. The measured Full Width at Half Maximum (FWHM) of the DSSSDs are 350 keV to 400 keV at approximately 60 MeV. In order

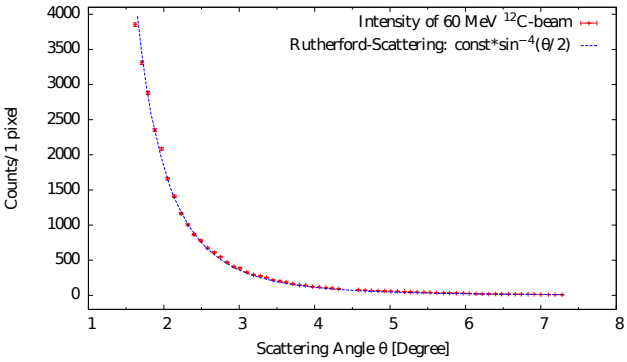

Figure 3: The measured intensity distribution of the elastically scattered ^{12}C-nuclei on ^{197}Au-target follows the expected distribution of the Rutherford scattering.

to investigate the exact angular distribution of the beam intensity after the elastic scattering, the measured data of the p- and n-side were correlated and, thus, the events in the DSSSDs were analyzed pixel by pixel. Figure 3 shows the intensity distribution of 64 contiguous pixels from two DSSSDs located vertically below the beam axis. The measured values, covering a range of 1.5 to 7.2 degree, reproduced the theoretically expected scattering-angle dependence of $\sin^{-4}(\theta/2)$ nicely.

Outlook

For further in-beam experiments at the Cologne tandem accelerator, a modified mechanical construction of the LYCCA chamber was realized by IKP's mechanical workshop. The new design consists of two octagon brackets and a back wall, which support up to 24 ΔE-E telescopes in operation (see Figure 4). The target ladder is located between the octagon brackets. This new construction increases the scattering-angle coverage from a maximum of 16 to a maximum of 120 degree, as well as the solid-angle coverage up to 60% of 4π significantly, which means that LYCCA can be used to further examine elastic and inelastic particle scattering. This configuration will be shortly installed and tested for the first time.

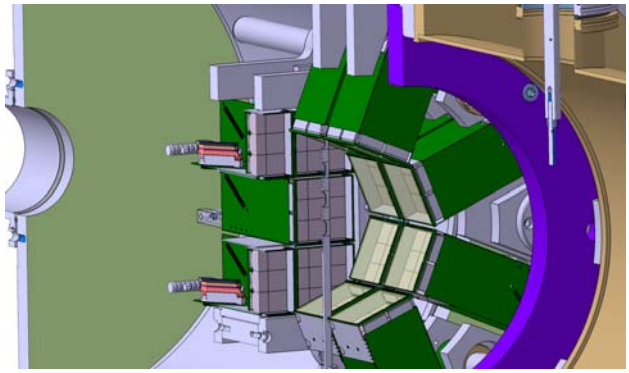

Figure 4: The new mechanical design of the LYCCA chamber. Each octagon bracket and the back wall support 8 ΔE-E telescopes.

References

[1] P. Golubev *et al.*, Nucl. Instr. & Meth. A 723 (2013).

[2] G. Guastalla *et al.*, Phys. Rev. Lett. 110, 172501 (2013).

[3] A. Wendt *et al.*, Phys. Rev. C 90, 054301 (2014).

[4] K. Moschner *et al.*, Phys. Rev. C 94, 054323 (2016).

DOI:10.15120/GR-2017-1

Collective behaviour of p-rich nuclei around A = 70

T. Arici [*1,2], *J. Gerl*[1], *and W.Korten*[3]

[1]GSI, Darmstadt, Germany; [2]Justus-Liebig University, Giessen, Germany; [3]CEA-Saclay, DAPNIA/SPhN, France

In N = Z nuclei, neutrons and protons occupy the same orbitals. This creates an opportunity to study the effect of the nucleon sequence on deformation changing effects caused by proton-neutron correlations. Moreover, in this region towards the proton drip line, nuclei experience a low binding energy which results in a shape change and in the vicinity of N = Z and around A = 70 this becomes even more rapidly due to the large shell gaps in the Nilsson diagram for nucleon numbers 34, 36 and 38. The ^{70}Kr, ^{72}Kr, ^{70}Br and ^{68}Se isotopes of this region were studied, where the valence protons and neutrons occupy these shells and let us to answer the fundamental questions of nuclear physics, such as the charge symmetry, independence of nuclear force and the collectivity.

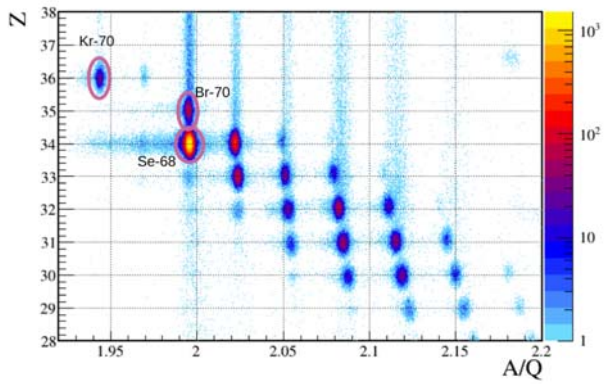

Figure 1: BigRIPS particle identification plot for ^{70}Kr setting. The circles show the particle gates used for each isotope of interest.

Exotic beams with intermediate energy have been used as a spectroscopic tool through inelastic scatterings. The inelastic scattering of ^{72}Kr, ^{70}Kr, ^{70}Br and ^{68}Se isotopes on ^{9}Be and ^{197}Au targets has been studied. Production of these very exotic nuclei, through the proton drip-line, was achieved at the Radioactive Isotope Beam Factory (RIBF) [1]. A ^{78}Kr primary beam with an energy of 345 MeV/u was impinged on a ^{9}Be target to produce the ions of interest as a secondary beam. The BigRIPS fragment separator was used in order to deliver the secondary beam isotopes, ^{72}Kr, ^{70}Br, ^{68}Se and ^{70}Kr at around 175 MeV/u to the secondary target for the measurements. Particle identification plot for selected isotopes is given in Figure 1 for ^{70}Br, ^{68}Se and ^{70}Kr. The reaction products were identified in the ZeroDegree Spectrometer (ZDS) employing the Bρ-ΔE-TOF method and γ-rays emitted due to the excitation were measured by an array of γ-ray detectors, DALI2, that was placed around the secondary target. Firstly, the exotic beam was scattered through the electromagnetic field of a heavy target gold. In this process, Coulomb excitation and nuclear interaction interfere. The fraction of these two kinds of excitation was identified. In order to separate these two interactions, the same setting was repeated to scatter the beam off a Beryllium target to increase the relative strength of nuclear scattering. For each isotope, the experimental conditions were simulated to obtain the response functions of the transitions. Experimental results were then fitted to these response functions from the simulations in order to determine the number of emitted γ-rays. The excitation cross-sections were deduced for both cases and used in order to determine the deformation lengths δ_n and δ_c, for nuclear and Coulomb excitation, respectively. These deformation lengths were obtained using ECIS-97 code [2]. In the even-even nuclei, degree of the deformation in the nucleus is related to reduced transition probability, B(E2) values with the following equation:

$$\beta = \frac{4\pi}{3ZR_0^2}\sqrt{B(E2\uparrow)/e^2} \qquad (1)$$

where A and Z mass and charge numbers, respectively, β is the deformation parameter and R_0 is the nuclear radius.

The chain for the experimental knowledge on Kr isotopes was extended with this study. Results also allow to make a direct comparison with ^{70}Se which gives important new information about the shape coexistence phenomenon (the existence of two stable shapes at the same excitation energies) across the N = Z line. We deduced the B(E2) value for the $2_1^+ \rightarrow 0_1^+$ transition of ^{70}Kr, T_z = - 1 for the first time. This quantity for the other measurements was determined before within different experiments and shows and aggrement with our results. The B(E2;$2_1^+ \rightarrow 0_1^+$) value for ^{70}Kr showed a rapid increase among these values. It was even approximately twice higher compared to its isobaric triplet members. This variation indicates an increase in the deformation in this isotope.

References

[1] T. KUBO, D. KAMEDA, H. SUZUKI, ET AL. BigRIPS separator and ZeroDegree spectrometer at RIKEN RI Beam Factory. Progress of Theoretical and Experimental Physics, 2012(1), 2012

[2] J. RAYNAL. Coupled channel code ECIS97. Unpublished.

* t.tarici@gsi.de

DOI:10.15120/GR-2017-1

Geant4 Simulations of the novel γ-ray detector array DEGAS *

C. Lizarazo[1,2], G. Li[2,3], N. Pietralla[1], J. Gerl[†2], and the PreSPEC Collaboration [1]

[1]Institut für Kernphysik, Technische Universität Darmstadt, Germany; [2]GSI, Darmstadt, Germany; [3]Institute of Modern Physics, CAS, Lanzhou, China

The performance of the novel HP-Ge detector array DEGAS that will be used at FAIR has been studied through GEANT4 simulations using real geometries of most of the detector components. Different possibilities of ancillary background shields were simulated and compared, showing that a system of active BGO Compton-suppressor back-catchers combined with additional side shields, provide a clear improvement of the photo-peak efficiency and the Peak-to-Total ratio in comparison to previous decay-spectroscopy arrays. Large differences in the performance of different clusters in DEGAS reveals that, due to geometrical effects, some particular positions in the array contribute stronger than others to achieve a superior performance.

Introduction. In the future FAIR facility, very exotic nuclei not yet accessible will be produced to perform RI-beams experiments that will allow to understand their nuclear structure and address open questions in astrophysical phenomena of high relevance such as the r-process. The DEcay SPECtroscopy experiments (DESPEC) are intended to measure and understand the decay processes of the exotic nuclei that will be studied at FAIR [1]. For this purpose, the beams will be slowed down and stopped into the implantation detector AIDA [2], a stack of 24×8 cm^2 Si-based 2-mm thick layers where the stopped nuclei eventually decay. The novel HP-Ge detector array DEGAS [3] is a key device for DESPEC, since it will be used as the high energy resolution γ-ray spectrometer device to detect the delayed γ-rays emitted by the stopped nuclei after isomer or beta decay. DEGAS must have a sensitivity good enough in order to detect with high efficiency the γ-rays emitted by the implanted nuclei and discriminate the intense background expected from the secondary radiation produced at RI-beams environments.

Simulations of complex detector systems are a powerful tool to get insights on their performance otherwise not possible to obtain, so they can help to improve the detector design beforehand its actual construction. In this report, we summarize the simulation studies of the DEGAS array using the Geant4 toolkit [4].

Simulation Description. The simulated experiment consists of an AIDA-shape γ-ray source surrounded by 72 HP-Ge crystals arranged in 26 triple-clusters (DEGAS configuration Phase-0), for extra details see Ref [5]. Besides the active Ge detector volume, additional elements of each crystal capsule such as the aluminum housing, mechanical components and the cooling rod were included. Realistic dimensions for these elements were achieved by using GDML geometry files based on the original CAD design of the detector. The translation from CAD to GDML format was done using the software FASTRAD [6] . For all the simulations performed, add-back energy reconstruction between crystals of the same cluster was conducted (e.g. *intra-cluster* add-back).

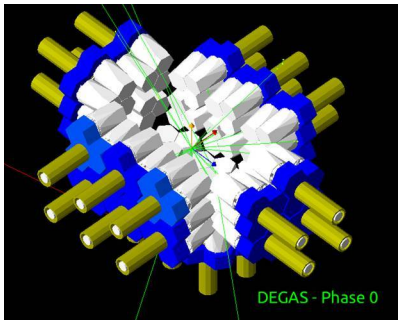

Figure 1: Snapshot of a simulated experiment. The 26 DEGAS triple-clusters in a squared-box geometry (grey) surround the source, the BGO back-catchers (blue), and additional elements (gold/grey). The AIDA-source lies in the x-z plane (red-blue axis). The trajectory of few γ-rays (green) emitted from the origin are shown.

The photo-peak efficiency (ϵ_{ph}) of the full DEGAS array and of each triple-cluster were obtained in the range of 25 keV to 3 MeV, see Figs. 2 and 3. For each energy value of the source, 2×10^6 γ-rays were simulated, isotropically emitted from a random point inside the volume of an AIDA layer centered at the origin.

In order to study the influence of an external γ-ray background, a second set of simulations was performed. Background γ-rays were emitted randomly from a spherical surface containing the experimental setup. A cosine-law angular emission distribution was used in order to have isotropic fluence inside the sphere volume [7]. A double decreasing exponential function was used as energy distribution in the range [25 keV, 3 MeV], using parameters to mimic a background distribution previously measured in decay spectroscopy experiments with the EURICA array. The ratio between background and γ-rays emited from the AIDA-source was chosen to be 1000:1. The DEGAS Peak-to-Total ratio in the range of 25 keV to 3 MeV was measured for each one of the following ancillary shield systems added to the setup:

* Work supported by T. U. Darmstadt in cooperation with GSI.

† j.gerl@gsi.de

- Compton-suppressor BGO back-catchers.
- BGO back-catchers and lead side-shields placed at the edges of the "Ge-faces" defined in the DEGAS-0 Configuration.
- Passive lead back-catchers and lead Side shields.

For a more detailed description of each one of these configurations, see Ref. [5].

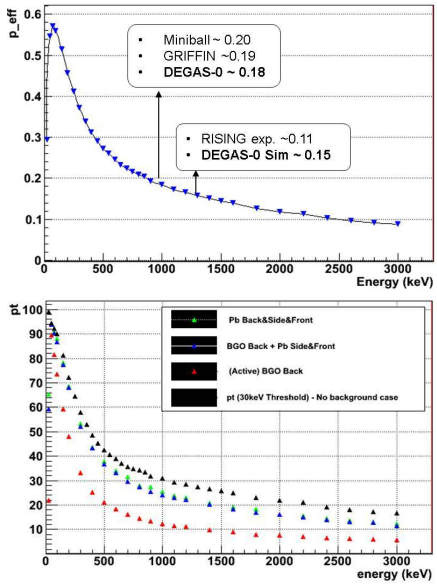

Figure 2: DEGAS ϵ_{ph} (top) and P/T ratio (bottom) in the range [25 keV, 3 MeV]. The P/T ratio is compared not only between different shields, but also to the background-free case, as it is the scenario with the best possible P/T value.

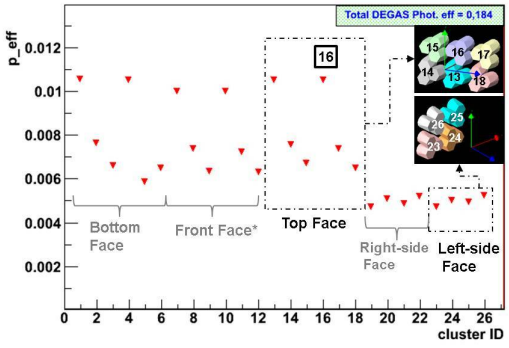

Figure 3: ϵ_{ph} of individual triple-clusters. Due to the geometry of the AIDA+DEGAS setup, cluster positions such as 13 or 16, double the performance of others like 19-26.

Results. The ϵ_{ph} obtained with inter-cluster addback, shown in Fig. 2, The obtained values are comparable to current state-of-the-art decay-spectroscopy arrays such as GRIFFIN (TRIUMF, Canada). As shown in Fig. 2 the DEGAS ϵ_{ph} at 1.3 MeV was found to be 0.15, in comparison to the measured value of 0.11 of EUROBALL during the RISING experiments, leading to an improvement of almost 40%. This is a direct consequence of the squared-box design of DEGAS since it is more suited than a spherical one (such as EUROBALL) for an implantation detector with the AIDA geometry. It is worth to mention that add-back reconstruction between neighbouring crystals regardless their cluster number (*inter-cluster* addback) can potentially double the impact of the add-back analysis on the efficiency, as it is not limited to only to the two adjacent crystals that belong to the same cluster.

In Fig. 3 it can be observed how the ϵ_{ph} changes drastically with the cluster position. Particular positions such as 16 and 13 double the ϵ_{ph} of clusters 19-26, and are even almost 40% bigger than the ϵ_{ph} for neighbouring positions 14,15,17,18. The reason for this phenomenon lies in the larger solid angle covered by clusters in central positions with respect to the AIDA-source, revealing them as determinant for the superior performance of DEGAS. This represents a challenge since all the beam-induced background particles emitted in the forward beam direction have larger probabilities to impact these central positions during the ion implantation process, worsening their performance. To overcome this limitation, it is expected to use AGATA type detectors at these forward positions in DEGAS Phase-2.

The P/T ratio has been used to evaluate the effectiveness of a shield system to allow DEGAS to identify a "good" γ-ray emitted from the AIDA-source against an intense external background. The results in Fig. 2 reveal that as soon as the external background is plugged into the simulation, the P/T ratio is strongly affected, decreasing from the black curve (no background case) to the red one (DEGAS+BGO). When Additional Pb Side shields are added, the P/T ratio improves considerably (blue curve), being almost similar to the case where only Pb is used as a shield (green curve). However, Compton-suppression allows in addition to discriminate events where a γ-ray escapes from the Ge detector and hits the Shield and viceversa. A further simulation with a new configuration of the clusters is currently under development, showing already an improvement in the total efficiency. Background components such as the known prompt-flash emitted during the stopping of the ions or, as well as beam-induced background particles such as high energetic protons or neutrons, can be studied in further simulations.

References

[1] http://www.fair-center.eu/for-users/experiments/nustar/experiments/hispecdespec.html

[2] http://www2.ph.ed.ac.uk/ td/AIDA/

[3] J. Gerl et. al. "Technical report for the design, construction and commissioning of the DESPEC Germanium Array DEGAS", v12.3, August 2014,

[4] http://geant4.cern.ch/

[5] G. Li, C.Lizarazo, et. al. "Simulation on the performance of the DEGAS gamma detector array", GSI Scientific Report 2015, DOI:10.15120/GR-2016-1

DOI:10.15120/GR-2017-1

[6] http://www.fastrad.net/

[7] G. Santin, ESA / ESTEC and RheaTech Ltd - Seminar at "Ecole Geant4", Annecy, 18-21 and 25-28 Nov 2008.

DOI:10.15120/GR-2017-1

DOI:10.15120/GR-2017-1

Superheavy element research – Status report 2016

M. Block[1,2,3], P. Chhetri [2,4], H. David[2], A. Di Nitto[1,2], C. Droese[6], Ch.E. Düllmann[1,2,3], F. Giacoppo[2,3], M. Götz[1,2,3], S. Götz [1,2,3], F.P. Heßberger[2,3], E. Jäger[2], O. Kaleja[1,5], J. Khuyagbaatar[2,3], J. Krier[2], M. Laatiaoui[2,3], L. Lens[1,2], A. Mistry[2,3], V. Pershina[2], S. Raeder[2,3], J. Runke[1,2], P. Scharrer[1,2,3], B. Schausten[2], A. Yakushev[2,3]for the SHE Physics and SHE Chemistry Departments

[1]Johannes-Gutenberg University Mainz, Germany; [2]GSI, Darmstadt, Germany; [3]Helmholtz-Institute Mainz, Germany; [4]TU Darmstadt, Germany; [5]Max-Planck Institute Heidelberg, Germany; [6]University Greifswald, Germany

The main activity at GSI was the ^{48}Ca UNILAC beamtime, where the experiments were devoted to the continuation of the laser spectroscopy study in No [1] and to the chemical investigation of element 113, which was recently named nihonium (Nh).

In 2015, for the first time optical spectroscopy of nobelium atoms was performed at SHIP, making nobelium the heaviest elements for which such studies were feasible. A strong atomic ground state-transition and several Rydberg states in the nobelium atom were identified by resonance ionization laser spectroscopy [1]. The data showed good agreement with theoretical predictions using relativistic coupled cluster and multi configuration Dirac-Fock approaches. Among the atomic and nuclear properties, a limit for the first ionization potential (IP) of nobelium was obtained. However, a more accurate determination of the IP from the convergence of a Rydberg series was hampered by quenching collisions with buffer gas atoms populating also lower-lying metastable states. In 2016, the laser spectroscopy in nobelium thus focused on the identification of different Rydberg series. To this end, measurements in which the second laser pulse (exciting to a Rydberg state) was delayed compared to the laser for the first excitation step were performed for different pressures in the optical cell. The decay of the RIS signal is indicative of the lifetime of the populated state and allowed us to identify different Rydberg series originating from either the $^1P_1$ state or the metastable $^3D_1$ state. From the convergence of the Rydberg series now the IP of nobelium can be determined with high precision. The data analysis is close to completion and the results will be subject of a forthcoming publication. A rate equation model describing the quenching process was developed and showed good agreement with the data. In addition, the location of the $^3D_1$ state that cannot be excited directly from the ground state was determined indirectly [2]. In the second part of the beamtime, first steps towards laser spectroscopy in the next heavier element, lawrencium, were performed. The stopping and neutralization followed by the evaporation from different filaments was investigated to optimized the conditions for the level search in Lr. In addition, the feasibility of producing ^{255}No by EC decay of ^{255}Lr for laser spectroscopy was demonstrated. This will allow us to extend the measurements of nuclear properties in the nobelium isotope chain.

Besides the laser spectroscopy experiment, the SHE physics department was engaged in several technical developments and upgrades of the setup. The relocation of the

SHIPTRAP setup was completed to fully integrate the new cryogenic stopping cell. The new gas cell operated at 40 K will boost the overall efficiency of SHIPTRAP by up to an order of magnitude and extend the reach for Penning trap mass measurements to heavier elements available with lower yield. In 2016, extensive commissioning experiments with radioactive source (offline) and in parasitic beamtime with ^{254}No were performed. In addition, the recently developed novel phase imaging method (PI-PICR) was further improved by installing new extraction optics. First online mass measurements with upgraded SHIPTRAP system are foreseen for 2018.

The new focal plane detector system for decay spectroscopy at SHIP was characterized in parasitic beamtime by measuring α- and α-γ – decay of ^{253,254}No produced in irradiations of ^{207,208}Pb with ^{48}Ca. The measurements were followed by studies of neutron-deficiency Np isotopes, produced in irradiations of ^{181}Ta with ^{48}Ca where specific emphasis was devoted to the isotopes ^{225,226}Np. The investigation of nuclides in this region near the N=126 shell at the proton drip line can be extended with the new detector system. This system features practically dead time free digital electronics and thus gives access to short-lived nuclides. The data analysis is ongoing. The further analysis of the decay studies of ^{257}Rf and ^{258}Db performed in 2014 resulted in confirmation of two low-lying isomeric states in ^{258}Db, the identification of two short-lived isomeric states in ^{258}Rf, populated by EC decay of ^{258}Db [3], and a low-lying isomer in ^{257}Lr, populated by EC decay of ^{257}Rf [4].

At TASCA, a first attempt on the chemical study of Nh (nihonium, element 113) was performed in 2016. The nuclear fusion reaction ^{48}Ca + ^{243}Am, recently investigated at TASCA in the Mc (moscovium, element 115) decay spectroscopy experiment [5], was selected for the production. The ^{288}Mc recoils were guided through TASCA to an exit window, and were thermalized in a gas flow inside a recoil transfer chamber. The short-lived ^{288}Mc ($T_{1/2}$ = 0.17 s) isotope decayed via alpha-particle emission to ^{284}Nh ($T_{1/2}$ = 0.97 s), the lifetime of which is long enough for the transport to the detection setup. A similar detection setup as in the recent experiments on Fl chemistry was used [6].

DOI:10.15120/GR-2017-1

However, to account for the expected higher reactivity of Nh compared to Fl, the first half of the first COMPACT detector array was covered with a SiO_2 surface, while the second half as well as the full second COMPACT array with gold. The latter was cooled to low temperature with a liquid nitrogen cryostat. Fl chemistry experiments at TASCA have demonstrated that one Fl decay chain per week can be observed. Similar cross sections for the production of Fl [7] and Mc [5], as well as comparable beam intensities and target thicknesses led us to expect the observation of about two to three decay chains originating from ^{288}Nh, if the volatility and reactivity of Nh is similar to that of Fl. However, no Nh atoms were detected. The final data analysis is ongoing.

A second chemical system, where studies continued in 2016, is that of carbonyl compounds of transition metal complexes, with $Sg(CO)_6$ having been first synthesized in 2013 [8]. Current techniques include the Sg synthesis, its isolation in a recoil separation, followed by chemical synthesis of the compound behind the separator [8]. A next step included an experiment designed to measure the thermal stability of the compounds in the spirit of [9], which was performed under the lead of the heavy element group from Paul Scherrer Institute (PSI), Villingen, Switzerland, at the RIKEN Nishina Center, Wako, Japan. The focus of the work of our group was on further developments to extend studies of carbonyl compounds of the heaviest elements to those beyond Sg. Fusion products from the asymmetric nuclear fusion reactions, as needed for the carbonyl studies with Sg, Bh, and Hs, have a relatively large angular and energy spread, thus the transmission efficiency through an on-line recoil separator is relatively low. In case of TASCA or GARIS (which was used in [8]), the efficiencies are in order of 13% for Sg [10]. Thus, the overall efficiency of the synthesis of carbonyl complexes in combination with physical preseparation is rather low. For future experiments, the possibilities for chemical investigation of the metal carbonyl complexes of SHE without using a preseparation stage are currently being explored, with the goal to avoid the corresponding losses of close to 90%. First experiments performed at the Tandem accelerator at JAEA Tokai, Japan, suggested the successful the synthesis of Os and W carbonyl complexes also without a preseparator to be feasible, if the thermalization of the evaporation residues is spatially decoupled from the chemical synthesis. The latter is required to occur in a beam-free environment [11]. Further experiments were performed at the research reactor TRIGA Mainz [12].

With the aim to support gas-phase experiments on study of stability and volatility of carbonyls of the heaviest elements, calculations of the electronic structure and properties of group-6 $M(CO)_6$ [13] and group-8 $M(CO)_5$ [14] have been performed using the most advanced relativistic quantum-chemical methods (ADF BAND, X2c-DFT, DIRAC). The results have shown that in contrast to earlier published works the carbonyls of Sg and Hs should be less stable than those of the lighter 5d-homologs. This finding is valuable for fixing the right conditions in measurements of the first bond dissociation energies of these complexes. In addition, using results of these calculations, volatilities of goup-8 carbonyls as adsorption energies on inert surfaces have been predicted via a model of mobile adsorption. It was shown that $Hs(CO)_5$ should slightly more strongly adsorb on neutral surfaces than $Os(CO)_5$.

To render assistance to gas-phase experiments on study of reactivity of elements 112 through 114 with various surfaces, calculations of the adsorption energies of these elements and their lighter homologs on a hydroxylated quartz surface have been performed using a periodic ADF BAND code [15, 16]. Such periodic calculations of adsorption energies have been performed for the first time for superheavy element systems. The results have shown that Cn should be indeed the most volatile element out of those under consideration. Also, Fl should not interact with quartz at room temperature. Element 113, Nh, on the contrary should strongly interact with quartz [16]. Such a different adsorption behavior allows for a good separation between all these elements using a combination of quartz and gold surfaces.

A further activity of the SHE Chemistry division concerned the development of a new detector system for ALpha-BEta-Gamma (ALBEGA) multicoincidence spectroscopy for chemically separated samples [17]. Efforts in 2016 were mainly dedicated to the study and development of the new alpha/beta detector. The new version will be characterized by a more densely packed configuration and a thinner dead-layer on the side in contact with the gas flux. The production of the device was performed at the ITE, Warsaw (Poland), for which an ad hoc technological development for its assembling was required. The new alpha/beta detector will not only provide a higher energy resolution and efficiency, but will also feature increased mechanical stability to sustain the pressure difference inside and outside of the gas channel.

Presently, one of the hot topics in the superheavy element research is the synthesis of elements beyond Og (Z=118). The lack of sufficient amounts of heavier actinides prevents a continuation beyond Og with ^{48}Ca-induced reactions. An obvious path is to continue with fusion-evaporation reactions, but with projectiles heavier than ^{48}Ca. Several experiments have already been performed to synthesize Z=119 and 120 by using the reactions ^{50}Ti+^{249}Bk (TASCA, GSI), ^{64}Ni+^{238}U (SHIP, GSI), ^{58}Fe+^{244}Pu (DGFRS, FLNR, JINR), ^{54}Cr+^{248}Cm (SHIP, GSI), and ^{50}Ti+^{249}Cf (TASCA, GSI). In total, about one year of accelerator beam time has been spent for these search experiments. However, none of them led to the discovery of a new element, suggesting that cross sections are significantly lower than for ^{48}Ca-induced reactions. To get a better guidance for future search experiments, a better understanding of the fusion reaction is needed. Therefore, to understand the reaction mechanism better, an intensive experimental campaign involving various heavy

DOI:10.15120/GR-2017-1

projectiles and actinide targets was carried out by a collaboration of scientists from GSI, HIM Mainz, Johannes Gutenberg University Mainz, and the Australian National University (ANU), Canberra, Australia at the ANU's Heavy Ion Accelerator Facility. Suitable actinide targets like ^{244}Pu, ^{248}Cm, and ^{249}Cf were produced at the Institute of Nuclear Chemistry at the Johannes Gutenberg University Mainz, and were irradiated with a variety of beams between ^{34}S and ^{64}Ni at energies around the Coulomb barriers. The mass and angular distribution of fission fragments originating from the nuclear reactions were measured, in many reactions for the first time. The data analysis is ongoing and preliminary results already show a difference in dynamics of reactions involving different projectiles.

Further studies of the fission mechanism were performed, e.g., a study of fission induced by ^{18}O+^{249}Cf multi-nucleon transfer reactions at 8 MeV/A, in which the SHE Chemistry department participated. The experiment was performed at the Tandem accelerator at JAEA Tokai (Japan). Such reactions, acting as surrogate of n-induced fission reactions, allow populating in a single experiment several isotopes at low angular momentum and at low excitation energy. The excitation energy of the fissioning system can be determined by the kinematical reconstruction of the binary process, by measuring the mass and kinetic energy of light ejectile of the transfer reaction. In particular, this experiment was performed with the aim to extend the current systematics of fission fragment mass distribution nearby the region of transition from asymmetric to symmetric fission.

A further activity, which led to widespread recognition, was the contribution of GSI, HIM, and Johannes Gutenberg Mainz scientists and technicians to the direct detection of the exotic low-lying nuclear isomer in ^{229}Th [18]. For this, ^{233}U targets, which yield the ^{229m}Th after alpha decay of ^{233}U, as well as ^{234}U targets (for control experiments serving to exclude an origin other than that of ^{229m}Th decay to the ground state as a source for the observed signal) were produced. They were used in these joint experiments, which were led by the group of P. Thirolf at the Ludwigs-Maximilians-University Munich, Germany.

Some further activities, also including contributions of the SHE Chemistry department to the upgrade of the UNILAC Accelerator, are detailed in individual contributions to this GSI Scientific Report 2016 (J. Konki et al., A. Di Nitto et al., S. Götz et al., M. Götz et al., V. Pershina et al., as well as P. Scharrer et al.)

References

[1] M. Laatiaoui et al., Nature 538, 495 (2016).
[2] P. Chhetri et al., Eur. Phys. J. D (submitted).
[3] F.P. Heßberger et al. EPJ A 52, 328 (2016).
[4] F.P. Heßberger et al. EPJ A 52, 192 (2016).
[5] D. Rudolph et al., Phys. Rev. Lett. 111, 112502 (2013).
[6] A. Yakushev et al., Inorg. Chem. 53, 1624 (2014).
[7] Ch.E. Düllmann et al., Phys. Rev. Lett. 104, 252701 (2010).
[8] J. Even et al., Science 345, 1491 (2014).
[9] I. Usoltsev et al., Radiochim. Acta 104, 141 (2016).
[10] H. Haba et al., Phys. Rev. C 85, 024611 (2012).
[11] Y. Wang et al., Radiochim. Acta 102, 69 (2014).
[12] V. Wolter, Master's Thesis, Johannes Gutenberg University Mainz, 2016.
[13] M. Ilias and V. Pershina, Inorg. Chem. 56, 1638 (2017);
[14] V. Pershina and M. Ilias, J. Chem. Phys. 146, 184306 (2017).
[15] V. Pershina, Phys. Chem. Chem. Phys. 18, 17750 (2016).
[16] V. Pershina, J. Phys. Chem. C 120, 20232-20238 (2016).
[17] A. Di Nitto, GSI Sci. Rep. 2014, p. 184 (MU-NUSTAR-SHE-C-06).
[18] L. von der Wense et al., Nature 533, 47 (2016).

DOI:10.15120/GR-2017-1

DOI:10.15120/GR-2017-1

The new isotopes ^{240}Es and ^{236}Bk

J. Konki[*1], *J. Khuyagbaatar*[2,3], *J. Uusitalo*[1], *P. T. Greenlees*[1], *K. Auranen*[1], *H. Badran*[1], *M. Block*[2,3,4], *R. Briselet*[5], *D. M. Cox*[6], *M. Dasgupta*[7], *A. Di Nitto*[3,4], *Ch. E. Düllmann*[2,3,4], *T. Grahn*[1], *K. Hauschild*[8], *A. Herzán*[1], *R.-D. Herzberg*[6], *F. P. Heßberger*[3], *D. J. Hinde*[7], *R. Julin*[1], *S. Juutinen*[1], *E. Jäger*[3], *B. Kindler*[3], *J. Krier*[3], *M. Leino*[1], *B. Lommel*[3], *A. Lopez-Martens*[8], *D. H. Luong*[7], *M. Mallaburn*[9], *K. Nishio*[10], *J. Pakarinen*[1], *P. Papadakis*[1], *J. Partanen*[1], *P. Peura*[1], *P. Rahkila*[1], *K. Rezynkina*[8], *P. Ruotsalainen*[1], *M. Sandzelius*[1], *J. Sarén*[1], *C. Scholey*[1], *J. Sorri*[1], *S. Stolze*[1], *B. Sulignano*[5], *Ch. Theisen*[5], *and A. Ward*[6]

[1]University of Jyväskylä, Finland; [2]Helmholz-Institut Mainz, Germany; [3]GSI, Darmstadt, Germany; [4]University of Mainz, Germany; [5]CEA Saclay, France; [6]University of Liverpool, UK; [7]ANU, Canberra, Australia; [8]CSNSM Orsay, France; [9]University of Manchester, UK; [10]JAEA, Tokai, Japan

Two new neutron-deficient nuclei ^{240}Es and ^{236}Bk were synthesised in an experiment carried out at the Accelerator Laboratory of the Department of Physics (JYFL), University of Jyväskylä, Finland [1]. The hitherto unknown isotopes were identified by their radioactive decay chains starting from ^{240}Es produced in the fusion-evaporation reaction ^{209}Bi(^{34}S,3n)^{240}Es.

Evaporation residues (ER) recoiling out of the target were separated from the primary beam and transfer reaction products by the gas-filled recoil separator RITU [2]. The ERs passed through a Multi-Wire Proportional Counter (MWPC) and were implanted in the two adjacent double-sided silicon detectors (DSSDs) of the GREAT focal plane spectrometer [3] where their subsequent decays were measured.

The energies of all signals from the detectors were time stamped and recorded using the triggerless Total Data Readout (TDR) data-acquisition system [4]. The spatial and temporal correlations in the data between the detectors were analysed using the GRAIN software package [5].

The results of this experiment were reported in Physics Letters B [1] in detail. Two groups of α particles with energies E_α=8.19(3) MeV and 8.09(3) MeV were assigned to ^{240}Es from correlated ER-α events. The new isotope ^{236}Bk was identified from its electron-capture delayed fission (ECDF) branch. Half-lives of 6(2) s and 22^{+13}_{-6} s were obtained for ^{240}Es and ^{236}Bk, respectively. The ECDF probabilities (P_{ECDF}) of ^{240}Es and ^{236}Bk were determined from correlated ER-fission and ER-α-fission events to be 0.16(6) and 0.04(2), respectively. The proposed decay schemes for the new ^{240}Es and ^{236}Bk isotopes are shown in Fig. 1.

The ECDF probabilities of the heavier odd-odd isotopes $^{242-248}$Es and ^{238,240}Bk have been measured previously (see e.g. [6] and the references therein). The new data from this work extend the systematics of the Es and Bk isotopes and show a continuation of the exponential increase of P_{ECDF} as a function of the Q-value of the EC decay (Q_{EC}) and the spontaneous fission barrier (B_{sf}) in more neutron-deficient isotopes. No deviations from this trend

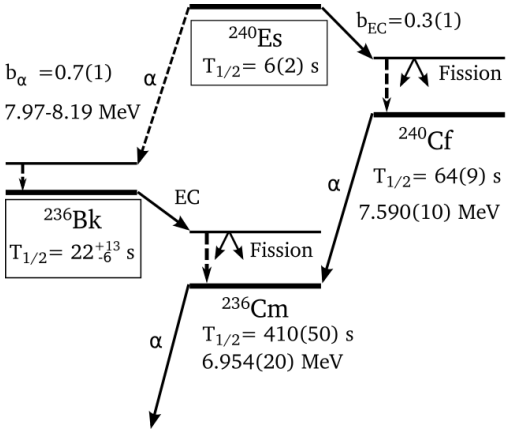

Figure 1: The proposed decay scheme of the new isotopes ^{240}Es and ^{236}Bk. The measured values for ^{240}Es and ^{236}Bk are from this work.

are observed. We note that P_{ECDF}-values for the new isotopes ^{240}Es and ^{236}Bk are the highest ones so far for Es and Bk isotopes, respectively.

The simple dependence of P_{ECDF} on $Q_{\mathrm{EC}} - B_{\mathrm{sf}}$ is not yet fully understood. There is a relative difference between Es and Bk isotopes in P_{ECDF} that could be attributed to the shape of the total fission barrier. In more neutron-deficient isotopes the P_{ECDF} is expected to approach saturation and more experimental data are needed there to shed a light on this complex decay process.

References

[1] J. Konki et al., Phys. Lett. B **764**, 265 (2017).

[2] M. Leino et al., NIM. B **99**, 653 (1995).

[3] R. D. Page et al., NIM. B **204**, 634 (2003).

[4] I. H. Lazarus et al., IEEE Trans. Nucl. Sci. **48**, 567 (2001).

[5] P. Rahkila et al., NIM. A **595**, 637 (2008).

[6] A. Andreyev et al., Rev. Mod. Phys. **85**, 1541 (2013).

*joonas.konki@jyu.fi

Hexacarbonyls of Mo, W, and Sg: Electronic Structure and Bonding

V. Pershina[1] and M. Iliaš[2,3]
[1]GSI Helmholtzzentrum für Schwerionenforschung, Darmstadt, Germany; [2]Helmholtz Institute Mainz, Germany;
[3]Matej Bel University, Banská Bystrica, Slovakia

The class of carbonyl compounds has recently been enriched by a new species, a hexacarbonyl of a superheavy element with Z=106, $Sg(CO)_6$ and its volatility has been studied both experimentally [1] and theoretically [2]. Now, experiments are under way to measure the First Sg-CO Bond Dissociation Energy (FBDE) [3]. Earlier predictions based on RECP calculations have indicated that the Sg-CO bond should be stronger than the W-CO one due to relativistic effects on the 6d AOs [4]. With an aim to prove these earlier predictions on a higher level of theory and to have an own set of data, in this work, we have calculated various properties of the group-6 hexa- and pentacarbonyls and have newly determined FBDEs. The following decomposition reaction was considered

$$M(CO)_6(O_h) \rightarrow M(CO)_5(C_{4v}) + CO.$$

The calculations were performed using a variety of nonrelativistic (NR), relativistic scalar (SR) and spin-orbit (SO) methods, such as ZORA-ADF, X2c+AMFI-CCSD(T) and Dirac-Coulomb-DFT one. The uncontracted Dyall vdz basis sets in the DIRAC CCSD(T) calculations were utilized. The present results for the FBDEs in comparison with those of the work [4] and experimental data for $Mo(CO)_6$ and $W(CO)_6$ [5] are given in Table 1.

Table 1. First M-CO Bond Dissociation Energies at various levels of theory (in kJ/mol)

Method	$Mo(CO)_6$	$W(CO)_6$	$Sg(CO)_6$
ADF (NR)	155.07	218.47	223.81
ADF (SR)	163.63	191.19	181.09
ADF (SO)	163.49	190.73	180.22
DC-DFT	163.20	189.83	177.42
X2c+CCSD(T)	158.19	181.45	176.22
RECP-CCSD[a]	170.71	197.90	204.59
RECP-CCSD(T)[a]	182.00	207.94	212.13
ZPT[b]	-5.17	-5.43	-5.59
Exp.[c]	167.4±8	192.5±8	-

[a]Ref. [4]; [b]Zero point and thermal contribution; [c]Ref. [5].

The main difference between the present relativistic ADF, ReSpect and DIRAC calculations on the one hand and the RECP ones [4] on the other hand is an opposite trend in the vibrational frequencies of the M-CO bond and FBDE from $W(CO)_6$ to $Sg(CO)_6$: all the former show a decrease in this direction, while the latter an increase (Fig. 1).

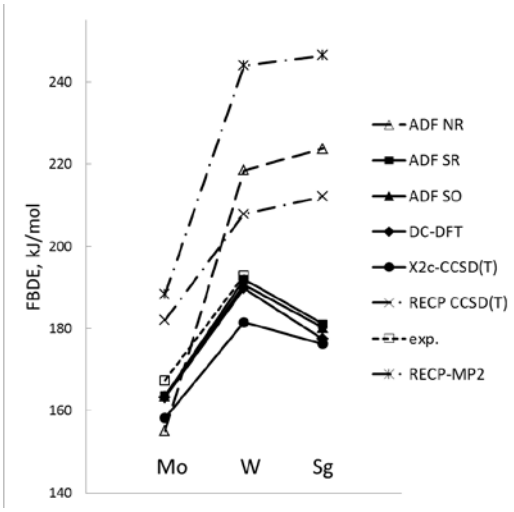

Figure 1. First Bond Dissociation Energies of $M(CO)_6$, where M = Mo, W and Sg, calculated using various methods in comparison with experimental data for the Mo and W carbonyls (open squares).

To find a reason for such a difference, a bond analysis of $M(CO)_6$ (M = Mo, W, and Sg) was performed using ADF Hirshfeld effective charges, q_M, Mulliken MO analysis based on the M and CO fragments and the DIRAC projection analysis. The obtained smaller relativistic q_M(Sg) than q_M(W) means that the electron density is not shifted so much in $Sg(CO)_6$ from Sg to CO as in $W(CO)_6$, so that the Sg-CO electrostatic interaction is smaller than the W-CO one, meaning that bonding is weaker in $Sg(CO)_6$. Non-relativistically, it is just the other way around: the largest q_M on Sg is the source of its largest ionic bonding with CO in the row of homologs. Thus, in difference to the earlier predictions [4], the decomposition of $Sg(CO)_6$ should occur at lower temperatures than those of $W(CO)_6$ [6], with a reversal of the trend from Sg to W.

References

[1] J. Even, et al. Science **345**, 1491 (2014).
[2] V. Pershina and J. Anton, J. Chem. Phys. **138**, 174301 (2013).
[3] R. Eichler, private communication.
[4] C. Nash and B. E. Bursten, J Am. Chem. Soc. **121**, 10830 (1999).
[5] K. E. Levis, et al. J. Am. Chem. Soc. **106**, 3905 (1984).
[6] I. Usoltsev, et al. Radiochim. Acta **104** (3) (2015).

DOI:10.15120/GR-2017-1

Identification of reaction products in ^{50}Ti + ^{249}Cf reactions at TASCA *

A. Di Nitto †[1,2], *J. Khuyagbaatar*[2,3], *D. Ackermann* ‡[2], *J.Adamczewski-Musch*[2], *L.-L. Andersson*[3,4], *E. Badura*[2], *M. Block*[2], *H. Brand*[2], *D.M. Cox*[4], *Ch.E. Düllmann*[1,2,3], *J. Dvorak*[3], *K. Eberhardt*[1], *P.A. Ellison*[5], *N.E. Esker*[5], *J. Even*[1,3], *C. Fahlander*[6], *U. Forsberg*[6], *J.M. Gates*[5], *P. Golubev*[6], *O. Gothe*[5], *K.E. Gregorich*[5], *W. Hartmann*[2], *R.D. Herzberg*[4], *F.P. Heßberger*[2,3], *J. Hoffmann*[2], *R. Hollinger*[2], *A. Hübner*[2], *E. Jäger*[2], *J. Jeppsson*[6], *B. Kindler*[2], *S. Klein*[1], *I. Kojouharov*[2], *J.V. Kratz*[1], *J. Krier*[2], *N. Kurz*[2], *S. Lahiri*[7], *S.Linev*[2], *B. Lommel*[2], *M. Maiti*[7], *R. Mändl*[2], *E. Merchan*[2], *S. Minami*[2], *A. Mistry*[4], *Ch. Mokry*[1], *H. Nitsche*[5], *J.P. Omtvedt*[8], *G.K. Pang*[5], *I. Pysmenetska*[2], *D. Renisch*[1,3], *D. Rudolph*[6], *J. Runke*[2], *L.G. Sarmiento*[6,9], *M. Schädel*[2,10], *H. Schaffner*[2], *B. Schausten*[2], *A. Semchenkov*[8], *J. Steiner*[2], *P. Thörle-Pospiech*[1], *T. Torres De Heidenreich*[2], *N. Trautmann*[1], *A. Türler*[11], *J. Uusitalo*[12], *D. Ward*[6], *M. Wegrzecki*[13], *P. Wieczorek*[2], *N. Wiehl*[1], *A. Yakushev*[2], *and V. Yakusheva*[3]

[1]U. Mainz, Germany; [2]GSI, Darmstadt, Germany; [3]HIM, Mainz, Germany; [4]U. Liverpool, UK; [5]LBNL+UC Berkeley, CA, USA; [6]Lund U., Sweden; [7]SINP, Kolkata, India; [8]U. Oslo, Norway; [9]UNAL Bogotá, Colombia; [10]JAEA Tokai, Japan; [11]U. Bern+PSI Villigen, Switzerland; [12]U. Jyväskylä, Finland; [13]ITE, Warsaw, Poland

During the last decades heavy ion induced reactions were applied to explore the chart of nuclei up to the superheavy elements (SHE), which has resulted in the discovery of the SHE up to Og ($Z = 118$) in complete fusion reactions [1]. Alternatively, recent model calculations suggest the possibility to produce exotic nuclei including SHE in non-fusion channels of heavy ion induced reactions [2]. Pioneering studies on the possible production of such exotic nuclei in non-fusion reactions were performed in the late 1970s by applying chemical separation techniques [3], which are suitable for longer-lived nuclei ($\gtrsim$1 h). Many properties of the multi-nucleon transfer reactions have been established, but still detailed information on the reaction mechanism/kinematics is missing [5, 6, 4].

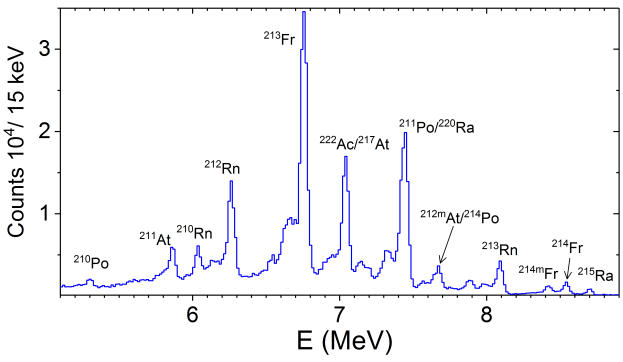

Figure 1: Energy spectrum measured with the focal plane detector during beam-off periods for the ^{50}Ti + ^{249}Cf reaction. Isotopic identification of some lines is given.

Recently, at the velocity filter SHIP new short-lived (down to 10^{-6} h) neutron-deficient nuclei of heavy elements have been synthesized in the ^{48}Ca + ^{248}Cm reaction [7]. These and other results at SHIP (see [8]), benefiting of the kinematic separation, demonstrate the relevance of the forward angle measurements for the investigation of the reaction dynamics.

At the gas-filled recoil separator TASCA, non-fusion products of the ^{50}Ti $+^{249}$ Cf reaction have been investigated. They were produced during the experiment for searching the SHE with $Z = 120$ [9]. The magnetic settings of TASCA were tuned to collect the products of fusion-evaporation reactions, but even under these conditions some amount of non-fusion products were passing through TASCA and were implanted into the focal plane detector. Here their subsequent radioactive decays were measured. A typical energy spectrum containing lines from the α decay of the implanted nuclei is shown in Figure 1. By exploiting the α decay properties, the identification of nuclei was performed employing a position and time correlation analyses between implantation and/or α-like events. In total, 57 isotopes with $Z = 83 - 90$ were identified.

Experimental details and the final analysis will be given in a forthcoming publication [10].

References

[1] Y. T. Oganessian and V. K. Utyonkov, Rep. Prog. Phys. 78, 036301 (2015).
[2] V. I. Zagrebaev and W. Greiner PRC **83**, 044618 (2011).
[3] M. Schädel et al., PRL **41**, 469 (1978), and **48**, 852 (1982).
[4] L. Corradi et al., Jour. of Phys. G **36**, 113101 (2009).
[5] J.V. Kratz et al., NPA **944**, 117 (2015).
[6] M. Götz et al., NPA **961**, 1 (2017).
[7] S. Heinz et al., EPJA **52**, 278 (2016).
[8] S. Heinz et al., EPJA **51**, 140 (2015).
[9] Ch. E. Düllmann et al. to be published.
[10] A. Di Nitto et al., to be published.

* We thank the ion-source and accelerator staff at GSI. Work supported by BMBF contract-No. 06MZ7164.
† a.dinitto@gsi.de
‡ Present address: GANIL, Caen, France

Speeding up gas-phase chemistry to access elements beyond Fl

S. Götz[*1,2,3], *S. Raeder*[1,2], *M. Block*[1,2,3], *Ch. E. Düllmann*[1,2,3], *P. Chhetri*[1,5], *F. Giacoppo*[1,2], *M. Götz*[1,2,3], *O. Kaleja*[1,3,4], *Ch. Mokry*[2,3], *J. Runke*[1,3], *P. Thörle-Pospiech*[2,3], *and A. Yakushev*[1,2]

[1]GSI, Darmstadt, Germany; [2]HIM, Mainz, Germany; [3]Johannes Gutenberg-University, Mainz, Germany; [4]MPIK, Heidelberg, Germany; [5]TU Darmstadt, Darmsatdt, Germany

The electronic structure of the heaviest elements is strongly influenced by relativistic effects, which may lead to chemical properties that deviate from those expected based on an extrapolation of trends present in the periodic table [1]. Chemical properties have been reproducibly studied for all elements up to Hs (Z=108) as well as for Cn (Z=112). Current research activities in the field focus on the elements Nh (Z=113) and Fl (Z=114) [2]. Due to the low production rates and short half-lifes, $T_{1/2}$, only single atoms are available in chemical experiments. Nevertheless, the required sensitivity can be achieved, best by combining chemical setups with electromagnetic preseparators [3]. Gas phase chemical methods have proven most successful for the heaviest elements, as they give access to isotopes with half-lifes of the order of at least about one second [2]. The successful gas-chromatography studies of Fl demonstrate the potential of the combination of the chromatography detector array COMPACT with the gas-filled separator TASCA at an one-atom-at-time level [4]. The most time-consuming step in the experiments performed with the current TASCA-COMPACT setup as it was used for the Fl experiments is the thermalization of the fusion-evaporation reaction products in the Recoil Transfer Chamber (RTC) [3] and their transport to the connected COMPACT detector array. Besides Cn and Fl, also Nh is in reach with this technique. The extraction time is, however, significantly longer than the half-lifes of the most long-lived isotopes of all elements wit $Z > 114$. For Mc (Z=115), for example, the most long-lived currently known isotope is ^{288}Mc with $T_{1/2}$ = 170 $\binom{+40}{-30}$ ms [5]. To overcome this limitation, exploratory experiments on the coupling of COMPACT to an existing gas-catcher operating with electric fields [6] were carried out.

To get access to shorter-lived isotopes, it is crucial to speed up the transport time, while maintaining a high efficiency of the setup [5]. To this end, a faster and more effective transport technique is currently being developed. For future experiments with Mc and beyond, the current RTC will be replaced by a gas-catcher, which uses electric fields to extract the ions [6, 7, 8, 9].

In 2016, first off-line measurements were performed with ^{223}Ra ($T_{1/2}$ = 11.43 d) and ^{225}Ac ($T_{1/2}$ = 10 d) recoil ion sources. The used sources were placed in axial symmetry in the center of the direct current electrodes-system (DC-cage), which is located within the gas-catcher. The DC-cage contains the stopping volume for the ions inside the gas-catcher. The system consists of 5 cylindrical electrodes with an outer diameter of 180 mm and an inner diameter of 160 mm. From the source the recoil ions ^{219}Rn$^+$ ($T_{1/2}$ = 3.96 s) or ^{217}At$^+$ ($T_{1/2}$ = 32.34 ms) are guided by the electric fields through the segmented DC electrode towards a funnel structure. This funnel guides the ions by applied DC and AC (RF: 140 V, gradient 7 V cm^{-1}) fields to the exit hole (5 mm diameter). After exiting, the ions are neutralized by collisions with the walls of a Teflon-tube. This neutralization section facilitates gas-chromatography studies of the element of interest in elemental form. After the neutralization zone the atoms are directed by a gas flow into the subsequent COMPACT-detector array [4]. The gas-catcher-COMPACT-setup was flushed with helium gas and kept at a pressure of 50 to 100 mbar. This ensured a viscous flow and allowed performing gas phase chromatography studies in COMPACT. For ^{219}Rn, only decay in-flight was observed as COMPACT was operated at ambient temperature. Due to the high adsorption tendency of ^{221}Fr no atoms of this element were observed in COMPACT in a first test, ^{217}At, however, was observed in the first COMPACT-detector. We studied the efficiency for transporting ^{217}At from the source to the COMPACT detector as well as the transport time. For the efficiency quantification, the measured rate in COMPACT was compared with the effective source strength, which was determined in a separate measurement of the rate at which ^{217}At$^+$ ions are recoiling from the source. To measure the transport time, the potential, at which the source was kept, was cyclically switched rapidly from negative (to avoid release of ^{217}At$^+$ ions) to positive. This was used as the start of a time-of-flight measurement. The stop signal was given by measured decay in COMPACT. Transport times well below 100 ms were measured, which would be fast enough for applications to, e.g., Mc.

References

[1] M. Schädel (Ed.), The Chemistry of the Superheavy Elements, Kluwer Academic Publishers, Dordrecht, The Netherlands, 2003.

[2] A. Türler et al., Nucl. Phys. A **944**, 640 (2015).

[3] J. Even et al., Nucl. Instrum. Meth. A **638**, 157-164 (2011)

[4] A. Yakushev et al., Inorg. Chem. **53**, 1624 (2014).

[5] D. Rudolph et al., AIP Conf. Proc. **1681**, 030015-1 (2015).

[6] J. Neumayr et al. Nucl. Instr. and Meth. B **244** (2006) 489.

[7] M. Wada et al., Nucl. Instrum. Methods B **204**, 570 (2003).

[8] G. Savard et al., Nucl. Instrum. Methods B **204**, 582 (2003).

[9] M. Block et al., Eur. Phys. J. D **45**, 39 (2007).

* s.goetz@gsi.de

DOI:10.15120/GR-2017-1

Radiochemical investigation of the kinematics of multi-nucleon transfer reactions

M. Götz[1,2,3], S. Götz[1,2,3], J. V. Kratz[1], Ch. E. Düllmann[1,2,3], Ch. Mokry[1,3], J. Runke[1,2], P. Thörle-Pospiech[1,3], N. Wiehl[1,3], M. Schädel[2], J. Ballof[4], H. Dorrer[1], J. Grund[1], E. Jäger[2], O. Keller[1], J. Krier[2], J. Khuyagbaatar[2,3], L. Lens[1,2], B. Lommel[2], M. Mendel[1], K. J. Moody[5], B. Schausten[2], M. Schmitt[1], D. Shaughnessy[5], J. Steiner[2], N. Trautmann[1], A. Yakushev[2,3], and V. Yakusheva[2]

[1]Institute of Nuclear Chemistry University Mainz, 55099 Mainz, Germany; [2]GSI Helmholtz Center for Heavy-Ion Research, 64291 Darmstadt, Germany; [3]HIM Helmholtz Institute Mainz, 55128 Mainz, Germany; [4]Advanced Science Research Center JAEA, Tokai-mura Ibaraki 319-1195, Japan; [5]Lawrence Livermore National Laboratory, Livermore CA, USA

Renewed interest in multi-nucleon transfer reactions as a promising tool for the production of neutron-rich transactinide isotopes [1] has motivated us to perform a ^{48}Ca+^{248}Cm bombardment at an incident energy 10% above the Coulomb barrier to study emission-angle resolved kinetic energies of isotopes of Bk through Fm [2]. The isotopes of interest were implanted into a stack of Ni foils mounted behind the target. They were isolated off-line using radiochemical separations and detected by alpha spectroscopy. This way, long-lived isotopes with mass numbers between 246 and 256 were accessible. Angular distributions and kinetic energies corresponding to recoil ranges in the Ni foils were evaluated and weighted mean values in the center of mass system were used to construct deflection functions, total kinetic energy TKE vs. Θ_{cm}. Fig. 1 shows the location of the centroid of the Fm activities in the TKE vs. Θ_{cm} plane corresponding to an average total kinetic energy loss TKEL = 70 $\pm$ 10.5 MeV at Θ_{cm} close to the grazing angle. Taking into account the ground state Q value for the most probable primary fragment results in an excitation energy corresponding within the uncertainty in the measured TKEL to the missing mass, i.e. the mass difference between the most probable secondary mass number and the most probable primary mass number calculated with Volkov's generalized Qgg systematics [3] (minimum potential energy corrected for the breaking of nucleon pairs in the multi-nucleon transfer process) indicating that the number of evaporated neutrons is 1.3 on the average. For products closer to the target, e.g. for Cf, the values of TKE spread much wider than for Fm, see Fig. 2. Here, TKEL values of ≈9, ≈34, and ≈54 MeV corresponding to the evaporation of 0, 1, and 3 neutrons are observed in the corresponding range bins.

Thus, values of TKE reach from quasi-elastic to completely damped values. For multi-nucleon transfer products (Fm), the distributions are peaked close to the grazing angle with laboratory kinetic energies close to 80 MeV. These are benchmarks for the design of a large acceptance separator for the separation and detection of short-lived neutron-rich transactinide isotopes.

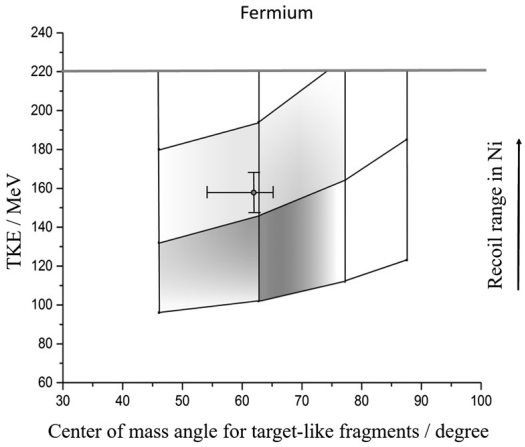

Figure 1: Centroid of the Fm distribution with standard deviations. The shades are meant to indicate the approximate width of the distribution.

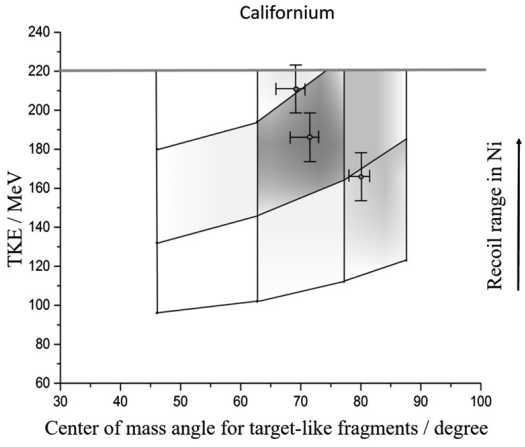

Figure 2: Same as Fig. 1 but for the Cf isotopes.

References

[1] V. Zagrebaev et al,. Nucl.Phys. A834, 366c (2010)

[2] M. Götz et al., Nucl. Phys. A961, 1 (2017)

[3] V.V. Volkov, Int. Conf. on Reactions between Complex Nuclei, Nashvillle 1974, (North Holland, Amsterdam) Vol. II, 363 (1974)

DOI:10.15120/GR-2017-1

DOI:10.15120/GR-2017-1

NeuLAND - from the demonstrator to the start version*

K. Boretzky† [3], *G. Alkhazov* [1], *L. Atar* [2,3,4], *T. Aumann* [2,3], *C. Beinrucker* [13], *D. Bemmerer* [5], *C. Caesar* [3], *M. Cherciu* [6], *L. Chulkov* [7], *T. Cowan* [5,8], *C.A. Douma* [9], *Z. Elekes* [10], *J. Enders* [2], *J. Frühauf* [3], *D. Galaviz Redondo* [11], *I. Gašparić* [12], *N. Gruzinsky* [1], *K. Göbel* [13], *T. Heftrich* [13], *H. Heggen* [3], *M. Heil* [3], *A. Heinz* [14], *J. Hoffmann* [3], *M. Holl* [2], *A. Horvat* [2], *Á. Horváth* [15], *H.T. Johansson* [14], *B. Jonson* [14], *J. Kahlbow* [2], *N. Kalantar-Nayestanaki* [9], *A. Kelić-Heil* [3], *K. Koch* [3], *N. Kozlenko* [1], *D. Kresan* [3], *N. Kurz* [3], *V. Kuznetsov* [1], *D. Körper* [3], *C. Langer* [13,3], *S. Lindberg* [14], *J. Mayer* [16], *M. Najafi* [9], *T. Nilsson* [14], *G. Nyman* [14], *A. Pelizza* [14], *S.G. Pickstone* [16], *R. Plag* [3], *M. Pohl* [13], *P. Potlog* [6], *R. Reifarth* [13], *S. Reinhardt* [8], *S. Reinicke* [5], *C. Rigollet* [9], *S. Röder* [5], *D. Rossi* [2], *D. Savran* [17], *H. Scheit* [2], *F. Schindler* [2], *P. Schrock* [2], *H. Simon* [3], *E. Stan* [6], *R. Thies* [14], *H. Törnqvist* [2], *L. Uvarov* [1], *S. Volkov* [1], *A. Wagner* [5], *V. Wagner* [2], *A. Zilges* [16], *K. Zuber* [8], *and the R^{3}B Collaboration* [1]

[1]Petersburg Nuclear Physics Institute Gatchina, Russia; [2]Technische Universität Darmstadt, Darmstadt, Germany; [3]GSI Helmholtzzentrum für Schwerionenforschung, Darmstadt, Germany; [4]University of Guelph, Canada; [5]Helmholtz-Zentrum Dresden-Rossendorf, Dresden, Germany; [6]Institute of Space Sciences, Magurele, Romania; [7]NRC Kurchatov Institute, Moscow, Russia; [8]Technische Universität Dresden, Germany; [9]KVI - CART, University of Groningen, The Netherlands; [10]ATOMKI Debrecen, Hungary; [11]Laboratory for Instrumentation and Experimental Particle Physics, Lisbon, Portugal; [12]RBI Zagreb, Croatia; [13]Johann Wolfgang Goethe-Universität Frankfurt, Germany; [14]Chalmers University of Technology, Gothenburg, Sweden; [15]Eoetvoes Lorand University, Budapest, Hungary; [16]Universität zu Köln, Germany; [17]Extreme Matter Institute, Darmstadt, Germany

Introduction

NeuLAND (New Large Area Neutron Detector) [1] is one of the key elements of the R^{3}B experiment, designed to measure fast neutrons with energies of typically 100 to 1000 MeV, and to determine their four-momenta with high precision. Acting primarily as a time-of-flight spectrometer with a time resolution of $\sigma_t \leq 150$ ps and spatial resolutions of $\sigma_{x,y,z} \approx 1.5$ cm, the calorimetric properties of this detector are essential for the reconstruction of multi-neutron events. NeuLAND with its front size of 2.5x2.5 m^2 and a total depth of 3 m is built from organic scintillator bars arranged in a double-plane structure. For details we refer to the GSI annual reports [2, 3]. In this document, we report about the achievements in the last two years. The two major activities are the continous production of further detector components, and the experimental campaign carried out at RIKEN with the NeuLAND demonstrator.

Production Status

Double Planes The final NeuLAND detector will consist of 30 double planes, each with a depth of 10 cm constitutes an independent subunit of 100 scintillators and 200 photomultipliers, see figure 1. The read-out electronics and the high voltage supply are mounted on each double plane frame, the form factor enables the dense packing of double planes, limited only by the depth of the scintillator bars.

The NeuLAND demonstrator, consists of four double-planes, which are still supplied by a commercially available high voltage system and the read-out system TacQuila [4] previously used for LAND. While it was shipped to RIKEN in 2014, the production of new double planes at GSI continued and big steps were made towards the final design. At the time of writing this report, a total of 11 double planes are complete. One to two more double planes will be built during 2017, thus providing a 40% detector.

Readout Electronics The read-out electronics for NeuLAND (NeuLAND-TAMEX) is a GSI in-house development based on the former TacQuila electronics. It delivers a very precise time measurement from an FPGA TDC and a charge measurement using the Time-over-Threshold (ToT) method. After in-beam tests of the first prototypes [5], major improvements in terms of compactness and performance were implemented. The functionality of the former frontend electronics (LANDFEE), the charge measuring board (QTC), and the monitoring and controls board (TRIPLEX) have been combined into one newly designed board (FQT). Together with the improved FPGA TDC board (TAMEX3), a very compact and cost-effective design has been established. This setup was tested in a GSI beam time in 2016 as read-out for the new Time-of-Flight wall for R^{3}B and demonstrated excellent performance with respect to timing and charge resolution, far beyond the needs for NeuLAND. The pre-series of the new read-out electronics (200 channels) was mounted inside the electronic boxes of one double-plane (see figure 1) and successfully taken into operation. The timing properties of the double-plane, determined using cosmic rays, exhibit results of typically $\sigma_t^{mean} \approx 120$ ps similar to earlier extracted val-

*This work is supported by the BMBF projects 05P15RDFN1, 05P2015PKFNA,05P15RFFN1, University of Groningen, the Croatian Science Foundation project SR-ETNo, HIC for FAIR and GSI (KZILGE1416)

† k.boretzky@gsi.de

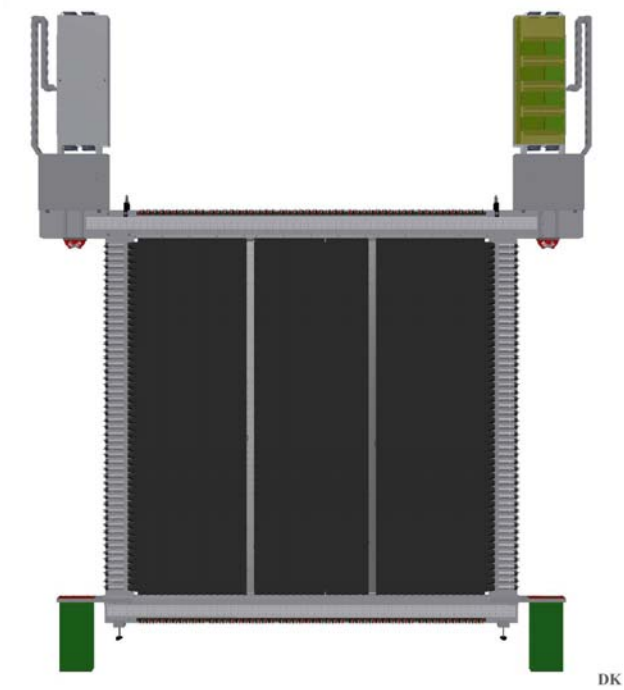

Figure 1: Schematic drawing of one double plane in a front view. Visible are the 50 horizontal bars read out on both sides by photomultipliers. The high-voltage modules (DB50) are mounted in the lower right and left corner, while the boxes on the top corners are hosting the cables and the read-out electronics. The 50 vertical bars are mounted on the backside of the horizontal bars.

ues using the former TacQuila electronics. The series production of the NeuLAND-TAMEX electronics is underway (3000 channels) and the installation and commissioning is scheduled for the end of 2017.

High Voltage Distribution System NeuLAND will be supplied with high voltage from two high voltage distribution systems (HVDS) called HV3200, each connected to up to 3200 photomultipliers (PMT). These systems are produced and delivered by PNPI, Russia, and their design has been optimized for usage with NeuLAND. The principle of operation of the HV3200 is based on individual down-regulation of a primary power supply output for each PMT. Each voltage regulator is located on an individual daughter-board. The 50-channel distribution board DB50 carries 50 regulators. Thus, four DB50 modules serve exactly one NeuLAND double plane. The communication with each individual channel, in order to adjust the high voltage and to monitor voltage and current, is provided via control monitor boards. Up to 16 DB50 boards can be daisy-chained. The pre-series (200 channels) and the first series delivery (1000 channels) have been taken into operation successfully. Together with the second series delivery (2000 ch) in autumn 2017, all existing NeuLAND double planes can be supplied, starting from 2018.

Support Structure The design of the support structure for the full-size NeuLAND was finalized, see figure 2. It consists of two identical supports, of which each can host up to 20 double planes. The two supports can be placed adjacent to each other, avoiding any gap between the double planes of the first and second support frame. Each of the supports consists of a frame to hold the double planes, and a platform on top which allows to access the electronics and PMTs from the top for maintenance. One of the support frames has been built, the existing double planes will be put into the frame after the delivery and installation of the maintenance platform.

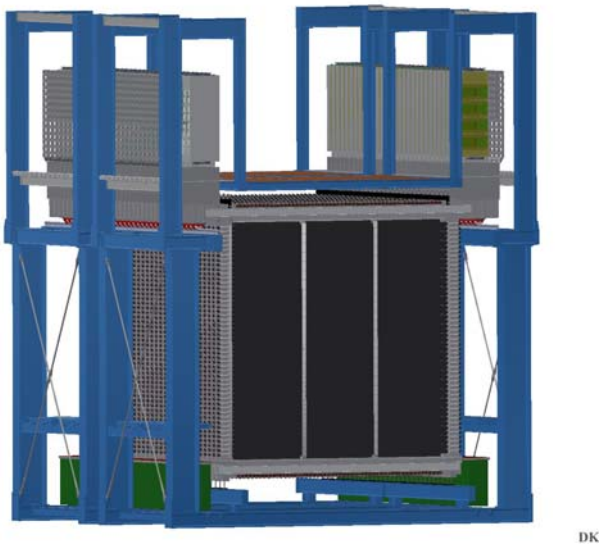

Figure 2: NeuLAND with 30 double-planes placed in the support structure, which is composed of two adjacent identical support frames and platforms.

NeuLAND Demonstrator at RIKEN

In the beginning of 2015, the NeuLAND demonstrator (4 double planes) arrived at RIKEN and was installed in the SAMURAI experimental hall [6], see figure 3. In the standard configuration, it is located in front of the NEBULA neutron detector from RIKEN [7, 8] at 0° with respect to the beam line downstream from the SAMURAI magnet, see figure 4. The NeuLAND demonstrator increases the neutron efficiency and improves the resolution in several experiments in a two year campaign.

Prior to the first experiment with NeuLAND@RIKEN, a one-day measurement was performed to study the neutron efficiency of NeuLAND at typical RIKEN beam energies, i.e. 100 and 250 MeV, using quasi mono-energetic neutrons from a ^{7}Li(p,n)^{7}Be reaction [9].

This calibration run was directly followed by an experiment aiming at identifying resonance states of the extremely neutron-rich oxygen isotopes ^{27}O and ^{28}O [10].

In spring 2016, experiments studying the nuclear EOS in central collisions of Sn isotopes were performed. Neu-

DOI:10.15120/GR-2017-1

Figure 3: Transportation of the NeuLAND demonstrator to the underground SAMURAI experimental hall at RIKEN.

Figure 4: The downstream area of the SAMURAI setup. The NeuLAND demonstrator, equipped with a VETO detector from RIKEN, is located in front of NEBULA. Neutrons impinging on NeuLAND come from the left.

LAND was placed at an angle of 30° with respect to the beam line in order to measure light charged particles, such as hydrogen and helium ions in addition to neutrons and γ-rays. In order to distinguish between neutral and charged particles, a RIKEN VETO detector in front of NeuLAND was used. Figure 5 presents the particle identification with NeuLAND, based on time of flight (ToF) and deposited energy (E_{dep}) in the first NeuLAND plane. In the upper part the spectrum is displayed without any condition on the VETO counter, in the lower part with rejection of events with a valid VETO hit. A clear signature of the various

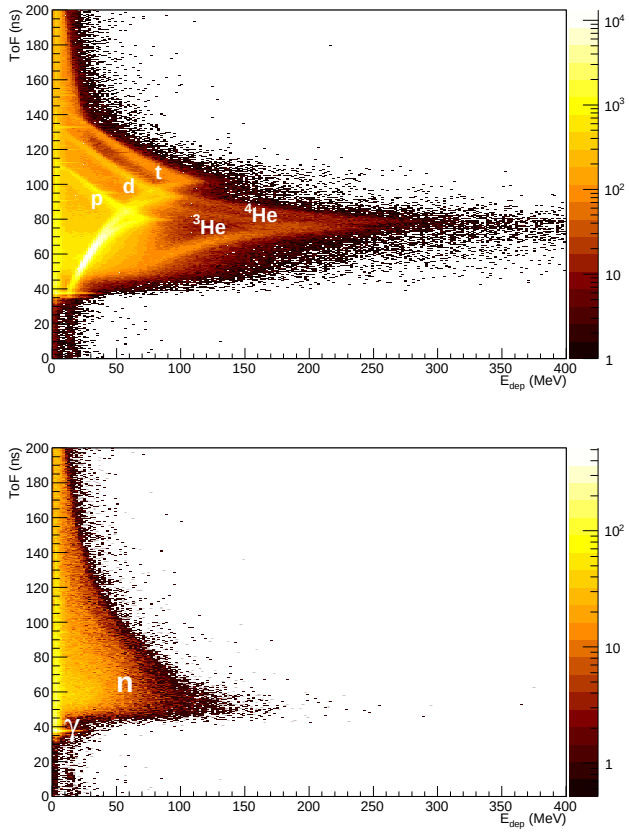

Figure 5: Particle identification in the first NeuLAND plane without (upper panel) and with VETO condition (lower panel).

charged isotopes is observed in the first case, and a clean suppression of these charged particles in case of the strict VETO condition [11]. Note, that the need for a VETO detector for NeuLAND at GSI/FAIR was studied recently with simulations [18].

For the autumn 2016 measurement campaign at SAMURAI, the NeuLAND demonstrator was moved back to its position at 0° to the beam line. Three experiments were carried out using light ions, comprising a study of the unbound states and ground-state properties of ^{31}Ne [12], an investigation of the level structure of ^{22}C combined with the search for ^{21}B [13], and an experiment exploiting a new technique to determine the neutron-decay lifetime of the ^{26}O ground state [14].

Five more experiments with NeuLAND participation are scheduled for the first half of 2017 at RIKEN. After these experiments the NeuLAND demonstrator will be moved back to GSI.

Preparation for Phase-0 Experiments at GSI

For the first phase-0 experiments of the R^{3}B setup in Cave C at GSI, about 40% of NeuLAND will be completed. The necessary calibration tools have been prepared [15],

DOI:10.15120/GR-2017-1

using the data taken in 2014 with the former electronics, and will be customized after the commissioning of the NeuLAND-TAMEX electronics. Detailed simulation studies using R3BRoot [16] are underway, investigating the NeuLAND response as a function of detector volume [17]. The 40% detector cannot provide the full design parameters with respect to efficiency, resolution and multi-neutron recognition capabilities. Multi-neutron detection is especially hampered due to the limits in calorimetric properties. The tools for neutron reconstruction need to be optimized for this scenario, depending on the demand of the physics cases to be investigated in the phase-0 campaign. In addition, the setup in Cave C does not allow a distance larger than 14 m between NeuLAND and the target, thus excluding high resolution performance, as laid out in the technical design report [1] for a distance of 35 m to the target. However, due to the excellent timing properties, the large granularity and the fully active converter material, the 40% detector will provide a major advance in the detection of fast neutrons.

References

[1] NeuLAND@R3B: A Fully-Active Detector for Time-of-Flight and Calorimetry of Fast Neutrons, NeuLAND Technical Design Report, http://www.fair-center.de/fileadmin/fair/experiments/NUSTAR/Pdf/TDRs/NeuLAND-TDR-Web.pdf

[2] K. Boretzky et al., NeuLAND - from Prototypes to Double-Planes, GSI Report 2014-1, 346-350 p. (2014) [10.15120/GR-2014-1-FG-S-FRS-11]

[3] K. Boretzky et al., NeuLAND - from double-planes to the demonstrator, GSI Report 2015-1, 200-202 p. (2015) [10.15120/GR-2015-1-MU-NUSTAR-NR-12]

[4] K. Koch et al., A New TAC-Based Multichannel Front-End Electronics for TOF Experiments With Very High Time Resolution, IEEE Trans. Nucl. Sci.52, 745 (2005)

[5] C. Ugur et al., A compact readout system for the R3B High-Resolution Neutron Time-of-Flight Spectrometer (NeuLAND), GSI Report 2015-1, 204-205 p. (2015) [10.15120/GR-2015-1-MU-NUSTAR-NR-14]

[6] T. Kobayashi et al., SAMURAI spectrometer for RI beam experiments, NIMB 317, 294 (2013)

[7] T. Nakamura and Y. Kondo, Large acceptance spectrometers for invariant mass spectroscopy of exotic nuclei and future developments, NIM B 376 (2016) 156–161

[8] Y. Kondo et al., Calibration methods of the neutron detector array NEBULA, RIKEN Accel. Prog. Rep. 45, 131 (2012)

[9] J. Kahlbow et al., Efficiency study of the NeuLAND demonstrator, contribution to this annual report

[10] Y. Kondo et al.,Spectroscopy of unbound oxygen isotopes II, RIKEN Accel. Prog. Rep. 49 (2016) 42, http://www.nishina.riken.jp/researcher/APR/APR049/pdf/42.pdf

[11] I. Gašparić et al., NeuLAND demonstrator performance in EOS experiments, submitted to RIKEN Accel. Prog. Rep. 50 (2017)

[12] T. Tomai et al., Search for unbound excited states of deformed halo nucleus ^{31}Ne using breakup reactions, submitted to RIKEN Accel. Prog. Rep. 50 (2017)

[13] SAMURAI36 and NeuLAND Collaborations, Exploring the N=16 sub-shell closure: level structure of ^{22}C and search for ^{21}B, submitted to RIKEN Accel. Prog. Rep. 50 (2017)

[14] C. Caesar et al., submitted to RIKEN Accel. Prog. Rep. 50 (2017)

[15] V. Wagner et al., Automated NeuLAND calibration in R3BRoot, contribution to this annual report

[16] D. Kresan et al., Status of the R3BRoot framework, contribution to this annual report

[17] J. Mayer et al., Neutron reconstruction with NeuLAND in FAIR Phase 0, contribution to this annual report

[18] C.A. Douma et al., Simulation studies of a NeuLAND VETO wall, contribution to this annual report

DOI:10.15120/GR-2017-1

Efficiency study of the NeuLAND demonstrator

J. Kahlbow[*1,2], *I. Gašparić*[3,2], *T. Aumann*[1,4], *K. Boretzky*[4,2], *Y. Kondo*[5,2], *T. Nakamura*[5,2], *H. Otsu*[2], *A. Saito*[5,2], *H. Simon*[4], *Y. Togano*[5,2], *H. Törnqvist*[1,2], *T. Uesaka*[2], *and the NeuLAND-SAMURAI Collaboration*[4,2]

[1]Institut für Kernphysik, TU Darmstadt, Germany; [2]RIKEN Nishina Center, Tokyo, Japan; [3]Ruder Bošković Institute, Zagreb, Croatia; [4]GSI, Darmstadt, Germany; [5]Department of Physics, Tokyo Institute of Technology, Japan

The NeuLAND demonstrator has been used for several experiments studying exotic (multi-)neutron unbound nuclear systems at SAMURAI, see K. Boretzky *et al.* [1]. An essential quantity in understanding this new detector and its response is the one-neutron detection efficiency. It has been studied in a one-day machine-study experiment using quasi-monoenergetic neutrons from the ^{7}Li(*p*,*n*)^{7}Be reaction at the beginning of the campaign at RIKEN.

NeuLAND was placed under zero degree $10.87\,\mathrm{m}$ downstream from the target followed by the two NEBULA subdetectors. In front of NeuLAND, a layer of eight $1\,\mathrm{cm}$ thin plastic scintillators was placed to veto charged-particle events. The active depth of the detector itself is $40\,\mathrm{cm}$ of organic scintillator material. The 800 PMT channels were read out with TacQuila electronics.

The charge-exchange reaction ^{7}Li(*p*,*n*)^{7}Be$(\mathrm{g.s.} + 430\,\mathrm{keV})$ produces almost monoenergetic neutrons as either the ^{7}Be ground state or excited state at $430\,\mathrm{keV}$ is directly populated. The zero-momentum transfer center-of-mass cross section for this reaction has been measured by Taddeucci *et al.* [2] and is used for the analysis here.

The proton beam was produced as a secondary beam from ^{48}Ca and delivered to SAMURAI after separation in BigRIPS. The incident proton beam with a rate of about $1\,\mathrm{MHz}$ impinged on the $1.05\,\mathrm{g/cm^2}$ thick natural Li target. Two plastic-scintillator veto-counters with a hole diameter of $3\,\mathrm{cm}$ were installed to determine the beam-spot size. The proton energies at the middle of the target were $109\,\mathrm{MeV}$ and $253\,\mathrm{MeV}$ leading to neutron energies of $106.8\,\mathrm{MeV}$ and $250.5\,\mathrm{MeV}$, respectively. The neutrons were emitted in the forward direction and detected by NeuLAND, whereas the unreacted protons were bent in the SAMURAI dipole magnet.

In order to identify one-neutron events in NeuLAND, the neutron velocity spectrum, shown in Fig. 1, is considered. The spectrum is obtained under the following conditions: The neutron velocity is determined from the time difference of the first valid hit in NeuLAND to the start detector. For NeuLAND the time is calculated from the two PMT times above threshold $\gtrsim 2\,\mathrm{MeVee}$ of one scintillator bar. The background from the empty-frame measurement is subtracted. In order to match the zero-momentum transfer condition in the lab frame, the position distribution is limited to a cone of $\pm 40\,\mathrm{mrad}$ in the x-y-plane.

The sharp peak marked by the fitted curve in the histogram is associated with the response to quasi-monoenergetic neutrons; the continuum is mainly caused by neutrons from other break-up reactions as ^{7}Li(*p*,x*n*). The uncertainty in determination of the prompt neutrons due to the overlap of the continuum and peak region is small in comparison to the 3% uncertainty arising from the uncertainty of the used cross section. For $250\,\mathrm{MeV}$ the acceptance cut was reduced to $\pm 14\,\mathrm{mrad}$ to reduce the continuum background further. By integrating the peak the number of detected neutrons is obtained. To calculate the efficiency, this value is normalized by the number of incident neutrons, corrected for the trigger efficiency. For a threshold energy cut $E > 5\,\mathrm{MeVee}$ the *preliminary* obtained one-neutron detection efficiency accounts for $(27.8 \pm 1.2)\%$ and $(26.6 \pm 1.1)\%$ at the neutron energies of $110\,\mathrm{MeV}$ and $250\,\mathrm{MeV}$, respectively. A first comparison to simulation data is provided by J. Mayer *et al.* [3].

A detailed study of the detector response is needed to provide final results. With the results from this calibration experiment, cross sections from measurements using NeuLAND at SAMURAI can be calculated.

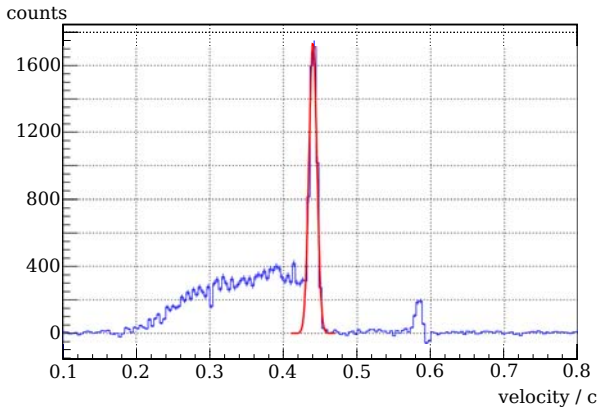

Figure 1: Experimental velocity spectrum of NeuLAND for $\approx 110\,\mathrm{MeV}$ neutrons with veto condition on charged particles, background subtraction, spatial cut, and an energy cut $E > 5\,\mathrm{MeVee}$.

References

[1] K. Boretzky *et al.*, contribution to this annual report and references therein

[2] T. N. Taddeucci *et al.*, Phys. Rev. C 41 (1990) 2548

[3] J. Mayer *et al.*, contribution to this annual report

*jkahlbow@ikp.tu-darmstadt.de

Work supported by the BMBF contract no. 05P15RDFN1.

Neutron reconstruction with NeuLAND in FAIR Phase 0

J. Mayer[*1], *K. Boretzky*[2], *M. Heil*[2], *D. Kresan*[2], *S.G. Pickstone*[1], *A. Zilges*[1], *and the R^3B collaboration*[2]

[1]Institut für Kernphysik, Universität zu Köln; [2]GSI Helmholtzzentrum für Schwerionenforschung GmbH, Darmstadt

The NeuLAND[1] simulation and analysis modules for the R3BRoot software package [2] have been rebuilt and extended. The data work flow can be separated into three main components, namely experimental mapping and calibration from raw data to hits, simulation specific inputs with detector response leading up to hit level, and shared neutron multiplicity and energy reconstruction.

Total detection efficiency

The 1n total detection efficiency for four double planes was studied during experiments with the NeuLAND@SAMURAI setup for neutron energies of 110 MeV and 250 MeV in 2015 [3, 4]. Several GEANT3 settings and GEANT4 physics lists were investigated together with the NeuLAND TacQuila Digitizer. This combination of simulation settings and detector response can be compared to experimental data [4]. Adjusting the hit energy threshold exposes differences in the energy deposition of the different physics lists. After applying equivalent acceptance cuts to both simulation and experiment, the preliminary comparison shows good agreement both for the adopted GEANT3 settings and GEANT4 physics lists which do not use the Bertini cascade.

For different detector depths, the total detection efficiency ϵ_{tot} can be described by a probabilistic approach. If n_{in} neutrons are impinging on n_{DP} double planes and the the hit energy acceptance threshold is low (up to $\approx$ 10 MeV), one finds:

$$\epsilon_{\mathrm{tot}} = 1 - (1 - p(n_{\mathrm{DP}}))^{n_{\mathrm{in}}}$$

where $p(n_{\mathrm{DP}}) = 1 - (1 - p_{\mathrm{DP}}))^{n_{\mathrm{DP}}}$, with the *double plane efficiency factor* p_{DP} as single free variable. For 600 MeV neutrons and 2 MeV threshold p_{DP} is ≈ 0.11.

Reconstruction

For FAIR Phase 0 experiments, at least 12 of the 30 proposed double planes will be available. A similar binomial approach can be made for the probability of different multi-neutron interaction channels. In the case of four incoming neutrons impinging on 30 double planes, all four will react in about 90% of all cases. For 12 double planes, this 4n-4n channel drops down to about 33% and competes with the 4n-3n and 4n-2n channels.

* jan.mayer@ikp.uni-koeln.de

Supported by the BMBF (05P2015PKFNA) and the GSI (KZILGE1416). J.M. is supported by the Bonn-Cologne Graduate School of Physics and Astronomy.

Reconstruction of the neutron multiplicity and the four-momentum for each neutron can be carried out using the combination of deposited energy and energy spread in the detector [1]. For limited detector depth, the capability of this calorimetric method is significantly reduced. Simulations show that while this method is still applicable to a reasonable degree for low multiplicities, the 4n reconstruction capability is not sufficient. Monte Carlo data shows that a reasonable four neutron reconstruction efficiency could be obtained, if the first hits in the active material could be distinguished with higher precision, displayed in Fig. 1 for a breakup scenario of ^{8}He to ^{4}He + 4n with a relative energy of E_{rel} = 100 keV.

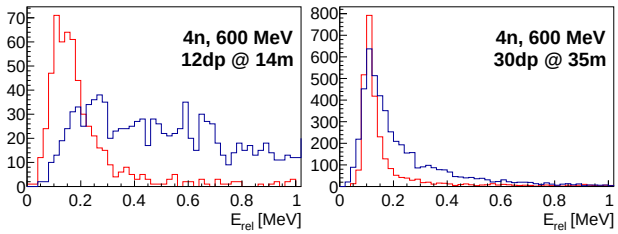

Figure 1: Simulated reconstructed relative energy spectra for 12 double planes at 14 m and 30 double planes at 35 m distance, gated on four neutrons (blue) obtained with the basic calorimetric method compared to the equivalent spectra using Monte Carlo data for reconstruction (red).

Reconstruction methods for 12 double planes at short distances are currently under revision for Phase 0 experiments.

References

[1] NeuLAND@R3B: A Fully-Active Detector for Time-of-Flight and Calorimetry of Fast Neutrons, NeuLAND Technical Design Report (2011)

[2] D. Kresan *et al.*, "R3BRoot: a FAIRRoot-based development for the analysis and simulation of the R3B experiment", GSI Report 2013-1 205 (2013)

[3] K. Boretzky *et al.*, "NeuLAND - from the demonstrator to the start version", contribution to this annual report.

[4] J. Kahlbow *et al.*, "Efficiency study of the NeuLAND demonstrator", contribution to this annual report.

DOI:10.15120/GR-2017-1

Simulation studies of a NeuLAND VETO wall

C. A. Douma[1], K. Boretzky[*2], I. Gasparic[3], N. Kalantar-Nayestanaki[1], D. Kresan[2], J. Mayer[4], C. Rigollet[1], and the R^{3}B collaboration[2]*

[1]KVI-CART, University of Groningen, The Netherlands; [2]GSI Helmholtzzentrum für Schwerionenforschung, Germany; [3]Ruđer Bošković Institute, Zagreb, Croatia; [4]Institut für Kernphysik, Universität zu Köln, Germany

Simulation Procedure

Simulations were carried out to investigate a possible layout and need of a VETO detector in front of NeuLAND (New Large Area Neutron Detector) [1] in order to reduce the background from charged particles.

All simulations were performed with R^{3}BRoot [2] according to the multi-neutron simulation procedure [1, 3]. The Geant4 Monte Carlo engine was chosen to include nucleus-nucleus collisions (like the target reaction) [3]. The physics list was benchmarked against the S438 experiment [4] to provide a production ratio of charged and uncharged particles close to reality.

The full R^{3}B setup in cave C was simulated, including a simplified model of the scattering chamber behind the GLAD magnet. This model included all tracking detector materials and the 4 mm thick stainless steel neutron exit flange. The simulation geometry is displayed in figure 1. The source code is available upon request.

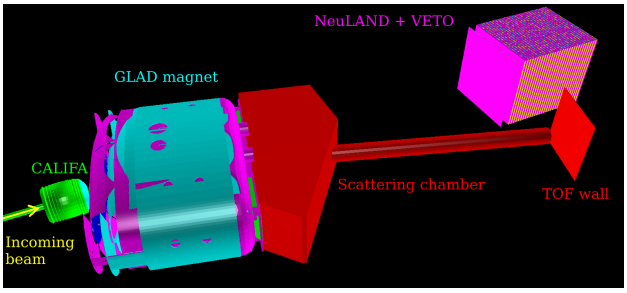

Figure 1: Simulated Geometry in R^{3}BRoot.

Several physics cases were investigated: a 1 GeV/u ^{208}Pb on a 500 mg/cm^2 lead target and a 600 MeV/u ^{48}Ca-beam on a 1.0 g/cm^2 carbon target and on a 2.2 g/cm^2 lead target. Results were evaluated by counting the number of successful events: events where the neutron multiplicity was correctly determined and all neutron interactions were correctly reconstructed and identified properly.

Design of the VETO wall

The VETO wall in the simulation was designed as a 250 cm $\times$ 250 cm wall of 16 distinct non-overlapping scintillators constructed from the same materials as NeuLAND [1] with 1.1 cm active scintillation crystal thickness, a time resolution below 300 ps and an energy deposition threshold below 1 MeV. This wall should be placed 30 cm in front of NeuLAND. Charged particles can then be eliminated by removing one neutron interaction point for each VETO signal. Our simulations show that this is the optimal design for the geometry and the position of the VETO detector.

Time Cuts

The background in NeuLAND originates from secondary scattering of projectiles (fragments) in the downstream detectors of the R3B setup. The neutron background was more than 50% higher than the charged background. To eliminate this neutron background, time cuts were applied on the raw data. This reduced the neutron background with a factor of 3.7 and the charged particle background with a factor of 5.7 while only 4% of the neutrons stemming from reactions in the target were lost. As a result, the number of successful events increased by 5%-25% (depending on neutron multiplicity). However, these time cuts influence the calorimetric properties of NeuLAND. This problem was solved by adjusting the neutron separation matrix accordingly [1].

VETO results

Our simulations show that about 1% of the target neutrons were eliminated by the VETO, while 46%-73% (depending on neutron multiplicity) of the contaminated events were turned into successful events. Due to the low number of charged background particles, this resulted in a small decrease in the total number of successful events in the configuration where the scattering chamber and the fragment arm are under vacuum making the VETO detector not very useful

However, with air in the scattering chamber, our ^{208}Pb physics case showed a significant increase in signal-to-noise ratio when using the VETO.

References

[1] The R^{3}B collaboration 2011 *Technical Design Report of NeuLAND* `http://www.fair-center.eu/fileadmin/fair/publications_exp/NeuLAND-TDR-Web.pdf`

[2] D. Bertini 2011 *J. Phys.: Conf. Series* **331** 032036 (2013) 56

[3] D. Kresan *R^{3}BRoot* `http://r3broot.gsi.de/`

[4] K. Boretzky *et al.* 2015 *NeuLAND - from double-planes to the demonstrator* GSI Report vol. 2015-1 MU-NUSTAR-NR-12

* k.boretzky@gsi.de

DOI:10.15120/GR-2017-1

Automated NeuLAND calibration in R3BRoot*

V. Wagner† [1,2], *D. Kresan*[2], *J. Enders*[1], *I. Gašparić*[3], *M. Heil*[2], *H.T. Johansson*[4], *and the R*^{3}*B Collaboration*[1]

[1]Institut für Kernphysik, TU Darmstadt, Germany; [2]GSI, Darmstadt, Germany; [3]RBI, Zagreb, Croatia; [4]Chalmers University of Technology, Göteborg, Sweden

Within the R3BRoot framework [1], an automated calibration chain for NeuLAND [2] has been developed and tested. The calibration is divided into three consecutive steps, from unpacked data to the fully calibrated hit level data, which is described below in detail.

Pedestal offset

The readout electronics used in NeuLAND have arbitrary zero energy channels, the so-called pedestals. These are determined by using a pedestal run, where all modules fire and record their readout value at zero energy deposit. In all following events these pedestal values are subtracted from the measured ones to get the proper values.

Time calibration

NeuLAND readout electronics has different time channel widths for each bin. To determine the width of each channel, any uncorrelated data, e.g. from cosmics, can be used. For uncorrelated data the events are uniformly distributed in time, thus the width of each channel is proportional to its number of counts and the calibration is derived from that.

The NeuLAND electronics has a walk effect, i.e. the time measurement of each hit is influenced by its amplitude. The dependency was determined by using an UV laser with variable amplitude and therefore the measured time can be corrected. Note that the signal from each PMT is time calibrated after this step but not synchronized yet. An automated synchronization is performed in the next step.

Position calibration, time synchronization and energy calibration

For the position calibration, time synchronization and energy calibration cosmic muons are used. The former two are based on the cosmic1 algorithm from the land02 software package [3]. The muons create long tracks inside NeuLAND and because of its design with alternating plane orientations, these tracks can be reconstructed in case enough planes were hit. After the reconstruction the coordinates of the hits alongside the bars are known. The time difference of the two signals in one bar linearly depends on the position of the hit, with the effective speed of light in the bar as its slope. For hits in the center of a bar the time difference between the signals of the two PMTs originates from different cable lengths. This effect is accounted for and removed in the synchronisation. With the offset and the effective speed of light, the position of each hit can be determined from the time difference. In the second step of synchronisation, the time relations of signals in different bars are adjusted. The time difference between the hits in the bars caused by the finite speed of the muons is calculated and subtracted and the remaining time difference is added to an overdetermined linear equation system which is solved at the end. For the gain calibration using muons, the deposited energy from a muon is divided by its path-length inside the bar. Since cosmic muons are minimum ionizing particles, the mean value corresponds to the well known energy deposition per length for the material. Thus the gain for each module can be determined.

The dataflow of the calibrations is shown in fig. 1.

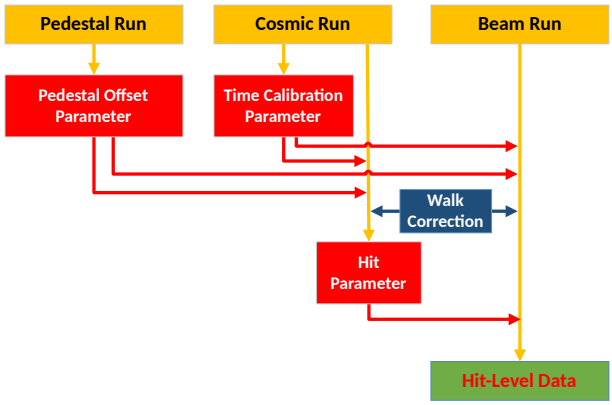

Figure 1: Dataflow of NeuLAND calibration.

Calibration Quality

The quality of the time calibration routine has been checked by determining the time resolution for high-energy gamma-rays stemming from reactions of ^{48}Ca reactions on a polyethylen target at 650 AMeV. The time resolution $\sigma = (144.6 \pm 5.6)$ ps without energy cut was below the goal of $\sigma = 150$ ps, specified in the TDR.

References

[1] R3BRoot : https://r3broot.gsi.de/

[2] K. Boretzky et al, "NeuLAND from the demonstrator to the start version", contribution to this annual report

[3] H. T. Johansson, The DAQ always runs, Chalmers, 2006

* Work supported by BMBF (05P15RDFN1)

† vwagner@ikp.tu-darmstadt.de

DOI:10.15120/GR-2017-1

Performance of PSP detectors for the R^{3}B setup *

I. Syndikus[1], S. Storck[1], D. Rossi[1], L. Atar[1], T. Aumann[1], R. Gernhäuser[2], M. Heil[3], B. Heiss[2], A. Ignatov[1], A. Inglessi[4], H. Johansson[5], J. Kahlbow[1], A. Kelic-Heil[3], O. Kiselev[3], P. Klenze[2], A. Krivshich[4], D. Körper[3], Y. Litvinov[3], B. Löher[3], C. Nociforo[3], S. Paschalis[6], M. Petri[6], R. Plag[3], H. Scheit[1], S. Scholl[1], H. Simon[3], J. Tscheuschner[1], H. Törnqvist[1], F. Wamers[3], and the R^{3}B collaboration[1]

[1]Institut für Kernphysik, TU Darmstadt, Germany; [2]TU München, Garching, Germany; [3]GSI, Darmstadt, Germany; [4]Petersburg Nuclear Physics Institute Gatchina, Russia; [5]Chalmers University of Technology, Göteborg, Sweden; [6]University of York, United Kingdom

A kinematically complete measurement of nuclear reactions is possible with the R^{3}B setup. To do so, several detectors are positioned in the beam tracking the incoming and outgoing isotopes. Position Sensitive Pin diodes (PSP) are used to determine the position of the passing particles and to measure their energy loss in the detector, respectively their charge.

Continuing the work of the previous years [1,2], we tested PSP detectors using the charge-division method to determine the interaction position of passing ions. This method has the advantage of a small number of electronic channels compared to micro-strip detectors providing a similar position resolution. After promising tests with detectors segmented into strips, reducing the noise and increasing the rate capability, we now tested new prototypes.

During a beam time in June 2016, several detectors were tested using a ^{124}Xe beam at $E = 600\,\mathrm{AMeV}$. We tested two different prototypes of X5 detectors from Micron Semiconductor Ltd. This model has strips on both sides perpendicular to each other, providing position information with a design goal of $100\,\mu\mathrm{m}$ in both directions and an active area of $10 \times 10\,\mathrm{cm}^2$. In addition, we used X1 detectors (same manufacturer, with strips only on one side and a smaller active area of $5 \times 5\,\mathrm{cm}^2$), to determine the influence of radiation damage from previous tests on the detector performance. All PSP detectors were read out with MPR-32 preamplifiers from Mesytec and their signals were digitized using the FEBEX3 [3] read-out system.

The focus of the ongoing analysis lies on the traditional prototype with read-out along the strips, while the analysis of the prototype with strips read out along the long edge is pending. During the beam time, the X5 detectors showed an unreasonably high leakage current. Still, the position and energy resolution of the detector were determined. Results are shown in Table 1 together with the results for the X1 detectors.

For the position resolution of the X5 detector, a cut on the interstrip events on the opposite side of the detector was applied. While the back side showed nice peaks and a promising resolution of $130 - 170\,\mu\mathrm{m}$, the front side showed a double-peak structure for every interstrip area. This structure lead to an unacceptably large position resolution of $350 - 800\,\mu\mathrm{m}$. The investigation of this phenomenon is still ongoing. Figure 1 shows the reconstructed positions for the interstrip events.

Table 1: Detector performance for Micron X1 detectors and X5 prototype.

Detector	X1	X1	X5 back	X5 front
$\Delta x/\mu\mathrm{m}$	90	120	150	> 350
$\frac{\Delta E}{E}/\%$	2.1	3.6	1.3	

For the energy resolution, only an upper limit can be given. Due to the presence of inhomogeneous material in the beam path for tests of other detectors, the PSP detectors require a position-dependent correction of the energy-loss, which cannot be performed yet at this time.

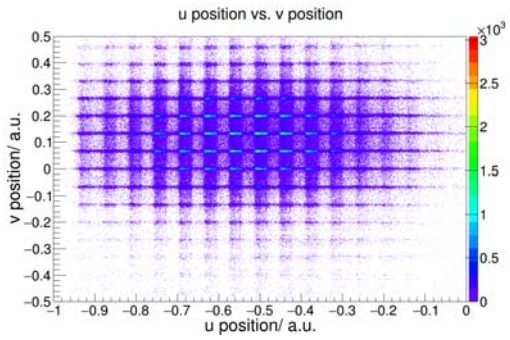

Figure 1: Position information from one Micron X5 prototype. The reconstructed lines in one direction correspond to the interstrip region of the opposite side of the detector.

References

[1] S. Paschalis and the R^{3}B collaboration, "Heavy-ion tracking detectors for the R^{3}B setup", GSI Scientific Report 2013 (2014) p.147, DOI:10.15120/GR-2014-1-NUSTAR-KR-10

[2] S. Paschalis and the R^{3}B collaboration, "The in-beam tracking detectors of R^{3}B", GSI Scientific Report 2014 (2015) p.206, DOI:10.15120/GR-2015-1-MU-NUSTAR-NR-15

[3] FEBEX3 homepage: https://www.gsi.de/work/forschung/electronics/digitalelektronik/digitalelektronik/module/lwl/febex/febex3a.htm

* Work supported by BMBF contract 05P15RDFN1, HGS HIRe and GSI-TU Darmstadt cooperation agreement.

Developing a fiber-detector for in-beam tracking at the R^{3}B-setup *

S. Scholl[1], J. Tscheuschner[1], D. Rossi[1], L. Atar[1], T. Aumann[1], R. Gernhäuser[2], M. Heil[3], B. Heiss[2], A. Ignatov[1], A. Inglessi[4], H. Johansson[5], J. Kahlbow[1], A. Kelic-Heil[3], O. Kiselev[3], P. Klenze[2], A. Krivshich[4], D. Körper[3], Y. Litvinov[3], B. Löher[3], C. Nociforo[3], S. Paschalis[6], M. Petri[6], R. Plag[3], H. Scheit[1], H. Simon[3], S. Storck[1], I. Syndikus[1], H. Törnqvist[1], F. Wamers[3], and the R^{3}B collaboration[1]

[1]Institut für Kernphysik, Technische Universität Darmstadt, Darmstadt, Germany; [2]Technische Universität München, Garching, Germany; [3]GSI, Darmstadt, Germany; [4]Petersburg Nuclear Physics Institute Gatchina, Gatchina, Russia; [5]Chalmers University of Technology, Göteborg, Sweden; [6]University of York, United Kingdom

The R^{3}B (**R**eactions with **R**elativistic **R**adioactive **B**eams) setup at FAIR is intended for kinematically complete measurements of reactions with relativistic heavy-ion beams up to 1 AGeV. In order to track the ions before and after the target, five plastic fiber detectors with active areas between 10×10 cm^2 and 120×80 cm^2 are foreseen. These detectors will provide position measurements perpendicular to the trajectory of charged particles to determine, *e.g.*, the magnetic rigidity $B\rho$ of the ions, and hence their mass-to-charge ratio. The light from the scintillating fiber is sensed using, for instance, SiPMs (silicon photomultipliers) and Multi-anode Photomultiplier Tubes. One advantage of such plastic fibers is the capability of handling beam rates up to several MHz.

Two prototype detectors were built to test the performance of the fibers and of the associated read-out system. These detectors were tested during a beam time in June 2016 at GSI. The first detector, made of 2×64 square fibers, had an active area of 1.28×1.28 cm^2 and consisted of two planes of fibers for measurements in the x and y directions. The fibers were individually coupled to 3×3 mm^2 Hamamatsu multi-pixel photon counters (MPPCs) [1] and read out with the FEBEX [2] system. The MPPCs are photon-counting devices using multiple avalanche photodiode pixels and have a very good acceptance for light emerging from the fiber. In normal operation, the MPPCs are operated in Geiger mode. The other detector was made of 2×8 fibers oriented vertically to measure the x-position. These fibers were coupled on one end to 3×3 mm^2 Hamamatsu MPPCs and to SiPMs from SensL [3] on the other, providing correlated data to compare the performance of both MPPC types directly. The read-out used PADI [4] combined with a VFTX2 TDC [5] with a time resolution of about 10 ps.

One of the results from this test is the capability to detect 600 AMeV ^{12}C ions using 200 μm plastic scintillating fibers. In figure 1 is shown the response of the different MPPCs. One can recognize the single pixels and a strong linear correlation between the detected photons on both sides. Here, no selection criteria were used. The time resolution between both ends is approximately 0.5 ns.

Although the fibers are rather thin, this test shows that if the dark rate is sufficiently low, it might be possible to track ions with even lower charge than carbon. The choice of read-out electronics is currently under investigation, with the goal of simplifying the electronics chain and reducing the cost per channel when compared to the present situation. Two different read-out systems will be tested in the near future, namely the GEMEX [6] (charge integration) read-out system and a PADI+TDC system, using a time-over-threshold approach.

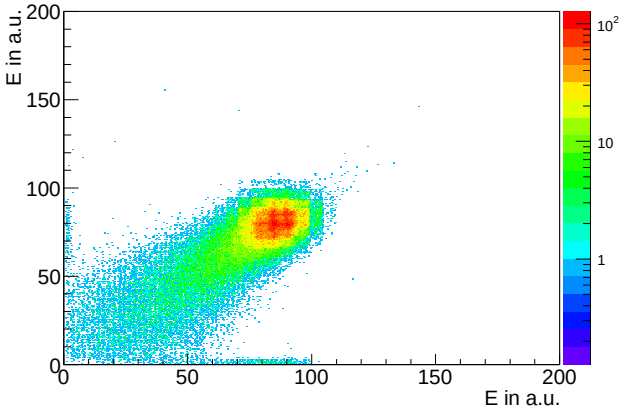

Figure 1: Energy signals from both sides of one fiber of the prototype detector using VFTX2 TDC + PADI with SensL SiPMs.

References

[1] http://www.hamamatsu.com/jp/en/4113.html

[2] https://www.gsi.de/en/work/research/experiment_electronics/digital_electronic/digital_electronics/modules/font_end_module/febex.htm

[3] http://sensl.com/products/c-series/

[4] M. Ciobanu et al., IEEE Transactions on Nuclear Science (2014), p.1015-1023, DOI:10.1109/TNS.2014.2305999

[5] https://www.gsi.de/fileadmin/EE/Module/Dokumente/vftx1_8.pdf

[6] B. Voss et al., 2012 IEEE NSS/MIC (2012), p.678-679, DOI:10.1109/NSSMIC.2012.6551191

* Work supported by BMBF (05P15RDFN1).

DOI:10.15120/GR-2017-1

Preliminary results of the PAS prototype test with a ^{12}C beam*

A. Krivshich[1], G. Alkhazov[1], V. Andreev[1], L. Atar[2], T. Aumann[2], R. Gernhäuser[3], M. Heil[4], B. Heiss[3], A. Ignatov[2], D. Ilin[1], A. Inglessi[1], H. T. Johansson[5], J. Kahlbow[2], A. Kelic-Heil[4], O. A. Kiselev[4], P. Klenze[3], D. Körper[4], Y. Litvinov[4], B. Löher[2], D. Maisuzenko[1], A. Nadtochiy[1], C. Nociforo[4], S. Paschalis[6], M. Petri[6],R. Plag[4], D. M. Rossi[2], H. Scheit[2], S. Scholl[2], N. Shvetsova[1], H. Simon[4], S. Storck[2], I. J. Syndikus[2], J. M. Tscheuschner[2], H. T. Törnqvist[2], F. Wamers[4], V. Yatsyura[1], and the R^{3}B collaboration

[1]Petersburg Nuclear Physics Institute Gatchina, Orlova Roscha, Leningrad district 188300, Gatchina, Russia; [2]Institut für Kernphysik, Technische Universität Darmstadt, 64289 Darmstadt, Germany; [3]Technische Universität München, James-Franck-Str 1, 85748, Garching, Germany; [4]GSI Helmholtzzentrum für Schwerionenforschung, Planckstraße 1, 64291, Darmstadt, Germany; [5]Chalmers University of Technology, Kemivagen 9, 412 96, Göteborg, Sweden; [6]University of York, United Kingdom

To test the operability of the PAS detector [1], we have fabricated a prototype of the detector module, structurally corresponding to the STW-X2 station. The performance of this prototype was studied at PNPI (using β-sources ^{90}Sr and photon source ^{55}Fe) and at a high-energy (600 MeV/u) beam of carbon ions at GSI. PAS is designed to measure precisely trajectory coordinates of protons emitted in nuclear reactions. The coordinate resolution of PAS is expected to be about 200 μm. The final version of PAS will be located in the vacuum chamber of the dipole magnet GLAD.

The PAS prototype consists of 96 thin-wall aluminum drift tubes (straws), which are arranged in three layers. Each layer is shifted by one tube radius with respect to the previous layer. All the tubes are of 110 cm length, diameter 10 mm and the wall thickness being 0.2 mm. The straw anode is a gold-plated tungsten wire with the diameter of 35 μm. The gas mixture is Ar+30%C_2H_6. The scheme of the experimental setup is presented in Fig. 1a. The general view of the detector and its location on a carbon beam at GSI is shown in Fig. 1b.

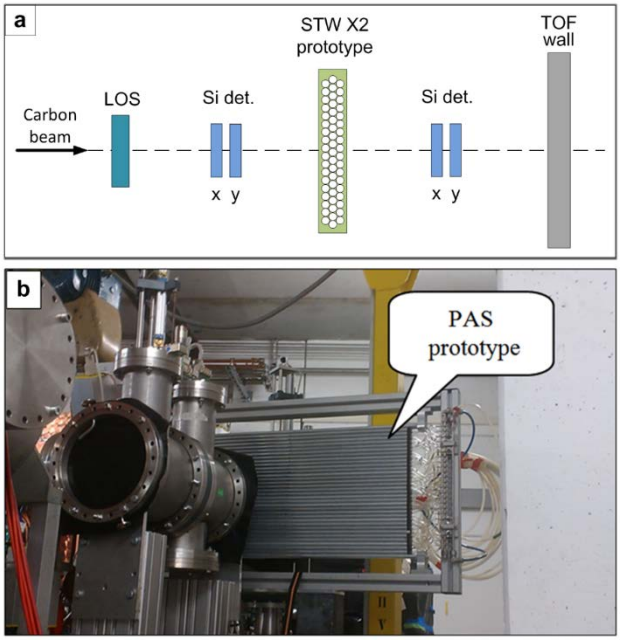

Figure 1: Scheme of the experimental setup (a); general view of the detector on a carbon beam (b).

During the beam test, data sampling and readout was performed using the VFTX-2 VME TDC module with the 10 ps time resolution. All events included a timestamp code which was distributed throughout all active detectors (LOS, TOF, PSP) providing synchronization of the time with other systems of the setup. A preliminary analysis was performed via standalone ROOT scripts, while an activity to integrate the Prototype in the R3BRoot framework is on the way.

The observed structure of the beam profile (Fig. 2a) and the dependence of the counting rate (Fig. 2b) on the high voltage do not match the same characteristics which are generated by monoenergetic particles (emitted protons). The map of the straw arrangement and the beam position are presented in Fig. 2c.

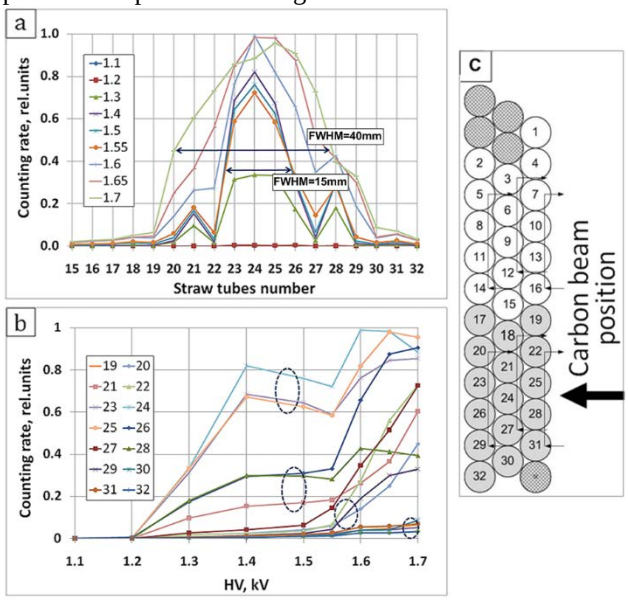

Figure 2: Counting rates of different straws for different high voltages (a); the counting rates via high voltage for different straws (b); straw map in the STW-X2 prototype and the beam position (c).

These results indicate that the carbon beam had a pronounced halo which contained a lot of accompanying particles (including delta-electrons) with different ioniz-

* Work supported in part by BMBF contracts 05P15RDFN1 and 05P15WOFNA, HGS HIRe and GSI-TU Darmstadt cooperation agreement.

ing power, which resulted in different counting rates from different straws. Such groups of particles are highlighted by dotted circles in Fig. 2b. This halo distorted the obtained time spectra due to a significant time dispersion of the detected signals with respect to the LOS trigger signal.

It was shown that for correct selection of particle tracks, special algorithms are required. Two of them were applied for the off-line data analysis (Fig.3), which allowed us to select events using information from either two or three layers of the detector straws.

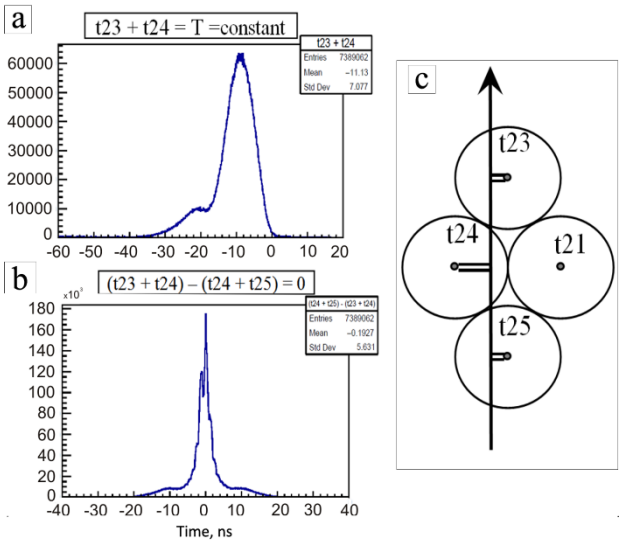

Figure 3: Time spectra and special algorithms for particle selection. Straw map and drift time information (c).

Both algorithms are based on the fact that the sum of the drift times of electrons from the single particle track to the anodes of two adjacent straws which are placed in two neighboring layers is a constant equal to the maximum electron drift time from the cathode to the anode (about 100 ns). The first algorithm (t23+t24=constant), which was initially used, was not sufficient to perform effective selection of events (Fig. 3a). To improve the particle selection, the third straw layer should be involved in the analysis. As one can see, the second algorithm ((t23 + t24) – (t24 + t25) = 0) makes it possible to detect most of particles within the time jitter of about ±8 ns, which corresponds to fluctuations in the measurement of the absolute coordinate of the particle track in the ±400 μm range (Fig. 3b). This data analysis has shown that the three layer design of each STWs was a proper choice.

A further development of the algorithms should include two following stages: (a) selection of useful events from PAS by using the scintillator wall TOFD; (b) synchronization of our data with the data from position-sensitive Si detector PSP. This will allow us to select the required events and to carry out measurements of the spatial resolution and the X-T relation of the PAS detector.

References

[1] Technical Report for the Design, Construction and Commissioning of the Tracking Detectors for R3B, pages 101-117, November 20.

DOI:10.15120/GR-2017-1

In-beam test of a CALIFA Demonstrator segment of R3B *

P. Cabanelas[†1,2], *P. Teubig*[3], *P. Remmels*[4], *P. Klenze*[4], *E. Galiana*[1,2], *H. Álvarez-Pol*[1,2], *E. Alves*[5], *J. M. Boillos*[1,2], *R. C. da Silva*[5], *D. Cortina-Gil*[1,2], *J. Cruz*[7], *D. Ferreira*[3], *M. Fonseca*[7], *D. Galaviz*[3,6], *R. Gernhäuser*[4], *D. González*[1,2], *A. Henriques*[3], *A.P. Jesus*[7], *H. Luís*[5], *J. Machado*[7], *L. Peralta*[3,6], *J. Rocha*[5], *A. M. Sánchez-Benítez*[8], *H. Silva*[7], *P. Velho*[3], *and the R3B Collaboration*

[1]Dpt. de Física de Partículas, Universidade de Santiago de Compostela, E-15782 Santiago de Compostela, Spain; [2]Instituto Galego de Física de Altas Enerxías (IGFAE), E-15782 Universidade de Santiago de Compostela, Spain; [3]Laboratório de Instrumentação e Física Experimental de Partículas (Lip), Av. Prof. Gama Pinto 2, 1640-003 Lisbon, Portugal; [4]Technische Universität München, 80333 Garching , Germany; [5]Campus Tecnológico e Nuclear, Instituto Superior Técnico, Universidade de Lisboa, 2695-066 Bobadela LRS, Portugal; [6]Departamento de Física, Faculdade de Ciências da Universidade de Lisboa, Campo Grande, P-1749-016 Lisbon, Portugal; [7]Laboratório de Instrumentação, Engenharia Biomédica e Física da Radiação (LIBPhys-UNL), Departamento de Física, Faculdade de Ciências e Tecnologia, Universidade Nova de Lisboa, P-2829-516 Caparica, Portugal; [8]Departamento de Ciencias Integradas, Facultad de Ciencias Experimentales, Campus de El Carmen, Universidad de Huelva, 21071 Huelva, Spain

Introduction

A devoted experiment to test the CALIFA [1] Barrel Demonstrator together with its Data Acquisition Chain was carried out in November of 2016. Two modules of the CALIFA Demonstrator, also known as petals, were exposed to gamma-rays up to 15 MeV coming from reactions of a proton beam with Al and LiF thin targets. A High Purity Germanium detector was included in the setup. The performances of the full detection system are being analyzed, and the physics of the produced nuclear reactions is being studied as well.

In this report, a complete description of the experiment is provided, together with a short summary on the status of the data analysis and the simulations of the experimental setup.

Experimental setup

Each of the two CALIFA modules consist of a petal box made of high resistance 5083 Aluminium with a 3 μm thick mylar window in the interaction point direction. Inside, a total of 64 CsI(Tl) scintillator crystals, with different shapes in groups of four, are located. The light collection and signal creation is made with Large Area Avalanche Photo Diodes (LAAPDs) directly coupled to the crystals, so that one read-out channel per crystal is available. The crystal + APD system used has an average energy resolution of $\Delta E/E < 6\%$ for 1 MeV gamma rays and very good light output uniformity. In this experiment, each petal had an approximate coverage of 30° in polar angle and 20° in azimuthal angle.

After a first pre-amplification stage, the signals were sent to a FEBEX-based Data Acquisition and trigger system [2], with 9 FEBEX boards available with 16 channels each (144 channels in total). The signal from the HPGe detector was read out with the FEBEX boards as well. The online data unpacking was done using a stand-alone program based on a MBS event structure [3]. The online monitoring was performed with Go4 [4]. A preliminary calibration was done and applied to the data on flight. In total, about 2 TB of data were recorded.

The experiment was performed at the 3 MV Cockcroft-Walton Tandem accelerator of the LATR (Laboratório de Aceleradores e Tecnologías de Radiação) facility located at the CTN/IST (Campus Tecnológico e Nuclear) campus near Lisbon, Portugal. Negatively charged hydrogen ions were produced in a duoplasmatron ion source and were injected with 14 keV energy into the Tandem accelerator. The final proton energies considered during this experiment ranged between 2 and 3 MeV. Following the two-step acceleration process, the positively charged ions were directed via an analysing magnet (90 degree) and further guided towards the reaction line where the detectors were mounted. Typical beam intensities of 100 - 300 nA were achieved throughout the experiment.

For this experimental campaign the nuclear reaction line was adapted to include a reaction chamber from the Technische Universität München. The reaction targets prepared for this experiment consisted in thin pure ^{27}Al foils as well as evaporated LiF foils (with thicknesses lower than 1 μm in both cases). A view of the experimental setup with the position of the CALIFA modules around the reaction chamber can be observed in figure 1.

The HPGe detector (40% relative efficiency) was also installed around the reaction target, positioned at 90 and 180 degrees from the nominal position of the two CALIFA petals. This detector provides a higher resolution of the energy lines observed during the measurements, and will also allow correlation studies between the CALIFA petals and the photons measured with this device.

Prior to the start of the experiment, calibration sources were used to verify the response of the detectors as well as

* Work supported by project No. POS-B/2016/015 of Xunta de Galicia, Grant 654002, ENSAR2, H2020-INFRAIA-2014-2015 of European Commission and Grant POCI-01-0145-FEDER-007334

† pablo.cabanelas@usc.es

Figure 1: Top view of the experimental setup during the experiment at the Tandem accelerator of the CTN/IST laboratory. The reaction target, at the end of the beam line, is surrounded by the two CALIFA petals used in the experiment, as well as by the HPGe detector.

a basis for energy calibration of the individual crystals. The sources used before and after the experiment were ^{60}Co, ^{137}Cs, and ^{152}Eu. A spectrum of the response of one single CALIFA crystal exposed to the ^{60}Co source can be observed in figure 2. The sufficiently good energy resolution allows as well for the separation and measurement of the natural background line from the ^{40}K decay, as shown in the figure.

The reactions studied during this experiment are listed in table 1. The two first reactions, ^{27}Al(p,γ)^{28}Si and ^{19}F(p,α)^{16}O, were chosen based on its high Q-value, allowing for the production of high energy photons (above 6 MeV) and thus providing a convenient tool to expose the CALIFA modules to energies similar to those expected in the future R^{3}B setup. The reaction ^{27}Al(p,α)^{24}Mg was also produced in the target, resulting in the emission of a photon of 1368.63 keV from the decay of the first excited state of ^{24}Mg. In addition to the particle capture reactions, the inelastic reaction ^{27}Al(p,p')^{27}Al* was also populated, resulting in the emission of the decay from the two first excited states in ^{27}Al at 843.79 keV (1/2$^+$) and 1014.56 keV (3/2$^+$) [5]. The spectrum obtained for this channel with one of the CALIFA modules can also be seen in figure 3.

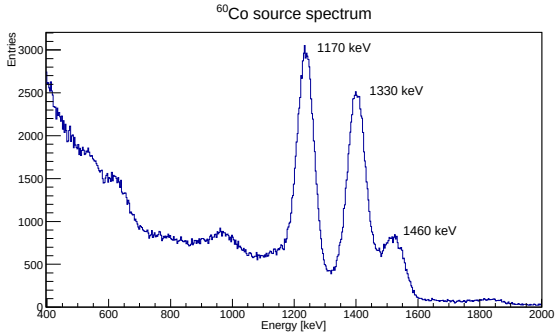

Figure 2: Spectrum measured by a single CsI(Tl) unit exposed to a ^{60}Co source during the preparations of the experimental campaign. The two gammas of 1.17 and 1.33 MeV from ^{60}Co are detected, together with the natural background 1.46 MeV peak from ^{40}K.

Table 1: List of reactions measured during the experimental campaign

Reaction	Q-value (MeV)
^{27}Al(p,γ)^{28}Si	11.6
^{19}F(p,α)^{16}O	8.1
^{27}Al(p,α)^{24}Mg	1.6
^{27}Al(p,p')^{27}Al*	< 0

Ongoing work

Experimental Data Analysis

The analysis of the experimental data is on-going. At the time of this internal report, the energy calibration of all individual modules is close to be finished. This will allow to explore the capabilities of the CALIFA modules in its petal configuration to reconstruct high energy photons in similar conditions as those to which they will be exposed in the future R^{3}B setup. Whereas the reconstruction of the full energy photon peak is one of the goals of the experiment,

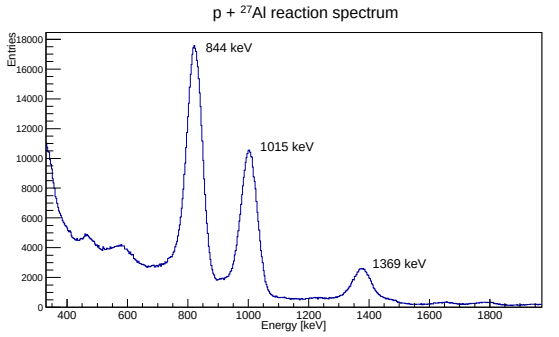

Figure 3: Spectrum measured by a single CsI(Tl) unit during the irradiation of protons on a ^{27}Al target. The two photons of 843.79 keV and 1014.56 keV from the inelastic reaction ^{27}Al(p,p')^{27}Al* are clearly observed, together with the 1368.63 keV photon from the first state of ^{24}Mg.

DOI:10.15120/GR-2017-1

the study of the clustering behaviour as a function of the photon energy will provide very valuable data for the upcoming experimental campaigns at GSI/FAIR. Additional outcomes from this experiment will be the data analysis tools that will be available for the first series of experiments with the CALIFA modules at the R^3B setup.

Simulation

At the same time, the full experiment is being simulated within the EnsarRoot framework [6]. The geometries of the CALIFA petals used in the experiment have been created, together with the reaction chamber and the HPGe detector, and placed in the space in their relative positions, as it is shown in figure 4. By means of simulation, the solid angle covered by the detection system was determined to be 12%. Figure 5 shows a detail of the CALIFA petals where the frame and the crystals inside the box are visible. Also, a dedicated event generator for this kind of proton induced reactions is under construction.

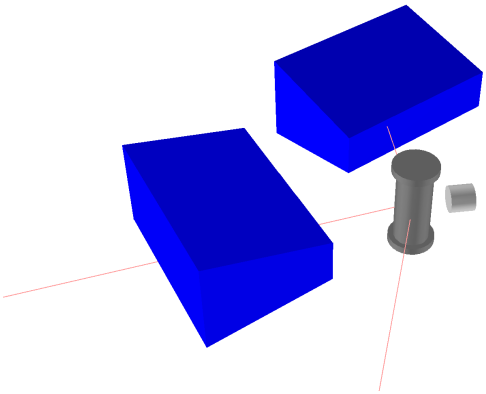

Figure 4: Simulated Setup for the experiment: the two CALIFA petals (big blue boxes), the HPGe detector (small light grey cylinder) and the reaction chamber are located in the space reproducing their real positions. An event with tree gammas coming from the interaction point inside the chamber is shown.

Conclusions

A segment of the CALIFA Barrel Demonstrator has been tested successfully under gamma-rays up to 15 MeV in a beam environment. Two demonstrator modules, or petals, with 64 CsI(Tl) crystals each (128 channels in total), were fully instrumented and the acquisition was performed with a FEBEX-based system of 144 channels. Also, a HPGe detector was included and data was sent to the same DAQ system. The data was unpacked and monitored online. The data from nuclear reactions of a proton beam on Al and LiF targets is now being analyzed. In addition, a complete simulation of the experiment is currently being performed.

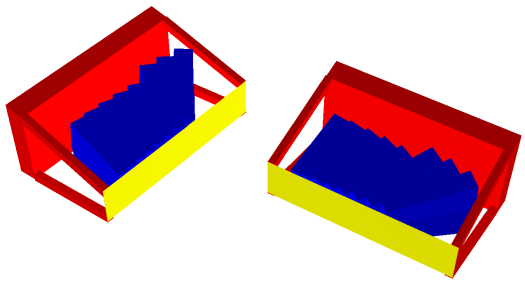

Figure 5: Detail of the CALIFA petals where the frame of the boxes and the 64 crystals inside each box are clearly observed.

References

[1] D. Cortina-Gil et al.,“CALIFA, a Dedicated Calorimeter for the R^3B/FAIR”, Nucl. Data. Sheets, Vol. 120, June 2014, p. 99-101

[2] See the dedicated contribution in this Annual Report

[3] https://www.gsi.de/mbs/

[4] http://go4.gsi.de

[5] National Nuclear Data Center. http://www.nndc.bnl.gov

[6] https://github.com/EnsarRootGroup/EnsarRoot, http://igfae.usc.es/satnurse

EPICS collector - making control parameters stick*

B. Löher[1], *H. Simon*[1], *H. T. Törnqvist*[1,2], *and H. T. Johansson*[3]

[1]GSI, Darmstadt, Germany; [2]Technische Universität Darmstadt, Darmstadt, Germany; [3]Chalmers Tekniska Högskola, Göteborg, Sweden

During experiment preparation and runtime, many important aspects of the experimental setup are controlled by adjusting parameters that may have an influence on the analysis of experimental data. Those parameters may include for example voltages, currents, and thresholds. To facilitate collection and long-term storage of these parameters and their chronological sequence, a helper library was created. Within the NuSTAR collaboration, all experiment control systems rely on EPICS[1] as a backend. Therefore, the helper library introduces an interface between the EPICS channel access protocol and the LMD data format used for detector data storage. This interface allows for timestamped correlation of control parameter values with detector data and gives the user direct access to these parameters during analysis.

Today, EPICS is already successfully in use in several experiments throughout GSI, mainly in the HADES, R3B, CBM and PANDA groups. However, the EPICS servers (IOC) and related software are mainly tailored to a specific use case and either no or only isolated infrastructural components exist. What is needed for future operations in the NuSTAR collaboration besides the IOCs and user interfaces for the individual device are therefore common infrastructural components.

The EPICS collector library focuses on monitoring a set of EPICS process variables (PVs) for changes of their state and value. Any change of state or value is then serialised into a binary format, receives a timestamp, and is written to an LMD data stream. The main benefit of this mechanism is the tight correlation between recorded detector data and control parameters, which makes these parameters directly available and reproducible when analysing data both online and at a later stage. Treating control parameter data similar to detector data automatically ensures also the same level of data protection, reducing the risk of data loss.

To guarantee that PVs have the state and value that was reported by the IOCs at a given time, any change is actively checked after a short time interval has passed. A confirmation flag is written to the data stream, if the PV can be guaranteed to be valid in this time interval. The PV is marked as valid if no further change was seen. Otherwise, the PV cannot be guaranteed to be valid for the interval and therefore receives no confirmation in the data.

The library allows the user to select the source for time information that is used when writing the data to file. Predefined time sources are the system time of the PC where the EPICS collector is running on, and any EPICS PV that exposes a timestamp.

By default, the EPICS collector reads a file `pv_list` or files in a directory named `pv_list.d` to load the list of PVs to track. PVs in the single file are treated as a single group (id $= 0$) and written to a single LMD subevent. Files in the `pv_list.d` directory must have a name starting with a unique group number (> 0, e.g. `01_los_hv`). This group number is used to generate the LMD subevent identifier and ensures that PVs from separate groups are written to separate subevents. The files contain a plain list of PV names, one per line.

Functional example clients, which use the library, are part of the distribution. The `standalone` client shows how the important parts of the library are used and outputs all available information to the terminal. The `watcher` client allows text-based monitoring of the value and state of PVs. The `lmd_source` client runs in an untriggered loop and produces LMD files. Additional clients include an `f_user.c` to show how the EPICS collector can be used from within an MBS node.

The LMD events written by the `lmd_source` and `f_user.c` clients are not marked with the standard type:subtype combination of 10:1, but instead with the proposed combination of ST:KY for so-called *sticky events*. Sticky events are a proposed extension to the LMD data format and represent a core concept for guaranteed delivery of information in a tree of data acquisition, transport, and analysis nodes. Information contained in sticky (sub-)events is cached at each node and delivered to any connecting client before sending any normal events. The cached information is stored until it is either overwritten by a sticky subevent with the same identifier or until it is actively revoked.

Careful consideration should be applied when choosing, which PVs are tracked by the EPICS collector. The persistent nature of information written to LMD files also applies to incorrect information or information that is falsified at a later stage. This means, that only information which is known to be correct is tracked by the EPICS collector and stored in sticky events. Information which is likely to change must not be stored in this way. It is strongly advised to store information organised by hardware (physical) name instead of any logical name. Physical to logical mappings are prone to contain errors, which are clearer to resolve when all mapping is done during analysis.

[1] A. Johnson, et al., Epics - experimental physics and industrial control system (2011).

* For the Common NUSTAR WG

DOI:10.15120/GR-2017-1

A FEBEX based real time high level trigger system

P. Klenze[1], M. Bendel[1], R. Gernhäuser[1], B. Heiss[1], P. Remmels[1], F. Stark[1], and M. Winkel[1]
[1]Physik Department, Technische Universität München

The CALIFA calorimeter with its 2600 scintillator crystals will be one key component for the upcoming R^3B experiment. In kinematically complete measurements, its large acceptance, efficiency and granularity will allow for a detailed event characterization. In addition the particle identification in the frontend electronics [1] and the spectroscopic quality energy measurement provide a substantial information for high level event selection.

The CALIFA trigger system is currently extended to allow for complex trigger conditions such as the total energy deposit, the gamma multiplicity or specific geometrical pattern, like "two protons in planar geometry", for the existing FEBEX readout platform developed at the GSI in Darmstadt [2]. This development will thus be useful for many NUSTAR experiments.

The aggregation of trigger information from the full detector is done in multiple layers using a newly developed low latency protocol named Trigger Transfer Tree Protocol (T^3P). On the lowest level of a tree structure (see figure 1), each FEBEX board sends information collected from its 16 channels to a Collector FEBEX Addon Board (C-FAB) module using a serial bus.

The C-FAB is a dedicated Addon Board for the FEBEX module which hosts one FPGA (Lattice MachXO2 featuring 334 IOs) which processes the information of eight FEBEX boards (128 channels) and sends it to a Receiver FEBEX Addon Board (R-FAB).

On the next level level, the R-FAB combines information from eight C-FABs in a similar manner. Already at the next layer, the information from the whole detector is collected in a single R-FAB and can be used for trigger decisions. Triggers are sent to the FPGA on its FEBEX card which then asserts a MLVDS trigger line on the crate's backplane connected to the EXPLODER [2]. From there, it can be used either to trigger CALIFA itself only or to sent out a signal to the R3B central trigger.

To accomodate trigger generation for auxilary detectors without long event buffers, these trigger decisions should not exceed a latency of $1\,\mu$s.

The only difference between the C-FAB and the R-FAB is the cabling used to connect different layers: For local collection on the first tree layer, the FEBEX boards will be connected using high density ribbon cable on the front side. For the global aggregation in the upper layers, where intercrate connections and longer distances are needed, CAT 7 cables with standard 8P8C connectors will be used.

Each tree connection features three point to point LVDS lines: a leafwards clock signal and two rootwards data signals. Each data line transmits a serialized word (typically one byte) describing the type of current trigger information. In the C-FAB and R-FAB, these informations are aggregated on the fly to decrease the overall latency. This works by receiving the least significant bit and then sending the resulting least significant bit of the operation out in the next clock cycle while processing the next bit. Any eight bits of trigger information can thus transferred from the FEBEX cards to the top level in 18 clock cycles.

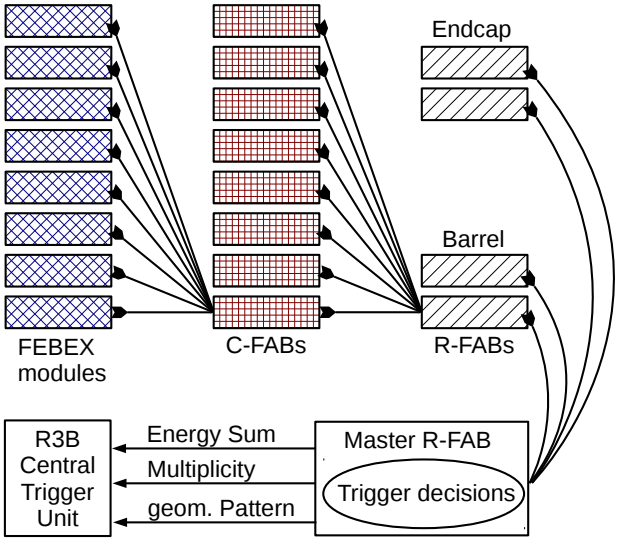

Figure 1: The Trigger Transfer Tree for the CALIFA Calorimeter in R3B

Prototypes for the C-FAB module were designed, produced and tested in the lab. For the FEBEX 3B modules, new branches of the CALIFA firmware were created: one which allows sending T^3P data from standard FEBEX cards and one which allows slow control access to the C-FAB FPGA via I^2C over GOSIP [2]. Additionally, firmware for the C-FAB FPGA was also developed – including HDL components for sending, combining and receiving trigger information. The transmission has been tested extensively in lab conditions and could be operated at a clock frequency of up to $66.5\,\mathrm{MHz}$. This results in an internal trigger delay of less than $300\,\mathrm{ns}$.

References

[1] CALIFA/R^3B Collaboration, Technical Report for the Design, Construction and Commissioning of The CALIFA Endcap, 2014

[2] https://www.gsi.de/en/work/research/electronics/digital_electronic/digital_electronics/modules/lwl.htm

DOI:10.15120/GR-2017-1

Implementation of the deexcitation model ABLA07 in GEANT4

J.L. Rodríguez-Sánchez[1], *A. Kelić-Heil*[2], *J. Benlliure*[3], *J.-C. David*[1], *and S. Leray*[1]

[1]IRFU, CEA, Université Paris-Saclay, Gif-sur-Yvette, France; [2]GSI, Darmstadt, Germany; [3]University of Santiago de Compostela, Spain

GEANT4 (for GEometry ANd Tracking) [1] is a platform for the simulation of the passage of particles through matter, using Monte Carlo methods. *GEANT4* software was the first in the use of object oriented programming and is written in C++. Therefore, in the last decades different codes, for example the intranuclear cascade model *INCL* [2], have been completely redesigned and rewritten in C++ [3] for their incorporation to the *GEANT4* software package.

The *INCL* model was developed to describe spallation reactions at kinetic energies from a few MeV to ∼3 GeV. Spallation reactions at relativistic energies are often described by means of a two-step process [4]: the collision itself, where part of the mass is removed from projectile and target nuclei and excitation energy is gained by the surviving remnants, and subsequent deexcitation processes by evaporation of particles or fission. For the description of the deexcitation stage, *INCL* is usually coupled to the *ABLA07* model [5] developed at GSI. However, *ABLA07* is written in *FORTRAN* and it cannot be used in *GEANT4*. For this reason, we have decided to rewrite *ABLA07* in C++.

The *ABLA07* model describes the deexcitation of an excited nucleus emitting γ-rays, neutrons, light-charged particles, and intermediate-mass fragments (*IMFs*) according to Weisskopf's formalism. For a more realistic description of the deexcitation, the separation energies and the emission barriers for charged particles are also considered according to the atomic mass evaluation from 2012 and the Bass potential, respectively. In addition, deexcitation by fission is also included according to a dynamical picture described in Ref. [6]. The coupling of *INCL+ABLA07* has been benchmarked in several works by using isotopic distributions of evaporation residues and fission fragments produced in spallation and fragmentation reactions of nuclei from iron to uranium, providing a satisfactory description of many observables [7, 8, 9, 10]. In what follows, the version of *ABLA07* rewritten in C++ will be called *ABLA++* and both models contain exactly the same physics and same input parameters.

In figure 1 we show the comparison of experimental data obtained for ^{238}U (1000A MeV) + p with calculations where *INCL* was coupled to different versions of *ABLA*. The dashed and solid lines correspond to *ABLA07* and *ABLA++* calculations, respectively, while the dotted line corresponds to a calculation using the previous version of *ABLA* implemented in C++, the so-called *ABLAv3p*. This version of *ABLA* only includes the evaporation of neutrons, protons, and α-particles, and the fission probability is described according to the Kramers picture [11]. As can be seen, *ABLAv3p* underestimates the production of light and intermediate residual nuclei and overestimates the production of fission fragments, while ABLA07 and ABLA++ provide a good description.

The new version of *ABLA07* in C++ will be included in the next *GEANT4* software package in order to describe the deexcitation of the compound nuclei produced in all kind of reactions, such as spallation, abrasion, fusion, etc.

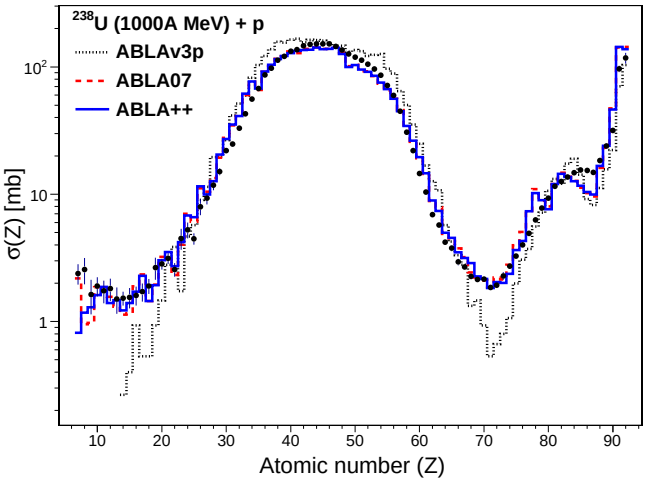

Figure 1: Comparison of *ABLAv3p* (dotted line), *ABLA07* (dashed line), and *ABLA++* (solid line) predictions with experimental data for proton-induced spallation reactions on ^{238}U.

References

[1] http://geant4.cern.ch

[2] A. Boudard et al., Phys. Rev. C **87**, 014606 (2013).

[3] D. Mancusi et al., Phys. Rev. C **90**, 054602 (2014).

[4] J.-C. David, Eur. Phys. J. A **51**, 68 (2015).

[5] A. Kelić, M. V. Ricciardi, and K.-H. Schmidt, Proceedings of Joint ICTP-IAEA Advanced Workshop on Model Codes for Spallation Reactions, ICTP Trieste, Italy, 4–8 February 2008, edited by D. Filges, S. Leray, Y. Yariv, A. Mengoni, A. Stanculescu, and G. Mank (IAEA INDC(NDS)-530, Vienna, 2008), pp. 181-221.

[6] B. Jurado et al., Nucl. Phys. A **747**, 14 (2005).

[7] C. Schmitt et al., Phys. Rev. C **81**, 064602 (2010).

[8] J. L. Rodríguez-Sánchez et al., Phys. Rev. C **91**, 064616 (2015); Phys. Rev. C **92**, 044612 (2015).

[9] Y. Ayyad et al., Phys. Rev. C **91**, 034601 (2015).

[10] J. Alcántara-Núñez et al., Phys. Rev. C **92**, 024607 (2015).

[11] H. A. Kramers, Physica **7**, 284 (1940).

DOI:10.15120/GR-2017-1